

# **NEW ANALYTICAL APPLICATIONS OF GOLD NANOPARTICLES**

**Dissertation**

**zur Erlangung des Doktorgrades der Naturwissenschaften**

**(doktorum rerum naturalis, Dr. Rer. Nat.)**

**der Fakultät für Chemie und Pharmazie**

**der Universität Regensburg**

**Deutschland**



**vorgelegt von**

**Fredy Kurniawan**

**aus Surabaya, Indonesia  
im März, 2008**

# **NEW ANALYTICAL APPLICATIONS OF GOLD NANOPARTICLES**

**Dissertation**

**Submitted in conformity with the requirements  
for the degree of doctor philosophy (Dr. rer. nat)**



Presented by

**Fredy Kurniawan**

(Surabaya, Indonesia)

March 2008

**Faculty of Chemistry and Pharmacy, University of Regensburg, Germany**

This study was performed in the Institute of Prof. Dr. Otto S. Wolfbeis, Institute of Analytical Chemistry, Chemo- and Biosensors, University of Regensburg, during the period from January 2005 to January 2008 under the supervision of Prof. Dr. Vladimir M. Mirsky.

Request for doctorate submitted in 22 February 2008

Date of defence: 27, March 2008

Board of examiners (Prüfungsausschuß):

Chairman (Vorsitzender): Prof. Dr. Otto S. Wolfbeis

First Examiner (Erstgutachter): Prof. Dr. Vladimir M. Mirsky

Second Examiner (Zweitgutachter): Prof. Dr. Werner Kunz

Third Examiner (Drittprüfer): Prof. Dr. Achim Göpferich

*Dedicated to my family*

# Table of Contents

1. Introduction .....	1
1.1. Early history of nanoparticles.....	1
1.2. Synthesis of metallic nanoparticles.....	3
1.2.1. Reductive synthesis of noble metal colloids.....	3
1.2.2. Synthesis of semiconductor nanoparticles.....	6
1.2.3. Other techniques for nanoparticle synthesis.....	6
1.3. Non-analytical applications of nanoparticles.....	7
1.3.1. Tissue engineering.....	7
1.3.2. Cancer therapy.....	8
1.3.3. Manipulation of cells and biomolecules.....	8
1.3.4. Commercial exploration.....	9
1.4. Analytical application of nanoparticles.....	12
1.4.1. Enzymatic biosensor based on gold nanoparticles .....	12
1.4.2. Application of gold nanoparticles for genosensors.....	16
1.4.3. Application of gold nanoparticles for immunosensors.....	19
1.4.4. Application of gold nanoparticles for electrocatalytic chemosensors.....	22
1.4.5. Multicolor optical coding for biological assays.....	23
1.4.6. Application of nanoparticles for signal amplification.....	24
1.5. Objectives of the work.....	26
2. Experimental.....	28
2.1. Reagents and materials.....	28
2.2. Methods of characterization.....	29
2.2.1. Cyclic voltammetry.....	29
2.2.2. Electrical Impedance Spectroscopy (EIS).....	36
2.2.3. Surface Plasmon Resonance (SPR).....	38
2.2.4. Conductive measurement.....	42
3. Results and Discussions.....	45
3.1. Conductive chemoassay for glucose .....	45
3.2. Silver mirror reaction in the paper support.....	46
3.3. Preparation of nanoparticles.....	47
3.4. Characterization of gold nanoparticles.....	57
3.5. Detection of glucose.....	65
3.6. Detection of dopamine.....	75
3.7. Nanoparticles as nucleation centers for protein crystallization.....	90
3.8. Localized Surface Plasmon Resonance (LSPR).....	96
3.9. Freezing indicator.....	100
3.10. Automation of Layer-by-Layer (LbL) deposition.....	109
4. Summary.....	114
5. Zusammenfassung.....	115

6. Kesimpulan.....	117
7. References.....	119
8. Curriculum vitae .....	142
9. List of publications and presentations.....	143
10. Acknowledgements.....	144

## **1. INTRODUCTION**

### **1.1. Early history of nanoparticles**

Nanotechnology, nanoscience, nanostructure, nanoparticles are now of the most widely used words in scientific literature. Nanoscale materials are very attractive for possible machine, which will be able to travel through the human body and repair damaged tissues or supercomputers which small enough to fit in shirt pocket. However, nanostructure materials have potentials application in many other areas, such as biological detection, controlled drug delivery, low-threshold laser, optical filters, and also sensors, among others.<sup>1,2</sup>

In fact, metal nanoparticles have been used a long time ago e.g. Damascus steel which used to make sword and Glass Lycurgus Cup which has unique color.<sup>3-5</sup> Even though, nanoparticles have been used along time ago, but no body realized that it reached nanoparticles scale. It is like just unintentionally technique to produce nanoparticles. After the modern device developed to analyzed material in nanoscale, scientist can prove nanotechnology has been developed and become an interesting subject for science today.

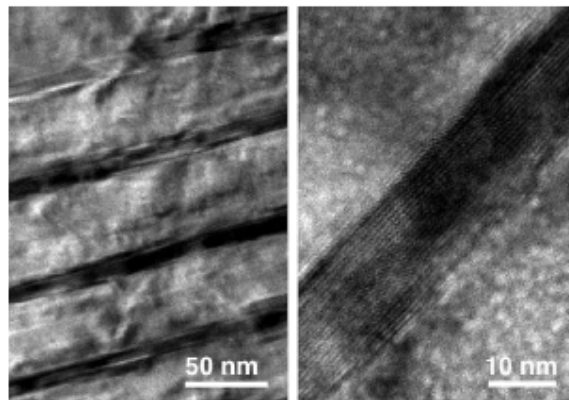


Fig 1.1 Nanowires in Damascus steel. The dark stripes indicate nanowires of several hundreds nanometers in length

Blade made from Damascus steel produce from about 500 AD in Damascus.<sup>6</sup> It become renowned because (1) the extreme strength (2) The sharpness (3) the resilience and (4) the beauty of their characteristic surface pattern<sup>7,8</sup>. The fascinating legend story it can cut clean through rock and still remain sharp enough to cut through a silk scarf dropped on the blade. Many scientist try to reveal this special properties and encounter multiwalled carbon nanotube in steel (MWNTs)<sup>5,9</sup>.

The famous Glass Lycurgus Cup from the Romans times (4<sup>th</sup> century AD) contains silver and gold nanoparticles in approximate ratio 7:3 which have size diameter about 70 nm<sup>10,11</sup>. The presence of these metal nanoparticles gives special color display for the glass. When viewed in reflected light, for example in daylight, it appears green. However, when a light is shone into the cup and transmitted through the glass, it appears red. This glass can still be seen in British museum.



Fig. 1.2 Lycurgus Cup (a) green color, if light source comes from outside of the cup (b) red color, if the light source comes from inside of the cup.

Nanoparticles (1-200nm) have unique electronic, optical, and catalytic properties. Its properties is also connected to the method how to prepare nanoparticles to control the shape and size of nanoparticles, provide exciting building blocks for nanoscaled assemblies, structure, and devices. Miniaturization of structures by mechanic methods and electron-beam lithography is reaching the



theoretical limits of about 50 nm. For further miniaturization of chemical object, alternative approaches must be developed and also to find the applications<sup>12-14</sup>.

## **1.2. Synthesis of metallic nanoparticles**

Many colloidal nanoparticles synthesis have been known<sup>15-17</sup>, but recent worked is dedicated to nanoparticles syntheses specifically for the construction of devices and nanostructures. These particles may consist of a particular material, be of a particular size, or have specialized surface functionality. It has even become possible to have some degree of control over the nanoparticles shape<sup>18,19</sup>. Stability of nanoparticles is also become one of the point. Special precautions have to be taken to avoid their aggregation or precipitation. Glassware is cleaned thoroughly, while reagent solutions and solvents are all filtered and of the highest purity. And syntheses sometimes also involve the use of a stabilizing agent, which associates with the surface of the particle, provides charge or solubility properties to keep the nanoparticles suspended, and thereby prevents their aggregation.

### **1.2.1. Reductive synthesis of noble metal colloids**

The simplest and by far the most commonly used preparation for gold nanoparticles is the aqueous reduction of  $\text{HAuCl}_4$  by sodium citrate at boiling point<sup>17,20</sup>. Although sodium citrate is the most common reducing agent, metal nanoparticles can also be synthesized by the use of borohydride and other reducing agents<sup>21,22</sup>. The application of alcohols as reductants for the production of platinum nanoparticles allows control over the size of the particles: Higher alcohols yield larger particles, which indicates that a more rapid reduction rate of the  $[\text{PtCl}_6]^{2-}$  ions is an important factor for the production of smaller particles<sup>23</sup>.

Particles synthesized by citrate reduction are nearly monodisperse spheres of a size controlled by the initial reagent concentrations (Fig. 1.3).<sup>24,25</sup> They have a negative surface charge as a consequence of a weakly bound citrate coating and are easily characterized by their plasmon absorbance band (at about 520 nm for 15 nm particles). Nanoparticles from other noble metals may also be prepared by citrate

reduction, such as silver particles from  $\text{AgNO}_3$ , palladium from  $\text{H}_2[\text{PdCl}_4]$ , and platinum from  $\text{H}_2[\text{PtCl}_6]$ .<sup>26-28</sup> The similarities in the preparation of these different metal colloids allows the synthesis of mixed-metal particles, which may have functionality different from each individual metal<sup>29</sup>. For example, the reduction of suitable mixtures of noble metal salts can lead to alloy or mixed grain particles.

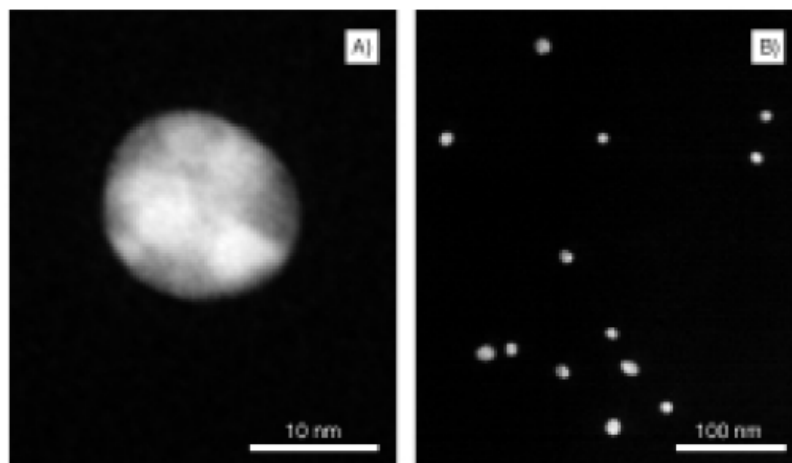


Fig. 1.3. Gold nanoparticles synthesized by citrate reduction.

More interestingly, composite particles can be built up in shells by the synthesis of a small colloidal nuclei followed by its enlargement with a different metal: a gold colloid can be covered with silver<sup>30,31</sup>. Well defined core/shell organosilicon micronetworks with topologically trapped gold particles have also been prepared using a molecular reactor technique.<sup>32</sup> Metallic nanoparticles can be capped with various shells, such as conductive, nonmetallic graphite<sup>26</sup>, or semiconductive  $\text{CdS}$ <sup>33</sup>. This capping can be done in situ if the reductive formation of nanoparticles is performed in the presence of the shell-forming material<sup>26</sup> or the shell can be organized later through a chemical reaction on the surface of the nanoparticles<sup>33</sup>. The enlargement of a nanoparticle can take place even after the colloidal seed particle has been immobilized on a substrate. In such cases, a colloid-functionalized glass substrate is introduced to a gold-<sup>34</sup> or silver-<sup>35</sup> depositing solution, to thereby enlarge the surface-bound nanoparticles and provide a method of control over their

size and density. Such core-shell particles have been studied extensively because their properties can differ from those of the core or shell materials<sup>32,36</sup>. The synthesis of particles that bear surface functionality is desirable for the purpose of nanoparticles handling and the construction of functional architectures. This functionalization of the nanoparticles surface can be accomplished during the nanoparticles synthesis by the addition of a suitable agent to the reaction vessel. As the nanoparticles form, the surface functionalization agent attaches to the nanoparticles, which also imparts an enhanced stability and gives additional control over their size. The borohydride reduction of  $\text{HAuCl}_4$  in the presence of ( $\gamma$ -mercaptopropyl)-trimethoxysilane gives rise to very small (1-5 nm) gold nanoparticles which bear a surface silane functionality<sup>37</sup>. Other borohydride reductions in the presence of thiols<sup>38</sup> have produced nanoparticles with a surface functionality from amines to carboxylic acids. Where the surface functionalization agent is not water soluble, a two phase synthesis can be used, as in the preparation of long chain alkanethiol surfaces on gold colloids<sup>39,40</sup>. The surface functionalization agent does not even need to bind covalently with the nanoparticles. Nanoparticles have been synthesized in the presence of dendrimeric<sup>41,42</sup> and polymeric<sup>43-45</sup> stabilizers, and have been formed in the cavities of micelles<sup>46,47</sup> and silicate sols<sup>48,49</sup>. Gold and silver nanoparticles functionalized by adsorbed disulfides have also been generated in the presence of sodium borohydride<sup>50</sup>. Disulfides offer the advantage that asymmetrical disulfides, that have two distinct functional groups ( $\text{RSSR}'$ ), may be used, which enables the possibility of generating mixed, self-assembled monolayers (SAMs) that possess a homogeneous distribution of functional groups or chain lengths. The use of disulfides also allows the functionalization of nanoparticles with groups such as quinones that are otherwise incompatible with thiols (normally, a thiol would be used rather than a disulfide). The application of different capping materials or the preparation of mixed bimetallic particles allows control of the size and shape of the nanoparticles.<sup>51-53</sup> For example, platinum nanoparticles with cubic, tetrahedral, polyhedral, or irregular-prismatic shapes could be generated selectively when the initial concentrations of  $[\text{PtCl}_6]^{2-}$  and polyacrylic acid were varied for the reductive particle formation<sup>51</sup>.

### 1.2.2. Synthesis of semiconductor nanoparticles

The production of semiconductor nanoparticles and their organization on solid supports is of great importance for the fabrication of nanoelectronic devices. The quantum properties of these particles have potential uses in information-processing devices and, in recognition of this, they are often called “Q particles”<sup>54</sup>. By far the most studied of these are cadmium sulfide particles<sup>55,56</sup>. These and related colloidal particles (for example, PbS<sup>57,58</sup>, Ag<sub>2</sub>S<sup>59,60</sup>, CdSe<sup>61,62</sup>, and TiO<sub>2</sub><sup>63,64</sup> can be prepared relatively easily by using inverse micelles as nanoscale reaction vessels<sup>65</sup>. Firstly, solutions of inverse micelles are prepared, one containing the metal salt (usually as the chloride) and the other containing Na<sub>2</sub>S (or Na<sub>2</sub>Se for the production of CdSe, and so forth). These solutions are mixed together and nanoparticles form as the different micelles exchange their contents. Alternatively, the sulfide can be introduced as H<sub>2</sub>S gas. After the particles are formed, they may be stabilized by the addition of a thiol, which bonds to the surface of the nanoparticles and may also contain other functionalities if a mixture of thiols is used, nanoparticles with a mixture of surface groups are produced<sup>56,58</sup>. The particles may be isolated after disrupting the micelles (provided that this has not already taken place in the stabilization step). The synthesis of CdS nanoparticles gives a highly monodisperse product but for some other materials, such as PbS, the procedure gives particles with a much wider size distribution. Several metal-sulfide nanoparticles have also been synthesized by a similar route involving a polymer (rather than micellar) stabilizer<sup>66</sup>, and related cadmium compounds have been synthesized from organometallic reagents<sup>67</sup>. Other semiconductor nanoparticles of interest include gallium nitride<sup>68,69</sup> and titania; nanoparticles of the latter can be synthesized either by precipitation<sup>70</sup> or in micelles<sup>71</sup>.

### 1.2.3. Other techniques for nanoparticle synthesis

Smaller nanoparticles may be formed in the gas phase<sup>72,73</sup>, or by ablation using high peak-power laser pulses<sup>74,75</sup>, while others have been etched<sup>76,77</sup>, electrodeposited<sup>78</sup>, or synthesized directly onto surfaces<sup>79,80</sup>, or in Langmuir-Blodgett (LB) layers<sup>81</sup>. These techniques cater for the specialized needs of researchers who

require colloids of particular sizes, shapes, or materials. For the cheap and easy synthesis of simple nanoparticles, there is no substitute for solution-state synthesis, which can be used to prepare bulk quantities without the need for specialized laboratory apparatus.

### **1.3. Non-analytical applications of nanoparticles**

Nanoparticles are important in a diverse set of fields, and they can generally be classified as two type i.e. engineered or nonengineered. Engineered nanoparticles are intentionally designed and created with physical properties tailored to meet the need of specific application. They can be end product in and of themselves, as in the case of quantum dots or pharmaceutical drugs, sensor for special purposes, or they can be component later incorporated into separate end products, such as carbon black in rubber products. Either way the particle's physical properties are extremely important to their performance or the performance of any product into which they are ultimately incorporated. Nonengineered nanoparticles, on the other hand, are unintentionally generated nanoparticles, such as atmospheric nanoparticles created during combustion. With nonengineered nanoparticles, physical properties also play importance role as they determine whether or not ill effect will occur as a result of the presence of these particles. For non analytical application nanoparticles based materials have been developed for drug and gene delivery<sup>82</sup>, tissue engineering<sup>83</sup>, tumor destruction<sup>84</sup>, separation and purification of biological molecules and cell<sup>85</sup>, and also - Phagokinetic studies<sup>86</sup>.

#### **1.3.1. Tissue engineering**

Natural bone surface is quite often contains features about 100 nm across. If the surface of an artificial bone implant were left smooth, the body would try to reject it. So production of a fibrous tissue covering the surface of the implant is preferable to get smooth surface. This thin layer will reduce the bone-implant contact, which may result in loosening of the implant and further inflammation. Nano-sized features can help to get smooth surface. It was demonstrated the hip or knee prosthesis which

produced from nano-sized particles could reduce the chances of rejection as well as to stimulate the production of osteoblasts. The osteoblasts are the cells which are responsible for the growth of the bone matrix and are found on the advancing surface of the developing bone. The effect was demonstrated with polymeric, ceramic and, metal materials<sup>87</sup>. More than 90% of the human bone cells from suspension adhered to the nanostructured metal surface<sup>88</sup>. Using nano-sized would allow to design a more durable and longer lasting hip or knee replacements and to reduce the chances of the implant getting loose.

### **1.3.2. Cancer therapy**

Photodynamic cancer therapy is based on the destruction of the cancer cells by laser generated singlet oxygen, which is cytotoxic. A greater quantity of a special dye that to generate the singlet oxygen is taken in by the cancer cells when compared with a healthy tissue. Hence, a given laser radiation to the cell will only destroy the cancer cells. Unfortunately, there is a side effect of this treatment. The remaining dye molecules migrate to the skin and the eyes and make the patient very sensitive to the daylight exposure. This effect can last for up to six weeks. An attempt to avoid this affect was enclosed the dye molecules inside a porous nanoparticles<sup>89</sup>. The dye stayed trapped inside the nanoparticles and did not spread to the other parts of the body. Even though the dye was trapped in the nanoparticles, the ability to generate oxygen was not effected due to the size of pore is about 1 nm which can freely allow the oxygen to diffuse out.

### **1.3.3. Manipulation of cells and biomolecules**

Functionalized magnetic nanoparticles have found many applications including cell separation and probing<sup>90</sup>. Most of the magnetic particles studied so far are spherical, which somewhat limits the possibilities to make these nanoparticles multifunctional. Alternative cylindrically shaped nanoparticles can be created by employing metal electrodeposition into nanoporous alumina template<sup>91</sup>. Depending on the properties of the template, nanocylinder radius can be selected in the range of

5 to 500 nm while their length can be as big as 60  $\mu\text{m}$ . By sequentially depositing various thicknesses of different metals, the structure and the magnetic properties of individual cylinders can be tuned widely. As surface chemistry for functionalisation of metal surfaces is well developed, different ligands can be selectively attached to different segments. For example, porphyrins with thiol or carboxyl linkers were simultaneously attached to the gold or nickel segments respectively. Thus, it is possible to produce magnetic nanowires with spatially segregated fluorescent parts. In addition, because of the large aspect ratios, the residual magnetisation of these nanowires can be high. Hence, weaker magnetic field can be used to drive them. It has been shown that a self-assembly of magnetic nanowires in suspension can be controlled by weak external magnetic fields. This would potentially allow controlling cell assembly in different shapes and forms. Moreover, an external magnetic field can be combined with a lithographically defined magnetic pattern ("magnetic trapping").

### **1.3.4. Commercial exploration**

Some of the companies involved in the development and commercialisation of nanomaterials (Table 1)<sup>92</sup>.

Table 1: Examples of Companies commercialising nanomaterials for bio- and medical applications.

<b>Company</b>	<b>Major area of activity</b>	<b>Technology</b>
Advectus Life Sciences Inc.	Drug delivery	Polymeric nanoparticles engineered to carry antitumour drug across the blood-brain barrier
Alnis Biosciences, Inc.	Bio-pharmaceutical	Biodegradable polymeric nanoparticles for drug delivery

Argonide	Membrane filtration	Nanoporous ceramic materials for endotoxin filtration, orthopaedic and dental implants, DNA and protein separation
BASF	Toothpaste	Hydroxyapatite nanoparticles seems to improve dental surface
Biophan Technologies, Inc.	MRI shielding	Nanomagnetic/carbon composite materials to shield medical devices from RF fields
Capsulation NanoScience AG	Pharmaceutical coatings to improve solubility of drugs	Layer-by-layer poly-electrolyte coatings, 8–50 nm
Dynal Biotech		Magnetic beads
Eiffel Technologies	Drug delivery	Reducing size of the drug particles to 50–100 nm.
EnviroSystems, Inc.	Surface disinfectant	Nanoemulsions
Evident Technologies	Luminescent biomarkers	Semiconductor quantum dots with amine or carboxyl groups on the surface, emission from 350 to 2500 nm
Immunicon	Tracking and separation of different cell types	magnetic core surrounded by a polymeric layer coated with antibodies for capturing cells
KES Science and Technology, Inc.	AiroCide filters	Nano-TiO <sub>2</sub> to destroy airborne pathogens
NanoBio Corporation	Pharmaceutical Antimicrobial	nano-emulsions



NanoCarrier Co., Ltd	Drug delivery	Micellar nanoparticles for encapsulation of drugs, proteins, DNA
NanoPharm AG	Drug delivery	Polybutylcyanoacrylate nanoparticles are coated with drugs and then with surfactant, can go across the blood-brain barrier
Nanoplex Technologies, Inc:	Nanobarcodes for bioanalysis	
Nanoprobes, Inc.	Gold nanoparticles for biological markers	Gold nanoparticles bio-conjugates for TEM and/or fluorescent microscopy
Nanoshpere, Inc.	Gold biomarkers	DNA barcode attached to each nanoprobe for identification purposes, PCR is used to amplify the signal; also catalytic silver deposition to amplify the signal using surface plasmon resonance
NanoMed Pharmaceutical, Inc.	Drug delivery	Nanoparticles for drug delivery
Oxonica Ltd	Sunscreens	Doped transparent nanoparticles to effectively absorb harmful UV and convert it into heat
PSiVida Ltd	Tissue engineering, implants, drugs and gene delivery, bio-filtration	Exploiting material properties of nanostructured porous silicone

Smith & Nephew	Acticoat bandages	Nanocrystal silver is highly toxic to pathogenes
QuantumDot Corporation	Luminescent biomarkers	Bioconjugated semiconductor quantum dots

#### **1.4. Analytical applications of nanoparticles**

The unique physical and chemical properties of nanostructured materials provide excellent prospects for interfacing biological recognition events with electronic signal transduction and for designing a new generation of bioelectronic devices with novel functions. Especially, Au nanoparticles (AuNPs) represent excellent biocompatibility and display unique structural, electronic, magnetic, optical and catalytic properties which have made them a very attractive material for biosensor, chemisensor and electrocatalyst<sup>93-95</sup>.

##### **1.4.1. Enzymatic biosensor based on gold nanoparticles**

The direct electron transfer (DET) from redox-protein to the electrode surface is a very important subject in bioelectrochemistry to understand the mechanism of many bioelectrochemical reactions and construct the biochemical sensors. Therefore, many scientists have devoted their efforts to realize the direct electrochemistry of proteins. An extremely important challenge in the direct electrochemistry of proteins is the establishment of satisfactory electrical communication between the active site of the enzyme and the electrode surface<sup>96,97</sup>. However, the redox center of most oxidoreductase is electrically insulated by a protein shell. Because of this shell, the protein cannot be oxidized or reduced at an electrode at any potential. In order to achieve this task, mediator (discrete, electroactive intermediaries between electrodes and solution couples) have been utilized. More recently, it is interesting to find that the DET of some redox-proteins can also take place with the help of nanoparticles without need of additional mediators. Modification of electrode surfaces with the AuNPs will provide a microenvironment similar to that of the redox-proteins in native

systems and gives the protein molecules more freedom in orientation, thereby reducing the insulating effect of the protein shell for the DET through the conducting tunnels of AuNPs. In 1996, Natan and co-workers<sup>98</sup> have reported a reversible electrochemistry of horse heart cytochrome *c* at SnO<sub>2</sub> electrodes modified with 12 nm-diameter AuNPs. Since then, a great deal of literatures have been reported to complete the DET of redox-proteins using AuNPs as promoter.

When nanoparticle/protein conjugates are assembled on the electrode via simple self-assembly technology, the third generation nanoparticles-based biosensors can be facilely fabricated. Dong's group<sup>99</sup> has developed a novel method to construct a third-generation horseradish peroxidase biosensor by self-assembling AuNPs into three-dimensional sol-gel network. Fig. 1.4 shows the stepwise preparation process of the biosensor. First, a clean gold electrode was modified with three-dimensional matrix by treatment with hydrolyzed (3-mercaptopropyl)-trimethoxysilane (MPS), then AuNPs were infiltrated into the matrix by forming Au-S covalent linkage. Finally horseradish peroxidase was introduced into the electrode surface by electrostatic attraction between negatively charged AuNPs and positively charged horseradish peroxidase.

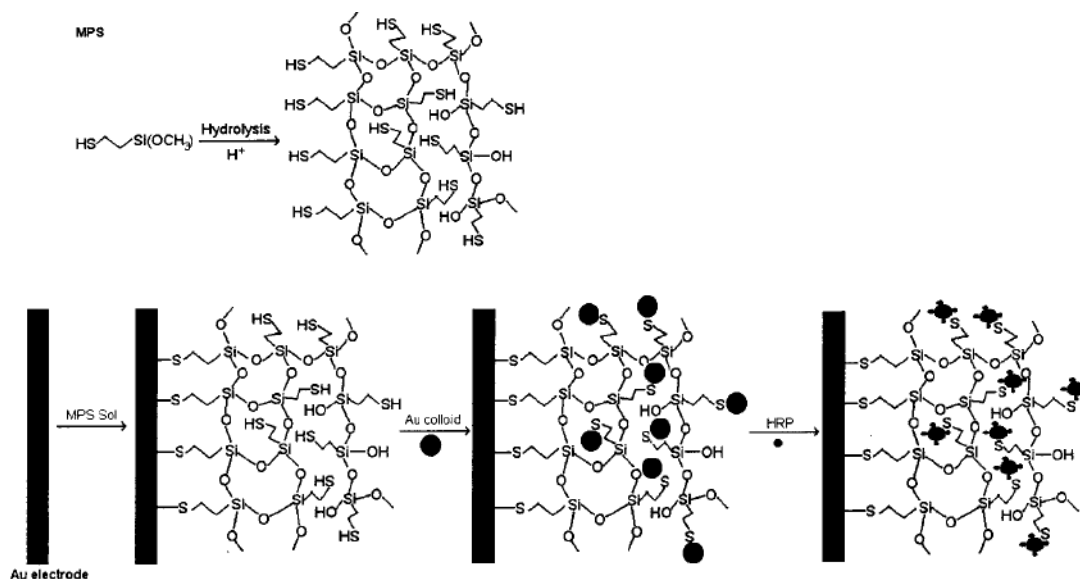


Fig. 1.4 Hydrolysis of MPS (A) and the stepwise biosensor fabrication process (B)<sup>99</sup>.

This biosensor could be fabricated reproducibly, exhibiting fast amperometric responses (2.5 s) to H<sub>2</sub>O<sub>2</sub>, high sensitivity and long-term stability. The detection limit of the biosensor could attain 2.0 μM, and the linear range was between 5.0 μM and 10.0 mM. Another group<sup>100</sup> has also completed direct electrochemistry of cytochrome c on a novel electrochemical interface constructed by self-assembling AuNPs onto a three-dimensional silica gel network. In addition, some thiols with specific functions could also be assembled on the electrode surface. Thus, AuNPs could be immobilized on the self-assembly monolayer surface and complete the DET of some redox-proteins. For instance, Gu et al have reported the DET of hemoglobin on the citrated-capped AuNPs assembled on a cysteamine modified gold substrate<sup>101</sup>. Furthermore, they investigated the electrocatalytic activity of nanoparticle/hemoglobin electrode towards H<sub>2</sub>O<sub>2</sub> reduction. As a result, a stable nanoparticle biosensor was constructed. In addition, the DET of glucose oxidase and horseradish peroxidase was well demonstrated by Pingarron and co-workers<sup>96</sup> and Chen<sup>102</sup> on AuNPs immobilized cysteamine modified gold electrode.

The AuNPs modified carbon paste electrodes have provided a good microenvironment for completing the DET of different redox-proteins. For instance, Ju and co-worker<sup>103</sup> [95] reported that the DET between immobilized myoglobin and colloidal gold modified carbon paste electrode was completed. The myoglobin immobilized on the colloidal AuNPs displayed a pair of redox peaks in 0.1M pH 7.0 PBS with a formal potential of about -0.108V (versus NHE). Furthermore, the preparation of a xanthine oxidase biosensor, based on a carbon paste electrode modified with electrodeposited AuNPs, for the amperometric determination of hypoxanthine was reported by Pingarron group<sup>104</sup>. Our group synthesized a kind of gold nanoparticle protected by a synthetic lipid (DDAB). With the help of these AuNPs, hemoglobin could exhibit a DET reaction on DDAB protected AuNPs modified glassy carbon electrode<sup>105</sup>. In addition, the AuNPs modified ITO and screen-printed rhodium-graphite electrodes could be also developed to complete the DET of some redox-protein such as myoglobin<sup>106</sup> and cytochrome P450sc<sup>107</sup>.

Recently, layer-by-layer (LbL) assembly technique based on electrostatic interaction<sup>108,109</sup> was suggested to be used to tailor the electrochemical interface for completing the DET of some redox-proteins and constructing novel electrochemical

biosensors. For instance, Hoshi et al.<sup>110</sup> prepared multilayer membranes by the LBL deposition of glucose oxidase and AuNPs on sensor substrates, such as a Pt electrode and a quartz glass plate, to prepare glucose sensors. Sun et al.<sup>111</sup> reported a feasible approach to construct multilayer films of glucose oxidase/ AuNPs on the Au electrode surface using a cysteamine as a covalent attachment cross-linker. The biosensor constructed with six bilayers of GOD/AuNPs showed a wide linear response to glucose in the range of 10  $\mu\text{M}$  – 0.013 M, with a fast response less than 4 s, high sensitivity of  $5.72 \mu\text{A}\text{mM}^{-1} \text{cm}^{-2}$ , as well as good stability and long-term life.

It is well-known that the polymer–nanoparticles composites possess the interesting electrical, optical and magnetic properties superior to those of the parent polymer and nanoparticles. The nanocomposite composed of AuNPs and biopolymer such as chitosan and carboxymethyl chitosan was also employed as excellent matrix for completing the DET of some redox protein and fabricating novel biosensor<sup>112,113</sup>. For instance, Chen's group<sup>113</sup> demonstrated a novel biocomposite made of chitosan hydrogel, glucose oxidase, and AuNPs by a direct and facile electrochemical deposition method under enzyme-friendly conditions for glucose biosensor. The biocomposite provided a shelter for the enzyme to retain its bioactivity at considerably extreme conditions, and the decorated AuNPs in the biocomposite offered excellent affinity to enzyme. The biosensor exhibited a rapid response (within 7 s) and a linear calibration range from 5.0  $\mu\text{M}$  to 2.4 mM with a detection limit of 2.7  $\mu\text{M}$  for the detection of glucose. Later, Zhu and co-workers<sup>114</sup> reported the DET of horseradish peroxidase based on biocompatible carboxymethyl chitosan–AuNPs nanocomposite. A novel biosensor for  $\text{H}_2\text{O}_2$  was constructed based on the above nanocomposite. The biosensor exhibited a fast amperometric response (5 s), a good wide linear range of concentrations from  $5.0 \times 10^{-6}$  to  $1.4 \times 10^{-3}$  M, and a low detection limit of  $4.01 \times 10^{-7}$  M. Furthermore, Indium tin oxide (ITO) electrode<sup>115</sup> could also be used to fabricate a novel disposable biosensor based on enzyme immobilized on Au-chitosan nanocomposite combined with flow injection analysis for the rapid determination of  $\text{H}_2\text{O}_2$ .

### 1.4.2. Application of gold nanoparticles for genosensors

The development of electrical DNA hybridization biosensors has attracted considerable research efforts<sup>116,117</sup>. Such DNA sensing applications require high sensitivity through amplified transduction of the oligonucleotide interaction. Electrochemical devices offer elegant routes for interfacing, at the molecular level, the DNA recognition and signal transduction elements, and are uniquely qualified for meeting the low-cost, low-volume, and power requirements of decentralized DNA diagnostics. The AuNPs modified electrochemical sensing interfaces offer elegant ways for interfacing DNA recognition events with electrochemical signal transduction, and for amplifying the resulting electrical response. AuNPs-based amplification schemes reported have led to improved sensitivity of bioelectronic assays by several orders of magnitude. Thus, AuNPs-based electrochemical device will provide new opportunity for gene diagnostics in the future.

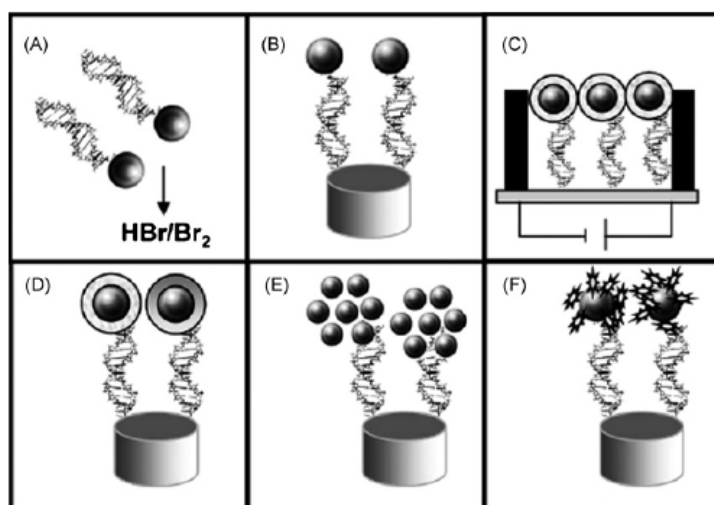


Fig. 1.5 Schematic procedure of the different strategies used for the integration of AuNPs into DNA sensing systems: (A) previous dissolving of AuNPs by using HBr/Br<sub>2</sub> mixture followed by Au(III) ions detection, (B) direct detection of AuNPs anchored onto the surface of the genosensor, (C) conductometric detection, (D) enhancement with silver or gold followed by detection, (E) AuNPs as carriers of other AuNPs, (F) AuNPs as carriers of other electroactive labels<sup>118</sup>.

Merkoci and co-workers reviewed<sup>118</sup> recent important achievements on the electrochemical sensing of DNA using AuNPs. In that review, the author discussed recent some novel strategies for genosensors based on AuNPs. Fig. 1.5 depicted a schematic of the most important strategies used to integrate AuNPs in DNA detection systems. These strategies consist of: (A) the electrochemical detection of AuNPs label by detecting the gold ions released after acidic dissolving; (B) direct detection of AuNPs anchored onto the surface of a conventional genosensor (based on stripping voltammetry); (C) silver enhancement using conductometric technique; (D) enhancement of AuNPs anchored to conventional genosensor surface by using silver or gold; (E) AuNPs as carriers of other AuNPs; (F) using AuNPs as carriers for other electroactive labels.

In 2001 both Wang's group<sup>119</sup> and that of Limoges<sup>120</sup> reported on the use of colloidal gold tags for electronic detection of DNA hybridization. This protocol relied on capturing the AuNPs to the hybridized target, followed by highly sensitive anodic stripping electrochemical measurement of the metal tracer. This approach could attain a detection limit in the picomolar range. In addition, the electrochemical genosensors based on AuNPs labels could be amplified by the catalytic electrodeposition of silver and its subsequent stripping. A better detection limit was reported when a silver enhancement method was employed, based on the precipitation of silver on AuNPs tags and its dissolution (in HNO<sub>3</sub>) and subsequent electrochemical potentiometric stripping detection<sup>121,122</sup>. This method was reported to obtain a detection limit in the femtomolar range.

Because the HBr/Br<sub>2</sub> solution is highly toxic and therefore methods based on direct electrochemical detection of AuNPs tags, which replace the chemical oxidation agent, have been also reported recently. For instance, Merkoci and co-workers reported a novel AuNPs-based protocol for detection of DNA hybridization based on a magnetically triggered direct electrochemical detection of gold quantum dot tracers. It relied on binding target DNA with Au<sub>67</sub> quantum dot in a ratio 1:1, followed by a genomagnetic hybridization assay between Au<sub>67</sub>-DNA and complementary probe DNA marked paramagnetic beads. Differential pulse voltammetry was used for a direct voltammetric detection of resulting Au<sub>67</sub> quantum dot-target DNA/complementary DNA-paramagnetic bead conjugate on magnetic graphite-epoxy

composite electrode. This method could attain a low detection limit in the nanomolar range<sup>123</sup>.

Enhancements by precipitation of silver or gold onto the AuNPs labels have been reported so as to achieve amplified signals and lower detection limits<sup>124</sup>. For instance, Fang's group demonstrated an electrochemical detection method for analyzing sequence-specific DNA using AuNPs marked DNA probes and subsequent signal amplification step by silver enhancement. The assay relied on the electrostatic adsorption of target oligonucleotides onto the sensing surface of the glassy carbon electrode (GCE) and its hybridization to the AuNPs-labeled oligonucleotides DNA probe. After silver deposition onto AuNPs, binding events between probe and target were monitored by the differential pulse voltammetry signal of the large number of silver atoms anchored on the hybrids at the electrode surface. A detection limit of 50 pM of complementary oligonucleotides was obtained based on this novel approach. In addition to silver enhanced technology, Rochelet-Dequaire et al.<sup>125</sup> developed a new efficient protocol for the sensitive quantification of a 35 base-pair human cytomegalovirus nucleic acid target (tDNA). In this assay, the hybridization of the target adsorbed on the bottom of microwells with an oligonucleotide modified AuNPs detection probe (pDNA-Au) was monitored by the anodic stripping detection of the chemically oxidized gold label at a screen-printed microband electrode (SPMBE). Thanks to the combination of the sensitive Au<sup>III</sup> determination at a SPMBE with the large amount of Au<sup>III</sup> released from each pDNA-Au, the picomolar detection limits of tDNA could be achieved. Further enhancement of the hybridization signal based on the autocatalytic reductive deposition of ionic gold (Au<sup>III</sup>) on the surface of the AuNPs labels anchored on the hybrids was first envisaged by incubating the commonly used mixture of Au<sup>III</sup> and hydroxylamine. This strategy, which led to an efficient increase of the hybridization response, allowed detection of tDNA concentrations as low as 600 aM (i.e. 10<sup>4</sup> lower than that without amplification).

Another signal amplification strategy is to attach electroactive ferrocenylhexanethiol molecules or electrogenerated chemiluminescence (ECL) indicator to the AuNPs labels. Zhou's group [126] reported that AuNPs/streptavidin conjugates covered with 6-ferrocenylhexanethiol were attached onto a biotinylated DNA detection probe of a sandwich DNA complex. Due to the elasticity of the DNA



strands, the ferrocene caps on AuNPs/streptavidin conjugates were positioned in close proximity to the underlying electrode modified with a mixed DNA capture probe/hexanethiol self-assembled monolayer and could undergo reversible electron-transfer reactions. A detection level, down to 2.0 pM for oligodeoxynucleotide samples could be obtained. In addition, a novel sensitive ECL method for the detection DNA hybridization based on AuNPs carrying multiple ECL probes was developed by Zhang and co-workers [129]. A detection limit of  $5.0 \times 10^{-12}$  mol L<sup>-1</sup> for target DNA was achieved<sup>126,127</sup>.

### 1.4.3. Application of gold nanoparticles for immunosensors

Immunosensors are important analytical tools based on the detection of the binding event between antibody and antigen. The recent development of immunoassay techniques focused in most cases on decreasing analysis times, improving assay sensitivity, simplification and automation of the assay procedures, low-volume analysis. Among types of immunosensors, electrochemical immunosensors are attractive tools and have received considerable attention because they are easy and economical to mass production, they are robust, and they achieve excellent detection limits with small analyte volumes. Furthermore, the availability of a variety of new materials with unique properties at nanoscale dimension, such as AuNPs, has attracted widespread attention in their utilization for the bioassay, especially for electrochemical detection. Recently, several novel strategies have been proposed to develop electrochemical immunosensors with high sensitivity using AuNPs<sup>128,129</sup>.

A novel and sensitive electrochemical immunoassay for immunoglobulin G (IgG) has been developed by Limoges and co-workers<sup>130</sup> using a colloidal gold label via anodic stripping voltammetry technology. A low detection limit (concentration as low as  $3 \times 10^{-12}$  M) could be obtained, which was competitive with colorimetric enzyme linked immuno-sorbent assay or with immunoassays based on fluorescent europium chelate labels. Furthermore, Shen's group<sup>131</sup> reported a novel electrochemical immunoassay based on the precipitation of silver on colloidal gold labels. After metal silver dissolution in an acidic solution, the signal was indirectly

determined by anodic stripping voltammetry at a glassy carbon electrode. A detection limit as low as  $1 \text{ ng mL}^{-1}$  human IgG was achieved. The enhancement in sensitivity for an electrochemical immunoassay by the autocatalytic deposition of  $\text{Au}^{3+}$  onto AuNPs has been studied by Huang's group<sup>132</sup>. By coupling the autocatalytic deposition with square-wave stripping voltammetry, the rabbit immunoglobulin G analyte could be determined quantitatively. A very low detection limit,  $0.25 \text{ pg mL}^{-1}$  ( $1.6 \text{ fM}$ ) was obtained, which is three orders of magnitude lower than that obtained by a conventional immunoassay using the same AuNPs labels.

Novel enzyme-labeled electrochemical immunosensors were well developed by several groups. For instance, Ju's group<sup>133</sup> reported that a highly hydrophilic and conductive colloidal AuNPs/titania sol-gel composite membrane could be employed as electrochemical sensing interface for horseradish peroxidase-labeled electrochemical immunosensor. Later, a novel electrochemical immunosensor for human chorionic gonadotrophin (hCG) was developed by the same group<sup>134</sup> via the immobilization of hCG on AuNPs doped three-dimensional (3D) sol-gel matrix. The 3D organized composite structure was prepared by assembling AuNPs into a hydrolyzed (3-mercaptopropyl)-trimethoxysilane sol-gel matrix, which showed good biocompatibility. After the interfacial competitive immunoreaction, the formed HRP-labeled immunoconjugate showed good enzymatic activity for the oxidation of o-phenylenediamine by  $\text{H}_2\text{O}_2$ . The immunosensor showed good precision, high sensitivity, acceptable stability and reproducibility.

Label-free electrochemical immunosensors using AuNPs as enhancing sensing component have been the focus of intense research due to their simplicity, speedy analysis and high sensitivity. The technique is mainly based on the detection of a change in physical properties as a result of antibody-antigen complex formation. The direct determination of immunospecies by detecting the change of impedance caused by immunoreactions has been demonstrated. A simple and sensitive label-free electrochemical immunoassay electrode for detection of carcinoembryonic antigen (CEA) has been developed by Yao's group. CEA antibody (CEAAb) was covalently attached on glutathione (GSH) monolayer-modified AuNPs and the resulting CEAAb-AuNPs bioconjugates were immobilized on Au electrode by electrocopolymerization with o-aminophenol (OAP). Electrochemical impedance

spectroscopy studies demonstrated that the formation CEA antibody–antigen complexes increased the electron-transfer resistance of  $[\text{Fe}(\text{CN})_6]^{3-/4-}$  redox pair at the poly-OAP/CEAAb-AuNPs/Au electrode. The immunosensor could detect the CEA with a detection limit of  $0.1 \text{ ng mL}^{-1}$  and a linear range of  $0.5\text{--}20 \text{ ng mL}^{-1}$ .<sup>135,136</sup>

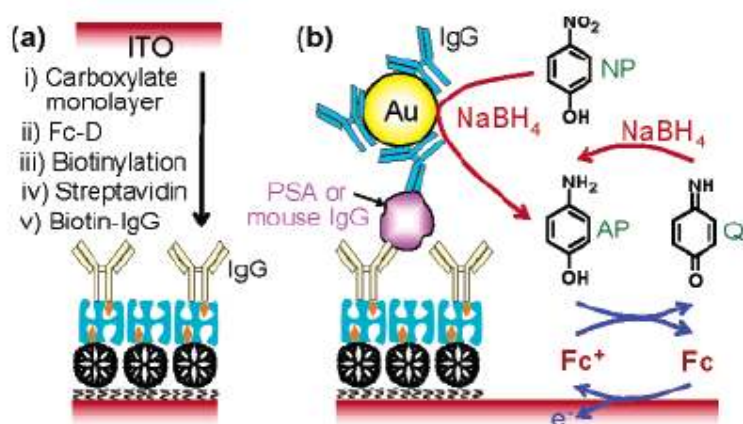


Fig. 1.6 (a) Schematic representation of the preparation of an immunosensing layer. (b) Schematic view of electrochemical detection of mouse IgG or PSA<sup>137</sup>.

DNA-free ultrasensitive electrochemical immunosensors have received considerable interests because of their advantage including simplify, rapidness and high sensitivity. Yang's group<sup>137</sup> developed an ultrasensitive and simple electrochemical method for the fabrication of a sandwich-type heterogeneous electrochemical immunosensor. Fig. 1.6 shows a typical fabrication procedure of DNA-free electrochemical immunosensor. An IgG layer was formed on an ITO electrode via a stepwise assembly process (Fig. 1.6a). First, partially ferrocenyltethered dendrimer (Fc-D) was immobilized to the ITO electrode by covalent bonding between dendrimer amines and carboxylic acids of a phosphonate self-assembled monolayer. Some of the unreacted amines of Fc-D were modified with biotin groups to allow the specific binding of streptavidin. Afterward, biotinylated antibodies were immobilized to the streptavidin-modified ITO electrode. An IgG-nanocatalyst conjugate was prepared via direct adsorption of IgG on 10 nm AuNPs. Mouse IgG or prostate specific antigen was chosen as a target protein (Fig. 1.6b).

The IgG-nanocatalyst conjugate and the immunosensing layer sandwiched the target protein. Signal amplification was achieved by catalytic reduction of p-nitrophenol (NP) to p-aminophenol (AP) using gold nanocatalyst labels and the chemical reduction of p-quinone imine (QI) by NaBH<sub>4</sub>. This novel DNA-free method could attain a very low detection limit (1 fg mL<sup>-1</sup>).

### **1.4.4. Application of gold nanoparticles for electrocatalytic chemosensors**

Nanometer-sized AuNPs exhibiting excellent catalytic activity have received considerable attention due to their relative high surface area-to-volume ratio, and their interface-dominated properties, which significantly differ from their bulk counterparts. Thus, interest in the catalytic properties of AuNPs has increased rapidly. In particular, AuNPs have been studied extensively for the design and fabrication of electrocatalysts and using as an enhancing component of catalytic activity or selectivity. The large surface-to-volume ratios and active sites of AuNPs constitute part of the driving force in developing nanosized electrocatalysts. Various methodologies have been used for the tailoring of AuNPs on electrode surfaces for electrocatalytic applications, which include the anchoring by electrostatic interaction, covalent linkage, and electrochemical deposition, etc. Thus AuNPs modified electrochemical interface behaving as nanoelectrode ensembles have been widely used as enhancing catalytic interface for the development of electrochemical sensors. In principle, the electroanalytical detection limit at a nanoelectrode ensemble can be much lower than that at an analogous macrosized electrode because the ratio between the faradaic and capacitive currents is higher<sup>138</sup>. Several groups<sup>139,140</sup> have been interested in the development of novel 2-D or 3-D AuNPs modified nanoelectrode ensembles for enhancing electrochemical responses.

AuNPs could also be employed as enhancing materials for electrochemical investigation of cell<sup>141</sup> and electrocatalyzing some small biomolecules such as glucose<sup>142</sup>, norepinephrine<sup>143</sup>, dopamine<sup>144</sup>, catechol<sup>145</sup>, epinephrine<sup>146</sup> and ascorbic acid<sup>147</sup>, etc. For instance, Raj and co-worker<sup>148</sup> reported a nonenzymatic electrochemical method for the detection of glucose by using AuNPs self-assembled

on a 3D silicate network obtained by using sol–gel processes. The nanosized Au particles have been self-assembled on the thiol tail groups of the silicate network and enlarged by hydroxylamine. The AuNPs efficiently catalyzed the oxidation of glucose at less-positive potential (0.16 V) in phosphate buffer solution (pH 9.2) in the absence of any enzymes or redox mediators. This novel nonenzymatic glucose sensor showed excellent sensitivity with a detection limit of 50 nM.

In addition to enhancing detection of small biomolecules, AuNPs derivated electrodes were also used to detect some toxic substances<sup>149-151</sup>. AuNPs modified carbon screen-printed, glassy carbon and basal plane pyrolytic graphite electrodes have been reported to detect Sb (III)<sup>149</sup> and As (III)<sup>150,151</sup> with high sensitivity. The electrolytic oxidation of nitric oxide and hydrazine was also developed by several groups<sup>152-155</sup>. It is found that the AuNPs modified electrode exhibited high catalytic activity for NO and hydrazine. For instance, Raj and co-worker<sup>155</sup> reported an ultrasensitive electrochemical detection of hydrazine using AuNPs self-assembled on a sol–gel-derived 3D silicate network, followed by seed-mediated growth of gold. This nanostructured platform was highly sensitive toward the electrochemical oxidation of hydrazine. A very large decrease in the overpotential (800 mV) and significant enhancement in the peak currents with respect to the bulk Au electrode were observed without using any redox mediator. The nanostructured platform showed excellent sensitivity with an experimental detection limit of 200 pM.

### **1.4.5. Multicolor optical coding for biological assays**

Increasing research in proteomics and genomic generates escalating number of sequence data and requires development of high throughput screening technologies. Various array technologies has been used in parallel analysis are likely to reach saturation when a number of array elements exceed several millions. A three-dimensional approach, based on optical "bar coding" of polymer particles in solution, is limited only by the number of unique tags one can reliably produce and detect. Single quantum dots of compound semiconductors were successfully used as a replacement of organic dyes in various bio-tagging applications<sup>156</sup>. By combining differently sized and having different fluorescent colors quantum dots, and also

combining them in polymeric microbeads will give further advantages<sup>157</sup>. A precise control of quantum dot ratios has been achieved. The selection of nanoparticles used in those experiments had 6 different colours as well as 10 intensities. It is enough to encode over 1 million combinations. The uniformity and reproducibility of beads was high letting for the bead identification accuracies of 99.99%.

### **1.4.6 Application of nanoparticles for signal amplification**

#### ***a. Silver nanoparticles enhance Local Plasmon Resonance signals***

Triangular silver nanoparticles (~100 nm wide and 50 nm high) have remarkable optical properties. In particular, the peak extinction wavelength,  $\lambda_{\max}$  of their localized surface plasmon resonance (LSPR) spectrum is unexpectedly sensitive to nanoparticle size, shape, and local (~10-30 nm) external dielectric environment. This sensitivity of the LSPR  $\lambda_{\max}$  to the nanoenvironment has allowed us to develop a new class of nanoscale affinity biosensors. The essential characteristics and operational principles of these LSPR nanobiosensors will be illustrated using the well-studied biotin-streptavidin system. Exposure of biotin-functionalized Ag nanotriangles to 100 nM streptavidin (SA) caused a 27.0 nm red-shift in the LSPR  $\lambda_{\max}$ . The LSPR  $\lambda_{\max}$  shift,  $\Delta R/\Delta R_{\max}$ , versus [SA] response curve was measured over the concentration range  $10^{-15} \text{ M} < [\text{SA}] < 10^{-6} \text{ M}$ . Comparison of the data with the theoretical normalized response expected for 1:1 binding of a ligand to a multivalent receptor with different sites but invariant affinities yielded approximate values for the saturation response,  $\Delta R_{\max} = 26.5 \text{ nm}$ , and the surface-confined thermodynamic binding constant  $K_{a,\text{surf}} = 10^{11} \text{ M}^{-1}$ . At present, the limit of detection (LOD) for the LSPR nanobiosensor is found to be in the low-picomolar to high-femtomolar region. A strategy to amplify the response of the LSPR nanobiosensor using biotinylated Au colloids and thereby further improve the LOD is demonstrated. Several control experiments were performed to define the LSPR nanobiosensor's response to nonspecific binding as well as to demonstrate its response to the specific binding of another protein. These include the following: (1) electrostatic binding of SA to a nonbiotinylated surface, (2) nonspecific interactions of prebiotinylated SA to a biotinylated surface, (3) nonspecific interactions of bovine

serum albumin to a biotinylated surface, and (4) specific binding of anti-biotin to a biotinylated surface. The LSPR nanobiosensor provides a pathway to ultrasensitive biodetection experiments with extremely simple, small, light, robust, low-cost instrumentation that will greatly facilitate field-portable environmental or point-of-service medical diagnostic applications<sup>158</sup>.

### ***b. Gold nanoparticles enhance the signal of Quartz Crystal Microbalance***

Amanda and Coworker report a novel strategy for the high-sensitive detection of target biomolecules with very low concentrations on a quartz crystal microbalance (QCM) device using gold nanoparticles as signal enhancement probes. By employing a streptavidin–biotin interaction as a model system, we could prepare biotin-conjugated gold nanoparticles maintaining good dispersion and long-term stability by controlling the biotin density on the surface of gold nanoparticles that have been investigated by UV-vis spectra and AFM images. These results showed that 10  $\mu\text{M}$  *N*-(6-[biotinamido]hexyl)-3'-(2'-pyridyldithio)propionamide (biotin-HPDP) was the critical concentration to prevent the nonspecific aggregation of gold nanoparticles in this system. For sensing streptavidin target molecules by QCM, biotinylated BSA was absorbed on the Au surface of the QCM electrode and subsequent coupling of the target streptavidin to the biotin in the sensing interface followed. Amplification of the sensing process was performed by the interaction of the target streptavidin on the sensing surface with gold nanoparticles modified with 10  $\mu\text{M}$  biotin-HPDP. The biotinylated gold nanoparticles were used as signal amplification probes to improve the detection limit, which was 50 ng/ml, of the streptavidin detection system without signal enhancement, and the calibration curve determined for the net frequency changes showed good linearity over a wide range from 1 ng/ml to 10  $\mu\text{g/ml}$  for the quantitative streptavidin target molecule analysis. In addition, the measured dissipation changes suggested that the layer of biotin-BSA adsorbed on the Au electrode and the streptavidin layer assembled on the biotin-BSA surface were highly compact and rigid. On the other hand, the structure formed by the biotinylated gold nanoparticles on the streptavidin layer was flexible and dissipative, being elongated outward from the sensing surface<sup>159</sup>.

### ***c. Nanoparticles enhance the Florescence***

Methodologies for glucose sensing based on the specific biological interactions between Con A, dextran-coated gold nanoparticles and glucose, and the interactions between dextran, glucose, and boronic-acid capped silver nanoparticles in solution have been developed. The new approaches promise new tunable glucose sensing platforms. Dextran-coated gold nanoparticles were aggregated with the addition of Con A resulting in increase an in absorbance of nanoparticles at 650 nm, where the post-addition of glucose caused the dissociation of the aggregates and thus a decrease in the absorbance at 650 nm. The interaction of glucose and dextran with boronic acid-capped silver nanoparticles in solution resulted in enhanced luminescence intensity cumulatively due to surface enhanced fluorescence and the decrease in absorbance at 400 nm, with an increase in absorbance at 640 nm. Lifetime measurements were used to distinguish the contribution from the surface-enhanced fluorescence. TEM was employed to assess the aggregation of nanoparticles. An enhancement of signal of fluorescence by specific shape, e.g gold rod and silver triangle of nanoparticles also observed<sup>160-162</sup>.

### **1.5. Objective of the work**

The main objectives of the work were screening of new bioanalytical application of metallic nanoparticles including electrocatalysis, localized plasmon resonance, accelerating of protein crystallization. The main attention was paid to gold nanoparticles. A part of the work was performed for industrial partner, this work included development of irreversible freezing indicator based on gold nanoparticles as well as an optimization of the indicator performance and a development of continuous synthesis of nanoparticles which can be scaled up easily. This experience was then used for development of automated Layer-by-Layer deposition of conductive polymers. Main scientific goals of the work were:

- optimization of a procedure for deposition of gold nanoparticles / polymer composites on the electrode surface;



- investigation of electrocatalytical activity of electrodes modified by gold nanoparticles to biologically important substances (glucose, dopamine) and of possibility to develop non-enzymatic sensor for these compounds;
- investigation of nucleation of proteins in the presence of gold nanoparticles.

## 2. EXPERIMENTAL

### 2.1. Reagents and Materials

#### *Reagents*

All chemicals and solvents used were purchased from Aldrich (Steinheim, Germany), Fluka (Buchs, Switzerland), Chempur (Karlsruhe) or Merck (Darmstadt, Germany). All chemical were utilized without further purification. All chemicals were of analytical grade unless otherwise stated. Dialysis tubes with a molecular weight cutoff of 12,000–14,000 were from Carl Roth. All experiments, if not specified, were carried out at room temperature ( $22\pm 2^\circ\text{C}$ ). All experiment used Millipore water.

#### *Buffers*

The following table outlines the buffers used in this work (Table 2.1). All buffers were prepared with MILLIPORE water. The pH was adjusted with 0.1 M and 1 M HCl or 0.1 M and 1 M NaOH when necessary.

Table 2.1 Buffer Solutions

Buffer	Composition	pH	Experiment
A	5,8362 gr $\text{NaH}_2\text{PO}_4$ 15,466 gr $\text{Na}_2\text{HPO}_4$ Dilute until 1 Liter	7	Determination of dopamine
B	4,0280 gr $\text{CH}_3\text{COONa}$ 9,7534 ml $\text{CH}_3\text{COOH}$ Dilute until 1 Liter	4	Determination of dopamine

The concentration of phosphate ion in Buffer A is 0,1 M and the concentration of acetate ion in buffer B is 0,2 M.

## ***Electrodes***

Thin film gold electrodes on glass or silicon support were formed by photolithography. The thickness of metal layer is about 250 nm; the electrode area is 0.38 mm<sup>2</sup>. Before use, the electrodes were cleaned by pure water, ethanol, acetone and chloroform consecutively. After dried, rinsed thoroughly with pure water and dried in the nitrogen gas flow.

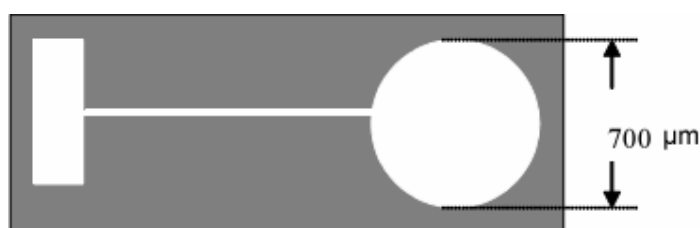


Fig. 2.1 Thin film of gold electrode on the silicon support.

## **2.2. Methods of Characterization.**

### **2.2.1. Cyclic Voltammetry**

Cyclic Voltammetry provides qualitative information chemical reactions. The information about an analyte is obtained by current measuring when the potential is varied. The power of cyclic voltammetry results from the ability to provide information on the thermodynamics of redox processes, on kinetics of heterogeneous electron transfer reaction, and on coupled chemical reactions or adsorption processes. Cyclic voltammetry is often the first experiment to be performed in an electroanalytical study.

In particular, it offers a rapid analysis of redox potentials of the electroactive species, as well as convenient evaluation of the effect of media upon the redox process.

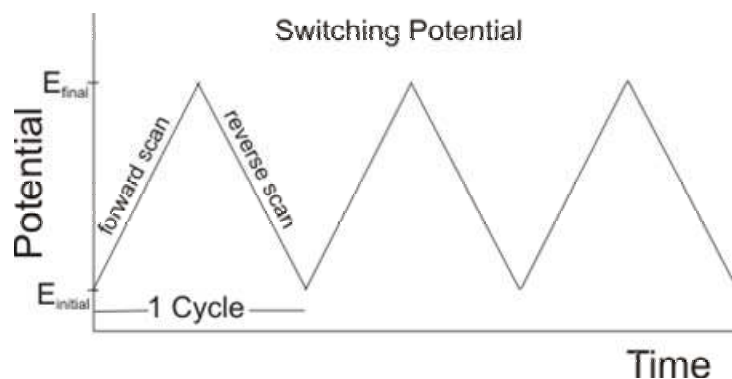


Fig. 2.2 Potential-time excitation signal in cyclic voltammetry experiment.

Cyclic voltammetry consists of linear scanning of the potential of working electrode using a triangular potential waveform (Fig. 2.2). Depending on the information sought, single or multiple cycles can be used. During the potential sweep, the potentiostat measures the current resulting from the applied potential. The resulting plot of current versus potential is termed a cyclic voltammogram. The cyclic voltammogram is a complicated time-dependent function of a large number of physical and chemical parameters.

Fig 2.3 illustrates the response of a reversible redox couple during a single potential cycle (in an unstirred solution). It is assumed that only the oxidized form O is present initially. Thus, a negative-going potential scan is chosen for the first half-cycle, starting from a value where no reduction occurred. As the applied potential approaches the characteristic  $E^{\circ}$  for the redox process, a cathodic current begins to increase, until a peak is reached. The sweep is reversed after traversing the potential region where the reduction process takes place (a least  $90/n$  mV beyond the peak). During the reverse scan, R molecules are reoxidized back to O and it results in an anodic peak.

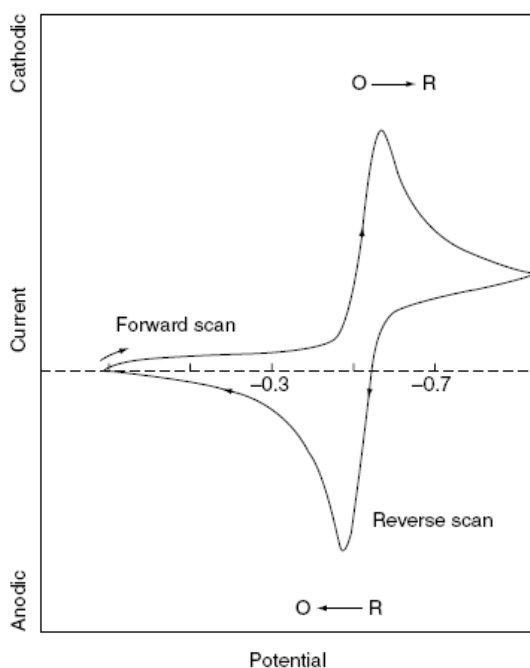


Fig. 2.3 Typical cyclic voltammogram for a reversible  $O + ne^- \rightleftharpoons R$  redox process

Formation of the diffusion layers near electrode surface layer gives the characteristic peaks in the cyclic voltammogram. These can be understood by examining the concentration-distance profiles during the potential sweep. Fig 2.4 illustrates for gradients of concentration for the reactant and product at different times. (a) the initial potential value, (b) and (d) the formal potential of the couple during the forward and reversed scans respectively, and (c) to the achievement of a zero reactant surface concentration. The continuous change in the surface concentration is coupled with an expansion of the diffusion layer thickness. The resulting current peaks reflect the continuous change of concentration gradient with the time. The increase of the peak current corresponds to the achievement of diffusion control, while the current drop (beyond the peak) exhibits a  $t^{-1/2}$  dependence (independent of applied potential). For the above reasons, the reversal current has the same shape as the forward one.

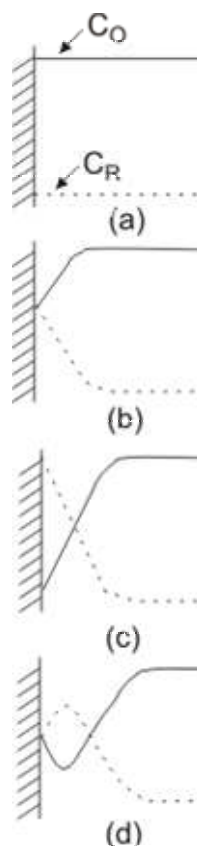


Figure 2.4 Concentration distribution of oxidized and reduced form of redox couple at different times during a cyclic voltammetric experiment corresponding to the initial potential (a), to the formal potential of couple during the forward and reversed scans (b,d) and to the achievement of a zero reactant surface concentration (c)

### ***Data interpretation***

There are several parameters which are important and can be used for characterization of redox reaction in the cyclic voltammogram. Four of these observables, the two peak currents and two peak potentials, provide the basis for diagnostics developed by Nicholson and Shain for analyzing the cyclic voltammetric response.

**Reversible systems**

The peak current for a reversible couple (at 25°C), is given by *Randles-Sevcik* equation

$$i_p = (2.69 \times 10^5) n^{3/2} A C D^{1/2} v^{1/2} \dots\dots\dots 2.1$$

Where *n* is the number of electrons, *A* is electrode area (in cm<sup>2</sup>), *C* is the concentration (in mol cm<sup>-3</sup>), *D* is the diffusion coefficient (in cm<sup>2</sup> s<sup>-1</sup>), and *v* is the scan rate (in V s<sup>-1</sup>). The ratio of the reverse to forward peak current, *I<sub>p,r</sub>/I<sub>p,f</sub>*, is unity for a simple reversible couple but very different when the redox reaction is slow or coupled with a chemical reaction. This peak ratio is strongly affected by chemical reaction coupled to redox process. The current peaks are commonly measured by extrapolating the preceding baseline current.

The position of the peaks on the potential axes (*E<sub>p</sub>*) is related to the formal potential of the redox process. The formal potential for a reversible couple is centered between *E<sub>p,a</sub>* and *E<sub>p,c</sub>*.

$$E^o = \frac{E_{p,a} + E_{p,c}}{2} \dots\dots\dots 2.2$$

The separation between the peak potentials (for a reversible couple) is given by

$$\Delta E_p = E_{p,a} - E_{p,c} = \frac{0,059}{n} V \dots\dots\dots 2.3$$

Thus, the peak separation can be used to determine the number of electrons transferred, and as a criterion for a Nerstian behavior. Accordingly, a fast one electron process exhibits a  $\Delta E_p$  of about 59 mV. Both the cathodic and anodic peak potentials are independent of the scan rate. It is possible to relate the half-peak

potential ( $E_{p/2}$ , where the current is half of the peak current) to the polarographic half-wave potential  $E_{1/2}$  :

$$E_{p/2} = E_{1/2} \pm \frac{0.028}{n} V \dots\dots\dots 2.4$$

(The sign is positive for reduction process)

***Irreversible and quasi-reversible systems.***

For irreversible processes (those with sluggish electron exchange), the individual peaks are reduced in size and widely separated (Fig. 2.5, curve A). Totally irreversible systems are characterized by a shift of the peak potential with the scan rate.

$$E_p = E^\circ - \frac{RT}{\alpha n_a F} \left[ 0.78 - \ln \frac{k^\circ}{D^{1/2}} + \ln \left( \frac{\alpha n_a F v}{RT} \right)^{1/2} \right] \dots\dots\dots 2.5$$

Where  $\alpha$  is the transfers coefficient and  $n_a$  is the number of electrons involved in the charge-transfer step. Thus,  $E_p$  occurs at potentials higher than  $E^\circ$ , with the overpotential related to  $k^\circ$  and  $\alpha$ . Independent of the value  $k^\circ$ , such as peaks displacement can be compensated by an appropriate change of the scan rate. The peak potential and the half-peak potential (at 25°C) will differ by 48/  $\alpha n$  mV. Hence, the voltammogram becomes more drawn-out as  $\alpha n$  decreases.

The peak current, given by

$$i_p = (2.99 \times 10^5) n (\alpha n_a)^{1/2} A C D^{1/2} v^{1/2} \dots\dots\dots 2.6$$



Is still proportional to the bulk concentration, but will be lower in height (depending upon the value of  $\alpha$ ). Assuming a value of 0.5, the ratio of the reversible to irreversible current peaks is 1.27 (i.e. the peak current for the irreversible process is about 80% of the peak for a reversible one).

For quasi reversible systems (with  $10^{-1} > k^0 > 10^{-5} \text{ cm s}^{-1}$ ) the current is controlled by both the charge transfer and mass transport. The shape of the cyclic voltammogram is a function of  $k^0 / \sqrt{\pi a D}$  (where  $a = nFv/RT$ ). As  $k^0 / \sqrt{\pi a D}$  increases, the process approaches the reversible case. For small values of  $k^0 / \sqrt{\pi a D}$  (i.e., at very fast  $v$ ) the system exhibit an irreversible behavior. Overall, the voltammogram of a quasi-reversible system are more drawn-out and exhibit a larger separation in peak potential compared to those of a reversible system (Fig. 2.5, curve B)

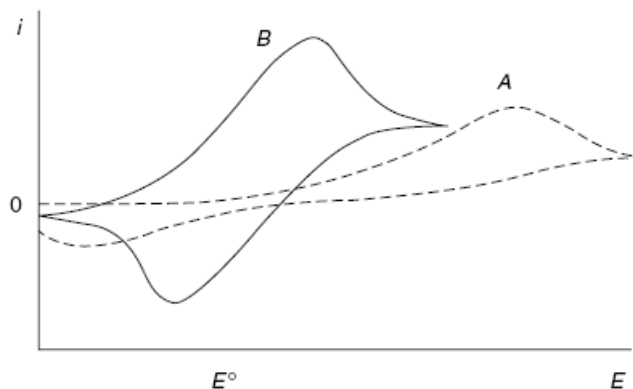


Fig. 2.5 Cyclic voltammogram for irreversible (curve A) and quasi-reversible (curve B) redox processes.

### **Qualitative applications**

Cyclic voltammetry can also be useful for quantitative response, based on measurement of the peak current (equation 2.1). Such quantitative applications require the establishment of proper baseline. For neighboring peaks (of mixture), the

base line for the second peak is obtained by extrapolating the current decay of the first one (in accordance with  $t^{-1/2}$ ). Background reaction, primarily those associated with the double-layer charging and redox-surface processes, limit the detection limit to around the  $1 \times 10^{-5} \text{M}$  level. Background-subtracted cyclic voltammetry can be employed for measuring lower concentration<sup>163</sup>. In particular fast-scan ( $1000 \text{Vs}^{-1}$ ) background-subtracted cyclic voltammetry is seeing increased use for the in-vivo monitoring in neurotransmitters (such as dopamine or serotonin) in the brain. Such coupling of digital background subtraction and fast voltammetric measurements provides the subsecond temporal resolution necessary for detecting dynamic concentration changes in the micromolar range occurring in the extracellular environment of the brain. The good temporal and chemical resolution of such in-vivo cyclic voltammetric experiment offers improved understanding of the chemistry of the brain. These repetitive scanning in-vivo experiments generate large quantities of data that are best represented as three-dimensional (potential, current, time) color contour images. For example, the temporal release of dopamine following electrical stimulation is evidenced from the rapid interferences from adsorption processes and chemical reactions that are coupled to the primary oxidation reaction of catecholamines neurotransmitters<sup>164</sup>.

### **2.2.2. Electrical Impedance Spectroscopy (EIS)**

Impedance spectroscopy is an effective technique for probing the features of chemically-modified electrodes and for understanding electrochemical reaction rates. Impedance is the totally complex resistance encountered when a current flows through a circuit made of combinations of resistors, capacitors, or inductors. Electrochemical transformations occurring at the electrode–solution interface can be modeled using components of the electronic equivalent circuitry that correspond to the experimental impedance spectra. Particularly useful to model interfacial phenomena is the Randles and Ershler electronic equivalent-circuit model (Fig. 2.6).

This includes the double-layer capacitance  $C_d$ , the ohmic resistance of the electrolyte solution  $R_s$ , the electron transfer resistance  $R_p$ , and the Warburg impedance  $W$  resulting from the diffusion of ions from the bulk solution to the

electrode surface. The impedance of the interface, derived by application of Ohm's law, consists of two parts, a real number  $Z'$  and an imaginary one,  $Z''$ :

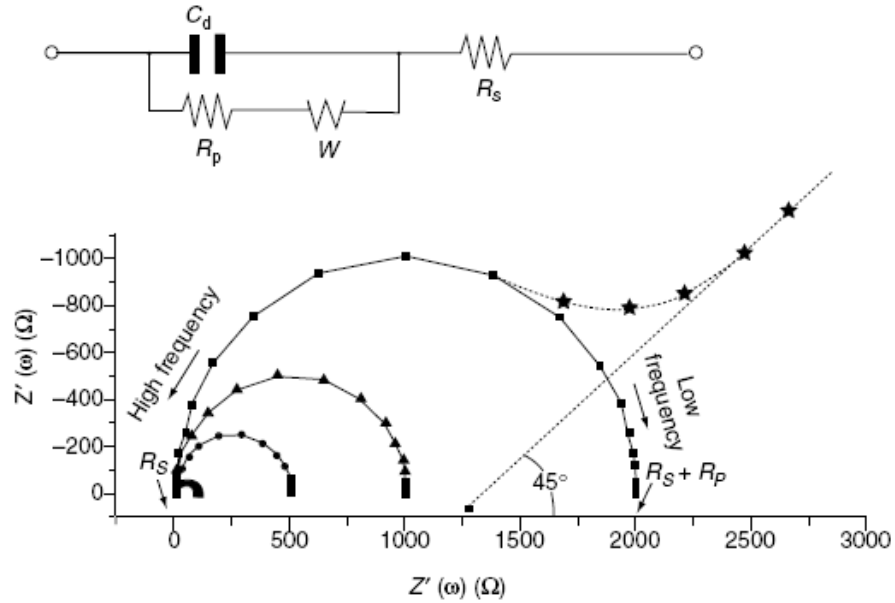


Figure 2.6 Faradaic impedance spectra presented in the form of Nyquist plots, along with the electronic equivalent circuit of the electrified interface.

$$R(\omega) = R_s + \frac{R_p}{(1 + \omega^2 R_p^2 C_d^2)} - \frac{j\omega R_p^2 C_d}{1 + \omega^2 R_p^2 C_d^2} = Z' + jZ'' \dots\dots\dots 2.7$$

where  $j^2 = -1$

Impedance spectroscopy requires an application of a small-amplitude perturbing sinusoidal voltage signal (at a  $\omega$  frequency) to the electrochemical cell and measuring the current response. The resulting faradaic impedance spectrum, known as a Nyquist plot, corresponds to the dependence of the imaginary impedance value on the real one (e.g., Fig. 2.6), and contains extensive information about the electrified interface and the electron transfer reaction. Nyquist plots commonly include a semicircle region lying on the axis followed by a straight line. The semicircle portion (observed at higher frequencies) corresponds to the electron-transfer-limited process, while the straight line (characteristic of the low-frequency range) represents the

diffusion-limited process. Such spectra can be used for extracting the electron transfer kinetics and diffusional characteristics. In the case of very fast electron transfer processes the impedance spectrum includes only the linear part, while very slow electron transfer processes are characterized by a large semicircular region. The diameter of the semicircle equals the electron transfer resistance. The intercepts of the semicircle with the  $Z'$  axis corresponds to those of  $R_s$ . In addition to fundamental electrochemical studies, the technique has been found extremely useful for transduction of bioaffinity events in connection to modern electrical immunosensors and DNA biosensors. Such transduction of bioaffinity events relies on the increased insulation of the electrode surface in respect to redox probes (e.g., ferrocyanide), present in the solution, on binding of large biomolecules (e.g., capture of an antigen that retards the electron transfer)<sup>164</sup>. Voltammetry and Impedance spectroscopy measurement on this work have been done using AUTOLAB PGSTAT 13 electrochemical work station.

### 2.2.3. Surface Plasmon Resonance(SPR)

Surface plasmon resonance (SPR) is a phenomenon which occurs when light is reflected off thin metal films.

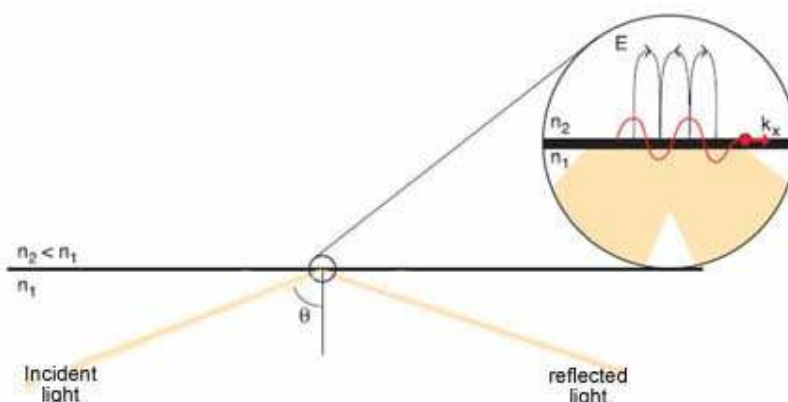


Fig. 2.7. Total Internal Reflection (TIR) for non-absorbing media. Refractive index ( $n$ ), evanescent field ( $E$ ) and angle of incidence ( $\theta$ )

When a light beam propagating in a medium of higher refractive index meets an interface at a medium of lower refractive index at an angle of incidence above a critical angle (Mirabella<sup>165</sup>, de Mello<sup>166</sup>), the light is totally reflected at the interface and propagates back into the high refractive index medium (see Fig. 2.7).

Although the fully reflected beam does not lose any net energy across the Total Internal Reflection (TIR) interface, the light beam leaks an electrical field intensity called an evanescent field wave into the low refractive index medium. The amplitude of this evanescent field wave decreases exponentially with distance from the interface, decaying over a distance of about one light wavelength from the surface (Fig. 2.8).

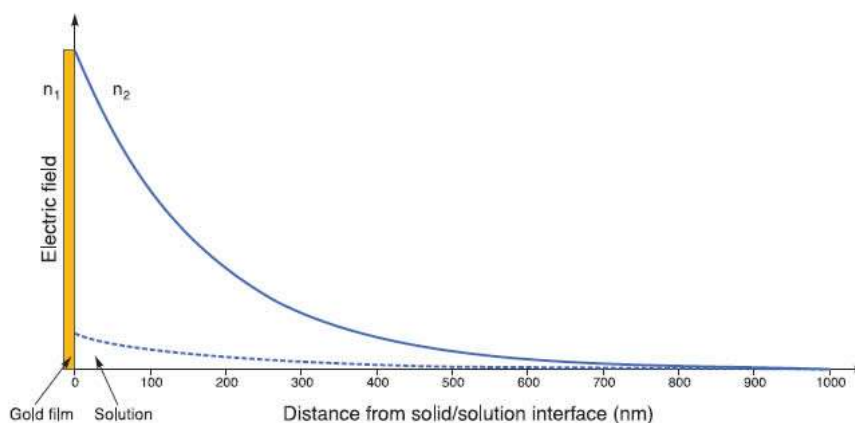


Fig. 2.8 Relative evanescent electric field amplitude (E) versus distance to solid/solution interface (nm). Continuous line for SPR-evanescent wave (gold film), dashed line for nonabsorbing TIR (no gold film).

If the lower refractive index media has a non-zero absorption coefficient, the evanescent field wave may transfer the matching photon energy to the medium. This is exploited in internal reflection spectroscopy (IRS) as reviewed by Mirabella<sup>165</sup>. The penetration depth of the evanescent field wave is usually defined as the distance over which the wave decays to  $1/e$ , or about 37%, of its maximum intensity. If the TIR-interface is coated with a layer of a suitable conducting material, such as a metal, of a suitable thickness the polarized component of the evanescent field wave, may penetrate the metal layer and excite electromagnetic surface plasmon waves

propagating within the conductor surface that is in contact with the low refractive index medium (Fig. 2.9). For a non-magnetic metal like gold, this surface plasmon wave will also be p-polarized and, due to its electromagnetic and surface propagating nature, will create an enhanced evanescent wave (Fig. 2.10).

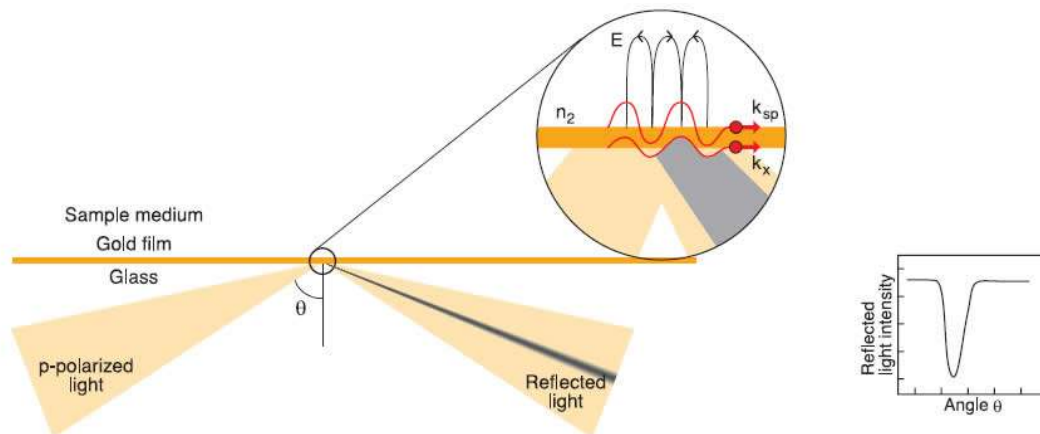


Fig. 2.9 SPR is excited by p-polarized totally internally reflected light at a glass/metal film interface, the surface plasmon enhancing the evanescent field amplitude (E). SPR is observed as a dip in the reflected light intensity at a specific angle of reflection.

This evanescent wave has electric field components directed in all spatial orientations during penetration into the low refractive index medium. Because the electric field penetrates a short distance into the lower refractive index medium, the conditions for SPR are sensitive to the refractive index at the gold surface. For plasmon excitation by a photon to take place the energy and momentum of these “quantum-particles” must both be conserved during the photon “transformation” into a plasmon. This requirement is met when the wavevector for the photon and plasmon are equal in magnitude and direction for the same frequency of the waves (the wavevector is a parameter in the mathematical formula for the electromagnetic wave related to the momentum). The direction of the wavevector is the direction of the wave propagation (i.e. the light ray direction), while its magnitude depends on the refractive indices of the media that the electromagnetic field wave interacts with along

its propagation path. Since the wave vector of the plasmon wave is bound to the conductor surface, it is the wavevector of the component of the incident light which is parallel to the conductor surface that can be equal to the wave-vector of the surface plasmons ( $k_{sp}$ ,  $k_x$  in Figure 2.9). The magnitude of the surfaceparallel wavevector,  $k_x$ , is the wavevector of the incident light times  $\sin(\theta)$ , (Fig. 2.9).

$$k_x = \frac{2\pi}{\lambda} \cdot n_1 \cdot \sin(\theta) \dots\dots\dots 2.8$$

The wavevector of the plasmon wave,  $k_{sp}$ , depends on the refractive indices of the conductor,  $n_{gold}$ , (being a constant complex number) and the sample medium,  $n_2$ , as

$$k_{sp} = \frac{2\pi}{\lambda} \times \left( \frac{n_{gold}^2 \times n_2^2}{n_{gold}^2 + n_2} \right)^{1/2} \dots\dots\dots 2.9$$

In both expressions the wavelength is the value for the light wave in vacuum. Thus, an increased refractive index of the sample,  $n_2$ , penetrated by the plasmon enhanced evanescent field increases the wavevector of the plasmon wave. The wavevector of the light  $k_x$  can be tuned to equate the plasmon wavevector by varying either the angle of incidence,  $\theta$ , or the wavelength of the light, Figure 2.9. The dielectric equations describing this dependence and the application of this technology are discussed in detail by Swalen<sup>167</sup>, Kovacs<sup>168</sup>, Kretschmann<sup>169</sup>, Liedberg<sup>170</sup>, Jönsson<sup>171</sup> and Davies<sup>172</sup>. The wavevector and energy match enables a resonant absorption of energy via the light-evanescent wave field, a plasmon excitation (SPR) causing a characteristic drop in the reflected light intensity. For a given wavelength of incident light, SPR is seen as a dip in the intensity of reflected p-polarized light at a specific angle of incidence (Fig. 2.9). Monochromatic light is focused in a wedge-shaped beam on the TIR interface and the angle of minimum reflectance intensity is determined using a two dimensional detector array (see Figure 2.10). The low refractive index medium is the surface coating of the sensor chip and the “surrounding” sample solution. Biomolecular interactions occurring at the sensor surface change the solute concentration and thus the refractive index within the

evanescent wave penetration range. The angle of incidence required to create the SPR phenomenon (the SPR angle) is therefore altered and it is this change which is measured as a response signal.

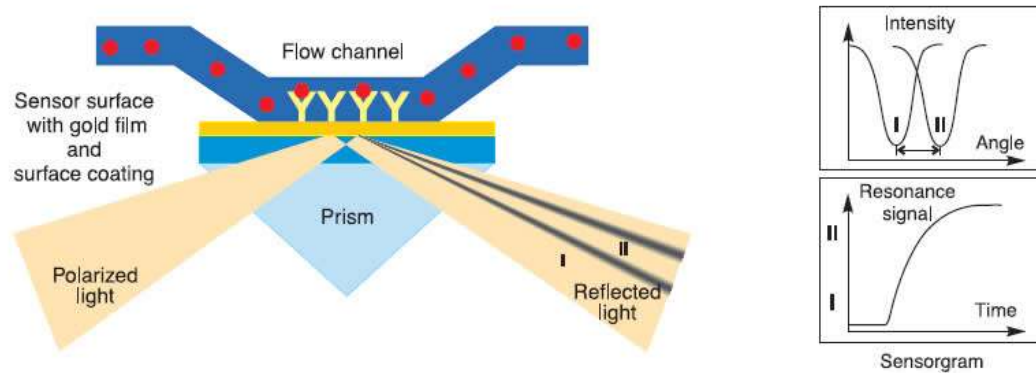


Fig. 2.10. Surface Plasmon Resonance (SPR) detection unit.

Fig 2.10. The incident p-polarized light is focused into a wedge-shaped beam providing simultaneously a continuous interval of light wavevectors  $k_x$ . This range covers the working range for the plasmon wavevector  $k_{sp}$  during biomolecular interaction analysis. An increased sample concentration in the surface coating of the sensor chip causes a corresponding increase in refractive index which alters the angle of incidence required to create the SPR phenomenon (the SPR angle). This SPR angle is monitored as a change in the detector position for the reflected intensity dip (from I to II). By monitoring the SPR-angle as a function of time the kinetic events in the surface are displayed in a sensorgram. All the SPR measurements in this work have been done by Biosuplar-3 from analytical  $\mu$ -Systems.

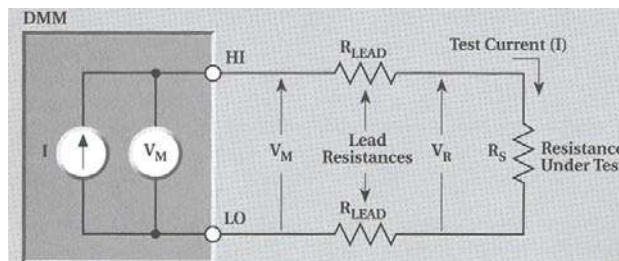
#### 2.2.4. Conductivity measurement

Resistance measurement in the normal range ( $>10\Omega$ ) are generally made using the 2-wire method shown in the figure 2.11 (a). The test current is forced through the test lead and the resistance being measured ( $R_S$ ). The meter then

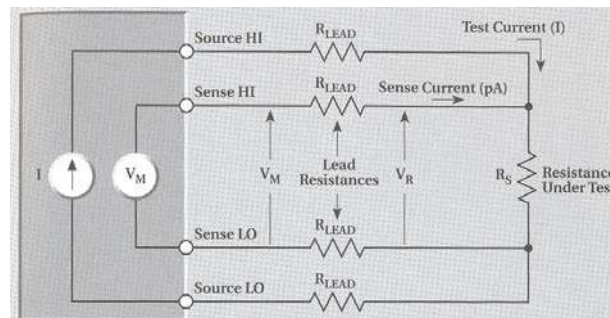


measures the voltage across the resistance through the same set of test leads and computes the resistance value accordingly.

The main problem with 2-wire method as applied to low resistance measurements is the lead resistance ( $R_{LEAD}$ ). Since the test current ( $I$ ) causes a small but significant voltage drop across the lead resistance, the voltage ( $V_M$ ) measured by the meter will not be exactly the same as the voltage ( $V_R$ ) directly across the test resistance ( $R_S$ ), and considerable error can result. Typical lead resistance lies in the range of  $1m\Omega$  to  $10m\Omega$ , so it is very difficult to obtain accurate 2-wire resistance measurement below  $10\Omega$  to  $100\Omega$  (depending on the lead resistance)



(a)



(b)

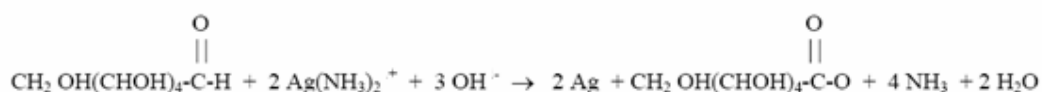
Fig. 2.11 Scheme Two point measurement system (a), Four point measurement system (b).

Due to the limitation of the 2-wire method, the 4-wire (Kelvin) connection method shown in the figure 2.11 (b) is generally preferred for low-resistance measurement. These measurements can be made using a DMM, micro ohmmeter, or a separate current source and voltmeter. With this configuration, the test current ( $I$ ) is forced through the test resistance ( $R_S$ ) through one set of test leads, while the voltage ( $V_M$ ) across the DUT is measured through a second set of the leads called sense leads, it is usually negligible (typically pA or less) and can generally be ignored for all practical purposes. Since the voltage drop across the sense leads is negligible, the voltage measured by the meter ( $V_M$ ) is essentially the same as the voltage ( $V_R$ ) across the resistance ( $R_S$ ). Consequently, the resistance value can be determined much more accurately than with 2-wire method. Note that the voltage-sensing leads should be connected as close to the resistor under test as possible to avoid including the resistance of the test leads in the measurement. Fig 2.11 is the scheme of the conductive measurement. The measurement has been performed using Keithley 617 and Keithley 2400. Absorbance spectra were measured using UV-Vis CARY 50 Bio.

### 3. RESULTS AND DISCUSSIONS

#### 3.1. Conductive chemoassay for glucose

This part of my experimental work is focused on the development of new assay for the glucose analysis. It should be fast, simple, cheap, and have low detection limit. One method which can promise fast, simple, cheap, and probably have low detection limit is conductivity measurement. The idea is to combine conductivity with silver mirror reaction which is the common method to produce silver mirror using glucose. It is produced by reacting glucose with ammoniacal silver solution. The reaction is described as the following.



The reaction can describe that the number of silver formed in the reaction depends on the number of glucose. If It is assumed that silver layer can be deposited in the surface of four point electrode (Fig. 3.1 ), then the resistance of the silver layer can be measured (i.e. silver particle). It is expected that the different amount of the silver which formed on the surface of the electrode will give different value of the resistance, while the number of silver which formed depends on the concentration of glucose.

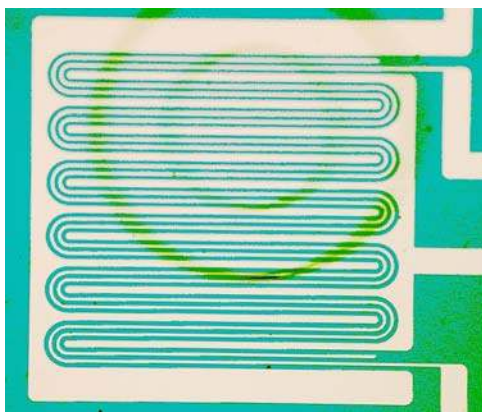


Fig. 3.1 Four points electrode.

After several attempts of measurement using different concentration of glucose, unfortunately this technique didn't give good result. No dependence has been observed during the experiments. This problem most probably is because of no homogeneous layer of silver has been formed on the surface of the electrode. Another attempt also has been done to improve this method by adding conductive polymer (i.e. polypyrrole) support on the surface of the electrode (Fig 3.2), but that also has given poor reproducibility.

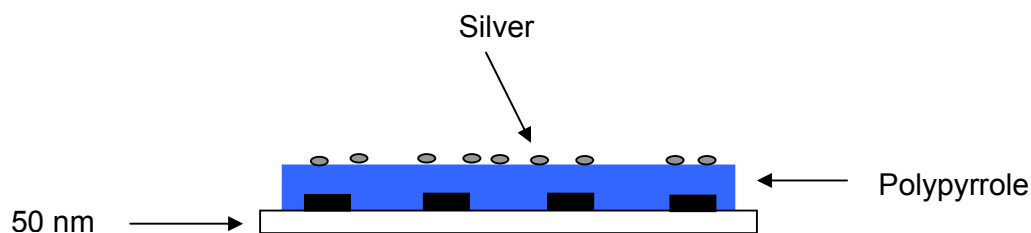


Fig 3.2 Scheme of conductive chemoassay for glucose with polypyrrole support

### 3.2. Silver mirror reaction in the paper support

Other attempt to analyze glucose is continued by silver mirror reaction in the paper support. The basic idea is to use the diffusion of glucose and  $\text{Ag}(\text{NH}_3)_2^+$  from two opposite directions that will meet at the reaction zone (about in the middle of the paper). The illustration of the experiment is demonstrated in fig 3.3.

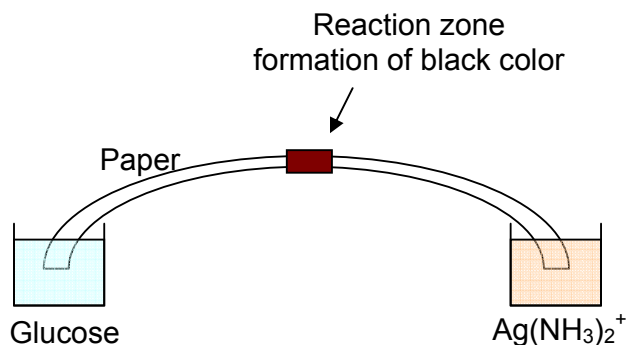


Fig. 3.3 Illustration of silver mirror reaction in the paper support.

The reaction between glucose and  $\text{Ag}(\text{NH}_3)_2^+$  will produce the black color on the paper support. The reaction from the different concentration of glucose (in constant concentration  $\text{Ag}(\text{NH}_3)_2^+$ ) will expectedly result different length and/or position of the black color in the paper support.

The experiment of the silver mirror reaction in the paper support using constant  $\text{Ag}(\text{NH}_3)_2^+$  and various glucose concentration is demonstrated in fig 3.4. The formation of black color in the paper support reveals as expected, but this technique has poor sensitivity and gives only semi quantitative analysis.

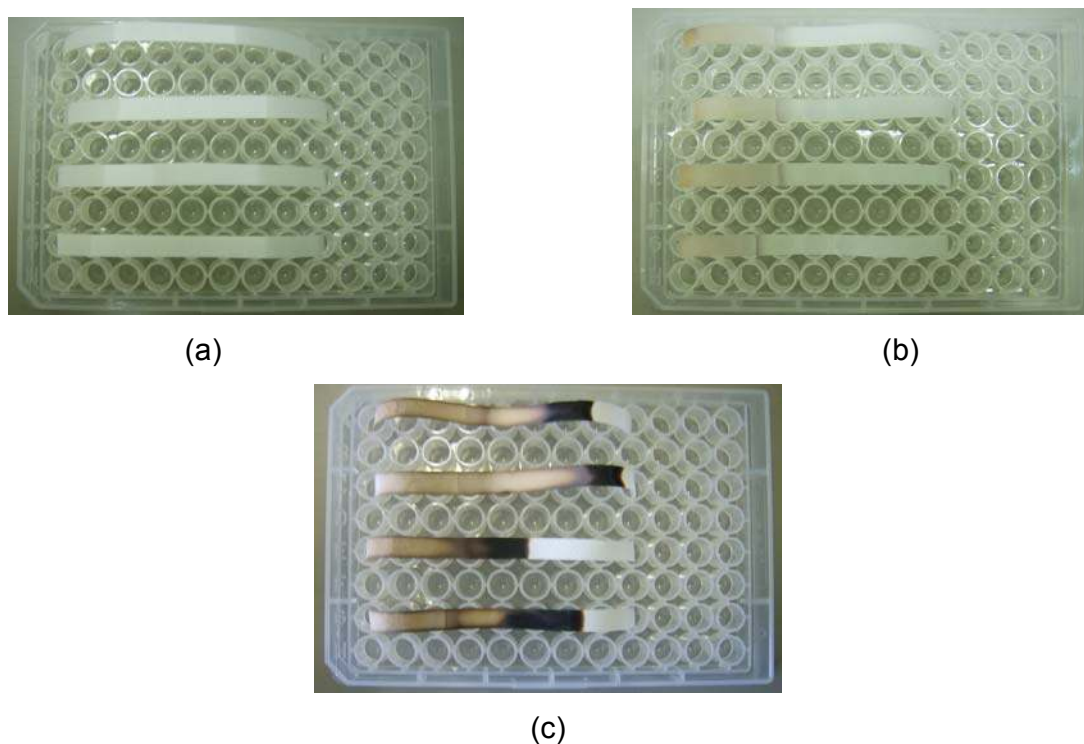


Fig 3.4 Detection of glucose using silver mirror reaction in the paper support technique. The concentrations of glucose are 500, 1000, 1500 and 2000 ppm from up to down respectively. Initial time (a), after 1 hours (b), after 1 day (c)

### 3.3. Preparation of nanoparticles

There are several ways to synthesize gold nanoparticles in this work i.e. either in aqueous or organic solution, or using different oxidation agent. Each way will

---

result in the different stability of the nanoparticles formed. The stability is very important to be considered for storage and application purpose.

### ***Preparation gold nanoparticles using sodium citrate in the aqueous solution***

Gold nanoparticles are produced from reduction of  $\text{HAuCl}_4$  by sodium citrate. This process has been done in boiling temperature of the solution. 1 mL of 1% sodium citrate has been added into 10 mL of 1 mM aqueous solution of  $\text{HAuCl}_4$  under intensive stirring (Fig 3.5).

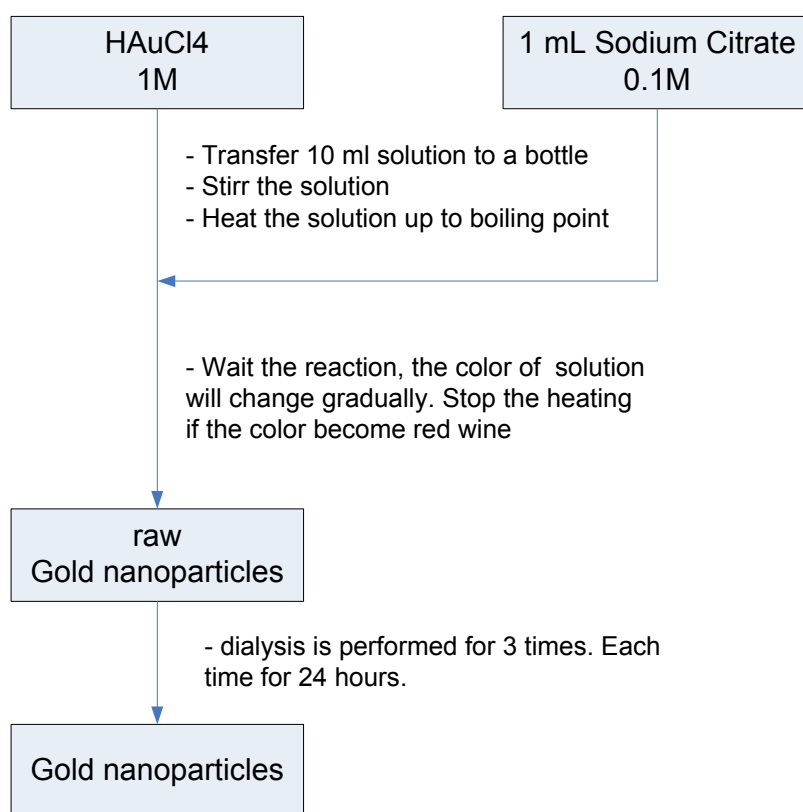


Fig. 3.5 Scheme of preparation of gold nanoparticles in aqueous solution

If the reagent is mixed in the room temperature, the color will change slowly become blue. That blue color will stay for long time or change to black color due to the aggregation of particles if the concentration of  $\text{HAuCl}_4$  is quite high. This blue or black color indicates that the size of the gold nanoparticles is relatively big. At this

condition, an attempt to boil this solution has been done expecting the solution would change to red, but the solution remains blue.

On the contrary, at the boiling temperature, the reaction begins immediately after the sodium citrate solution is added into the  $\text{HAuCl}_4$  solution. The reaction can be observed from the changes of the color of the solution. The figure 3.6 demonstrates the changes of color during the reaction.

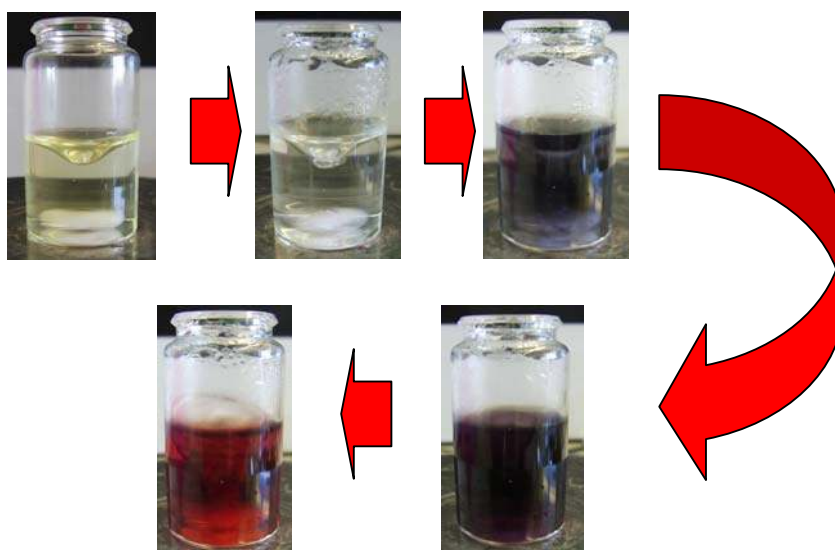


Fig. 3.6 Changes of color during the reaction of the reduction  $\text{HAuCl}_4$  by sodium citrate gold nanoparticles synthesis in boiling temperature.

The initial color of  $\text{HAuCl}_4$  is yellow, and soon after addition of sodium citrate in boiling state, the color changes in sequence to colorless, dark blue, and finally red wine. At this final state the solution is then cooled in the room temperature. The obtained suspension of nanoparticles is stored at room temperature and used within several days. The optical absorbance of the gold plasmon band in the suspension is about 1.5 (at  $\lambda = 519$  nm, this corresponds to the spectral maximum); the spectrophotometer UV Vis CARY 50 Bio is used. The mean diameter of nanoparticles determined by SEM (LEO SUPRA35 ) is about 14 nm (the details of characterization will be explained later).

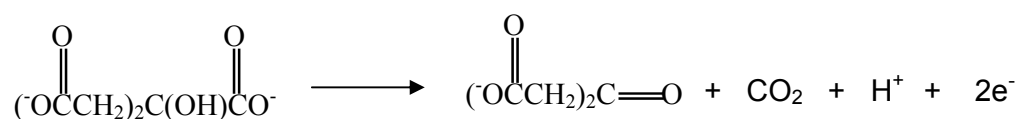
If we consider the changes of color of the solution during the reaction, probably the big particles are formed (blue and black color) in the beginning of the

## RESULTS AND DISCUSSIONS

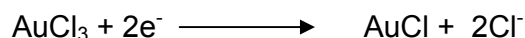
---

reaction, then the big particles cleavage to smaller size and finally formed nanoparticles (red wine color). However, it is not clear why the solution remains blue after boils the solution which is mixed in the room temperature.

Unfortunately, no one has studied the detailed reaction which takes place in the above mixture until this time. But the following is mechanism of this chemical process proposed by S. Kumar, K.S Gandhi and R. Kumar.<sup>173</sup> The reaction occurs as a multiple-step process. The initial step is the oxidation of citrate which yields dicarboxy acetone :



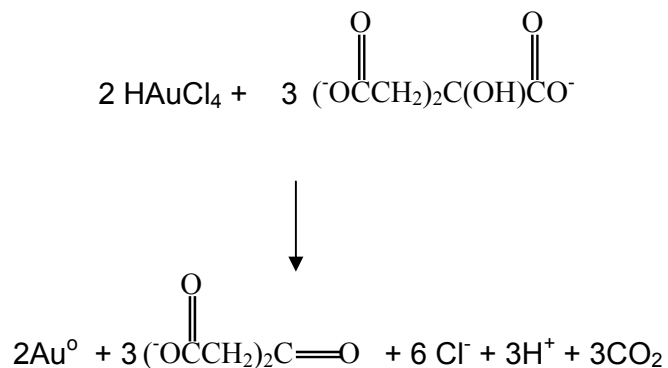
The second step is the reduction of auric salt to aurous salt :



The third step is the disproportionation of aurous species to gold atoms



The overall stoichiometry of reduction reaction can then be presented as.





***Purification of gold nanoparticles.***

Nanoparticles which are produced by reducing  $\text{HAuCl}_4$  with sodium citrate have very limited time storage. In order to get highly stable nanoparticles, purification has been performed for industrial purpose. Removal of the side product of the reaction between  $\text{HAuCl}_4$  with sodium citrate is considered to make gold nanoparticles more stable. The purification is done using dialysis technique. The dialysis is done in three days by immersing the dialysis tube containing gold nanoparticles in 5 L millipore water (Fig. 3.7). The water is changed every 24 hour. The result demonstrates that gold nanoparticles are more stable after the purification process. The stability of the gold nanoparticles will be described more detail in the part freezing indicator.



Fig 3.7. Dialysis device.

***Silver nanoparticles synthesis using Sodium Citrate***

An attempt in my work also tries to synthesize silver nanoparticles. Silver nanoparticles are produced by reduction of silver nitrate by sodium citrate. The procedure is similar to production of gold nanoparticles using sodium citrate which is

described above. The reaction is done in boiling temperature of  $\text{AgNO}_3$ . The color changes from colorless to yellow (Fig. 3.8).

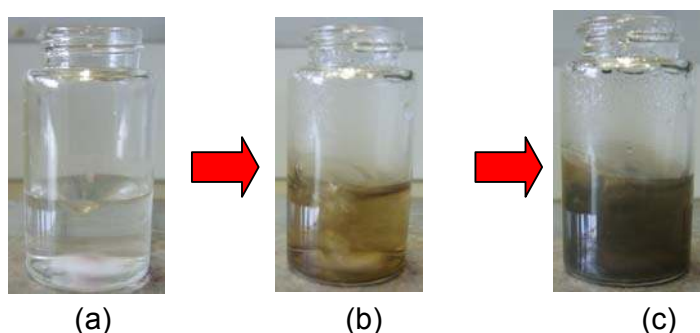


Fig 3.8 Changes of color during the synthesis of silver nanoparticles. Initial (a), in the middle of reaction (b), end of the reaction (c).

***Preparation of gold nanoparticles using sodium borohydride.***

The limited stability of gold nanoparticles prepared by reduction of  $\text{HAuCl}_4$  using sodium citrate is the reason to try other reducing agents. The basic procedure for the synthesis of gold nanoparticles using sodium borohydride is similar to the procedure in using of sodium citrate. 0.5 ml of 0.5 mM sodium borohydride is added to 1 mM 10 ml  $\text{HAuCl}_4$  with stirring. The color of the solution has changed from yellow to red/purple (Fig.3.9b). The reaction takes place at room temperature. This reaction does not need high temperature to proceed. The changes of color are very fast. Fig 3.9 demonstrates the change of the color, and finally aggregation of nanoparticles occurred.

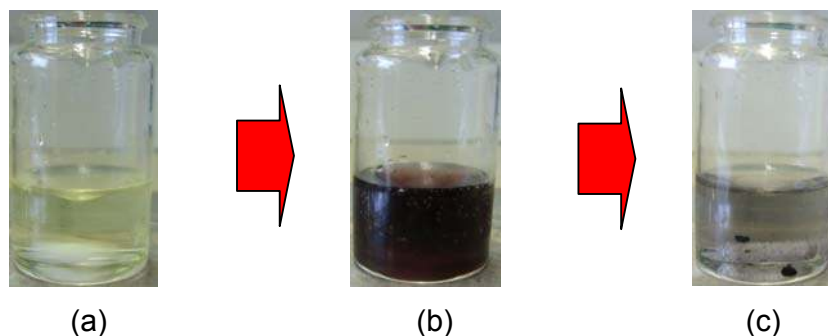


Fig. 3.9. Changes of color in reduction  $\text{HAuCl}_4$  by  $\text{NaBH}_4$  in gold nanoparticles synthesis. (a) initial, (b) gold nanoparticles, (c) aggregation of nanoparticles

The rate of reaction depends on the concentration of the reduction agent ( $\text{NaBH}_4$ ). It can be changed from several minutes until several days by addition of corresponding concentration of the reagent. But this part is not our main concern. Our concern is to get nanoparticles fast and stable for long time. Synthesis gold nanoparticles using  $\text{NaBH}_4$  is found difficult to be stopped. However once the reaction is started, the gold nanoparticles grow along the time. After red color has been achieved which shows the formation gold nanoparticles, the solution becomes dark, and continues growing and growing, and finally the particles settle down in the bottom of the flask (Fig 3.9c). An attempt to stop the reaction is by bubbling oxygen into the flask to oxidize the remained  $\text{NaBH}_4$ . Thousand times of oxygen is introduced into the solution. After two hours bubbling oxygen into the flask and let the solution for one night, the agglomeration of gold nanoparticles is still happened. This method is not suitable for industrial preparation purpose which need fast and stable product for a long periods.

### ***Preparation suspension of gold nanoparticles in non-polar medium***

Gold nanoparticles in organic solution are performed for nucleation agent of protein and freezing indicator experiments. 6 ml 30 mM hydrogen tetrachloroaurate aqueous solution is mixed with 16 ml of 50 mM tetraoctylammonium bromide in toluene. The mixture is stirred vigorously until all tetrachloro aurate transfer to toluene phase which is shown by change of the color. The color of aqueous solution changes from yellow to colorless. The organic solution changes from colorless to red. After separation of organic phase from the aqueous phase, 34 mg of dodecanethiol is added to the organic phase solution. Freshly prepared 4 ml 0,5 mM sodium borohydride solution is added slowly with vigorously stirring for 3 hours. Solvent is evaporated until 2 ml using vacuum devices, and continued with the addition 80 ml ethanol. The solution is kept at  $-18^\circ\text{C}$  for 4 hours in the refrigerator, and let for overnight. To remove the excess of dodecanethiol, the cleaning of gold nanoparticles using ethanol is repeated. 80 ml ethanol is added to the precipitate after removal of the ethanol from the solution, then let the solution for overnight. The precipitate is separated from the ethanol, and dried using vacuum device (Fig 3.10). These gold nanoparticles which are covered by dodecanethiol is soluble in non-polar medium<sup>174</sup>.

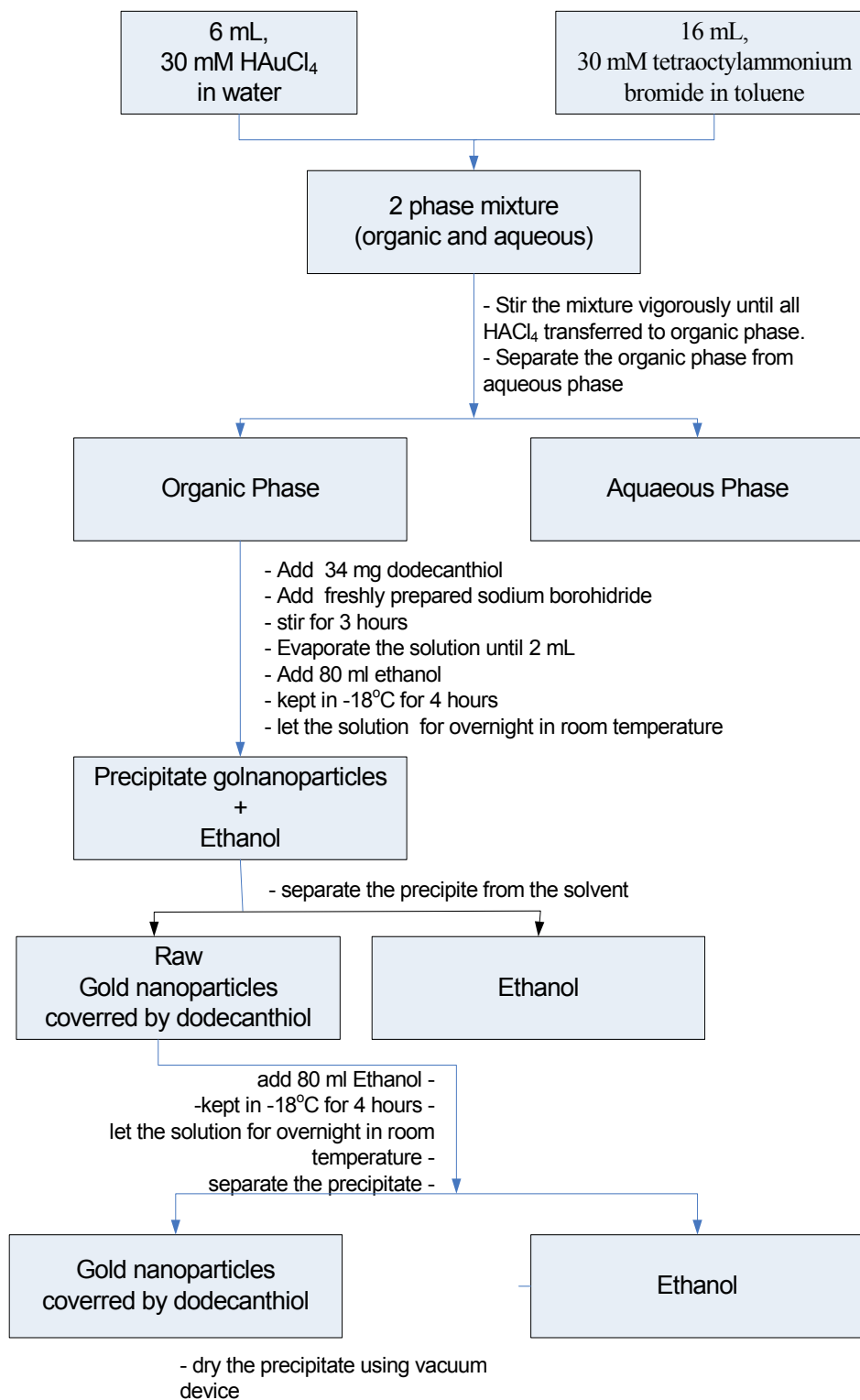


Fig. 3.10. Scheme of preparation gold nanoparticles in the organic solution

***Continuous synthesis of gold nanoparticles***

After producing gold nanoparticles in small scale successfully, it is a challenge to produce gold nanoparticles in big scale for industrial purposes. If we consider the way in “Preparation gold nanoparticles using sodium citrate in the aqueous solution” as described in detail previously, big scale synthesis of gold nanoparticles will need big reactor which is equipped with good stirring device. So, the reaction can run homogenously. If the stirring is not sufficient to make solution homogenously, gold nanoparticles may not grow perfectly as in small scale. This is a common problem if we want to develop from laboratory to industrial scale. Considering the above reasons, I have made some experiments to introduce a continuous synthesis of gold nanoparticles based on the principal reaction in batch method. Fig 3.11 is the initial scheme of continuous synthesis of gold nanoparticles.

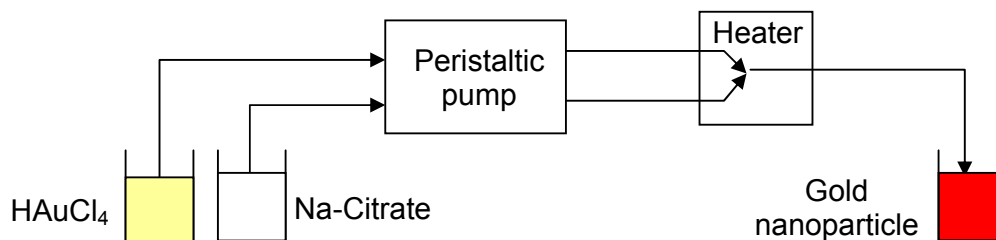


Fig. 3.11. Scheme of automation of gold nanoparticles synthesis.

Concentration of  $\text{HAuCl}_4$  and sodium citrate introduced into peristaltic pump are 1 mM and 0.01% respectively. Silicon tube is used for this experiment. Formation of gold nanoparticles starts when both of the solution mixed in the heater (water bath). This initial scheme raises two problems which make the reaction of formation of gold nanoparticles incompletely. The formation of gas ( $\text{CO}_2$ ) has caused inconstant rate of the output that influences the quality of the gold nanoparticles formed. Degassation of  $\text{HAuCl}_4$  and sodium citrate solution has been performed, but that can not help. The second problem, poor thermal conductivity of the silicon tube has made the temperature of the mixed solution is relatively lower than the expected temperature

(i.e. boiling point). One special shape of glass (Fig 3.12) is then introduced in the heater to solve those problems.

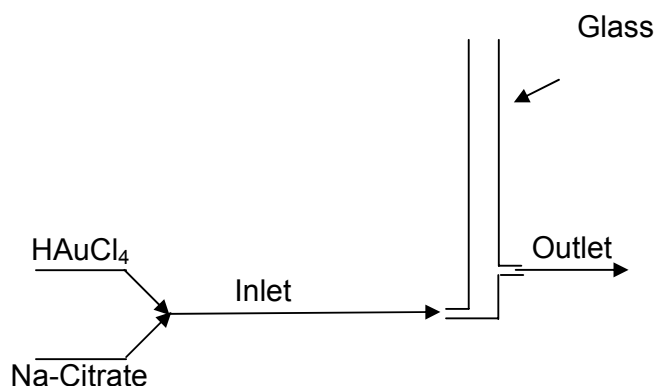


Fig 3.12 Illustration of the special shape of glass to remove gas during reaction and to help optimization of the heating for continuous gold nanoparticles synthesis.

When the mixed solution (i.e.  $\text{HAuCl}_4$  and sodium citrate) in the silicon tube comes to the special glass, the solution will be held for definite time in the glass (Fig 3.12). In that place, the mixed solution gets heating better than in the silicon tube, so that formation of gold nanoparticles can be performed completely, as well as the gas which formed during the reaction can be released. This addition of special shape of glass can produce better quality of gold nanoparticles. An attempt has also been tried to mix the reagents, i.e.  $\text{HAuCl}_4$  and sodium citrate, before peristaltic pump to find the optimize production of gold nanoparticles. Mixing of  $\text{HAuCl}_4$  and sodium citrate before peristaltic pump gives blue color solution product that indicates formation of big size of gold particles.

The flow rate of the reactants is controlled by the peristaltic pump which can be adjusted to get suitable complete time reaction of gold nanoparticles formation. Various flow rates (0.91, 1.14, 1.47, 1.90, 2.22, 2.62 and 2.99  $\mu\text{L/s}$ ) of the pump have been applied to observe the influence of the quality of gold nanoparticles produced. The gold nanoparticles produced give red color similar look as produced in the batch method synthesis but with different intensity of the color due to lower concentration of

H<sub>2</sub>AuCl<sub>4</sub> solution used. The details information of the spectrum of plasmon band of gold nanoparticles using UV-Vis spectrophotometer will be given the later.

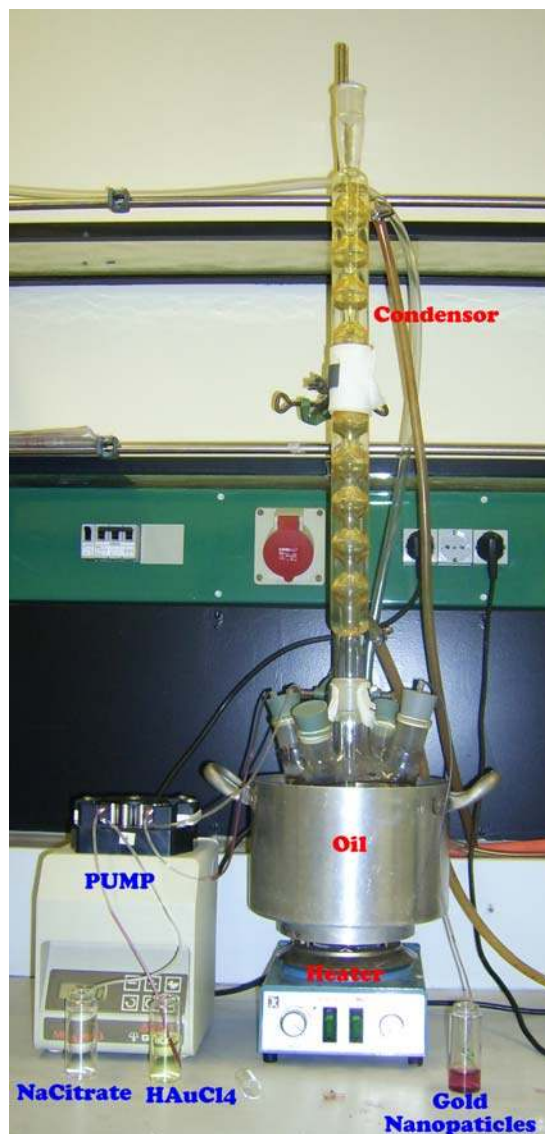


Fig. 3.13. The device for continuous gold nanoparticles synthesis.

### 3.4 Characterization of Nanoparticles

After the synthesis of the nanoparticles, the next step is the characterization. The characterization will give information about the spectrum of the plasmon band,

size and also shape of the nanoparticles. The first characterization has been performed by UV-Vis spectrophotometer. Fig 3.14 is the spectrum of gold nanoparticles that are produced using sodium citrate reducing agent in batch method.

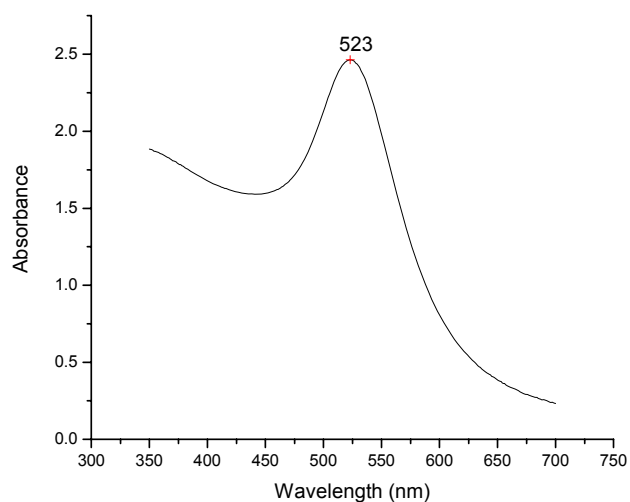


Fig. 3.14. UV-VIS spectrum of 1 mM gold nanoparticles solution by batch technique

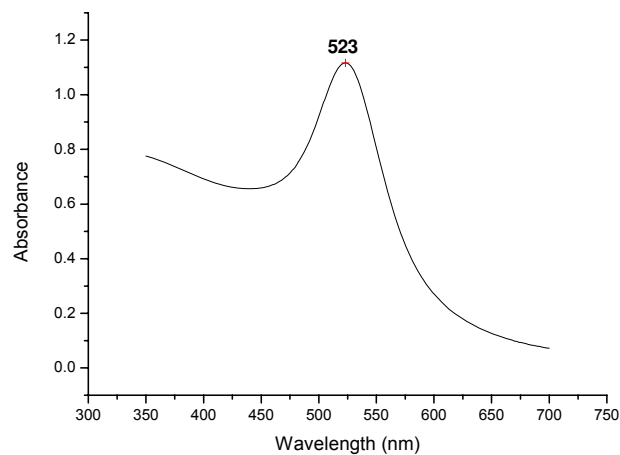


Fig. 3.15 UV-Vis spectrum of 1 mM gold nanoparticles solution by continuous technique.



Fig 3.14 demonstrates that the peak of the spectrum of the gold nanoparticles using batch technique is at 523 nm, and the same value of the peak also has been given by the continuous technique (Fig 3.15). That indicates that both the synthesis techniques produce the same size of the gold nanoparticles.

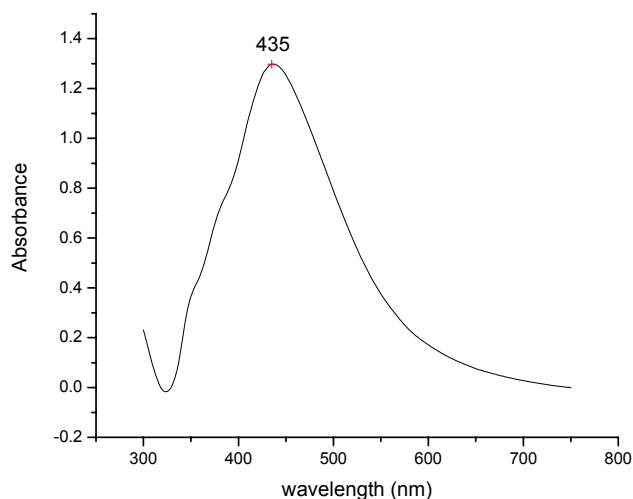


Fig. 3.16 UV-Vis spectra of silver nanoparticles solution by batch method.

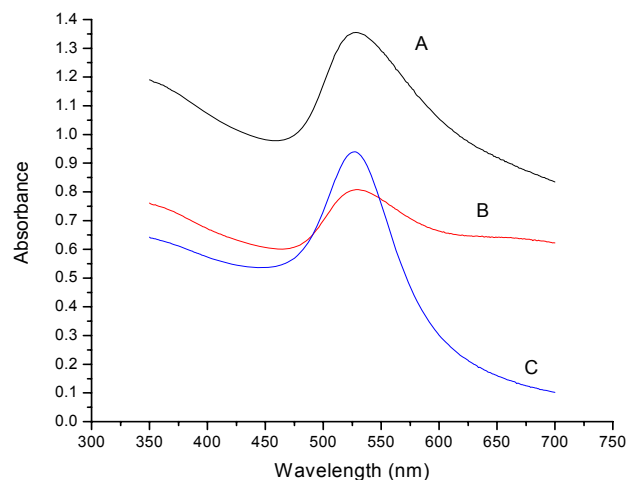


Fig 3.17 UV Spectrum of the gold nanoparticles synthesized at room temperature (without heating, blue color appeared) (A), continued with heating at boiling point for 7 minutes (B). The UV-Vis spectrum of gold nanoparticles synthesized using continuous method at boiling temperature(C)

Fig. 3.16 demonstrates the spectrum of the silver nanoparticles which is produced by batch technique using sodium citrate reducing agent. The peak of the spectrum is at 435 nm.

Fig 3.17 demonstrates the different results of the gold nanoparticles which are synthesized using different temperature treatment. The three spectrums show almost similar peak (at 523 nm), but each line has different absorbance value in each point of the wavelength. This indicates that the gold nanoparticles produced have different size of distribution. The narrower the spectrum of the plasmon band indicates the more homogenous size of distribution.

If the height of the peak is calculated from the based line of the spectrum, spectrum (C) shows the highest absorbance, that indicates the highest number of the gold nanoparticles in the solution. Spectrum (A) has higher absolute absorbance (i.e. 1.4) than spectrum (C) (i.e. 0.95) but lower peak height (calculated from the based line of the spectrum). Most probably that is because the spectrum (A) has more numbers of big particles in the solution that reflects much more light than the spectrum (B). After gold nanoparticles solution synthesized at room temperature (A) is boiled, the spectrum shows lower absorbance (B). Most probably the precipitation of big particles is the explanation of the decreasing of absorbance value.

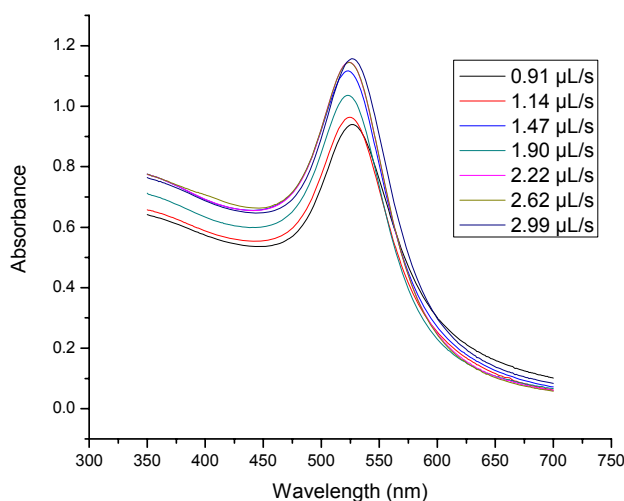


Fig. 3.18 UV-Vis spectrum of 1 mM gold nanoparticles solution by continuous synthesis technique in various flow rates.

Fig 3.18 demonstrates the spectrums of the plasmon band of gold nanoparticles which have been produced using continuous system in various flow rates of the pump. Fig 3.19 demonstrates that the optimum flow rate for continuous synthesis of the gold nanoparticles is 2.25  $\mu\text{L/s}$ . Most probably, big particles are formed if the gold nanoparticles solution is too long in the heater (lower than the optimum flow rate)

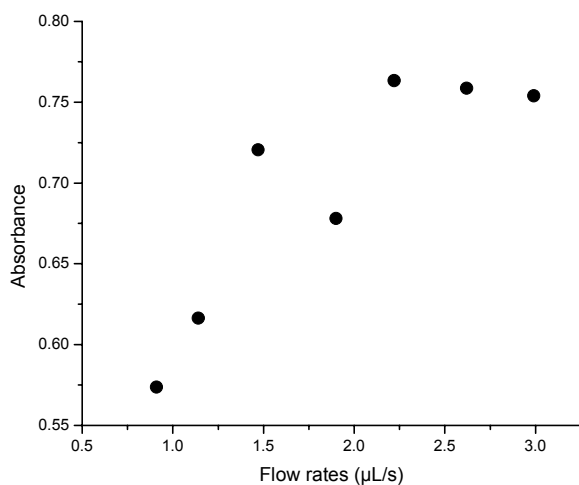


Fig 3.19 Dependence of absorbance upon flow rates of the pump. Absorbance calculated from the based line of the UV-Vis spectrum at 523 nm.

The second type of the characterization of nanoparticles is SEM and TEM to determine the size of the nanoparticles. Fig 3.20 is TEM image of the gold nanoparticles before dialysis. The size of the nanoparticles is estimated about 14 nm



Fig. 3.20 TEM image of the gold nanoparticles before dialysis.

Fig 3.21 shows that the size of the gold nanoparticles after dialysis is bigger than before dialysis. Some of nanoparticles most probably undergo aggregation during the dialysis process. The size of gold nanoparticles is estimated between 20 nm – 50 nm.



Fig. 3.21 SEM image of the gold nanoparticles after dialysis.

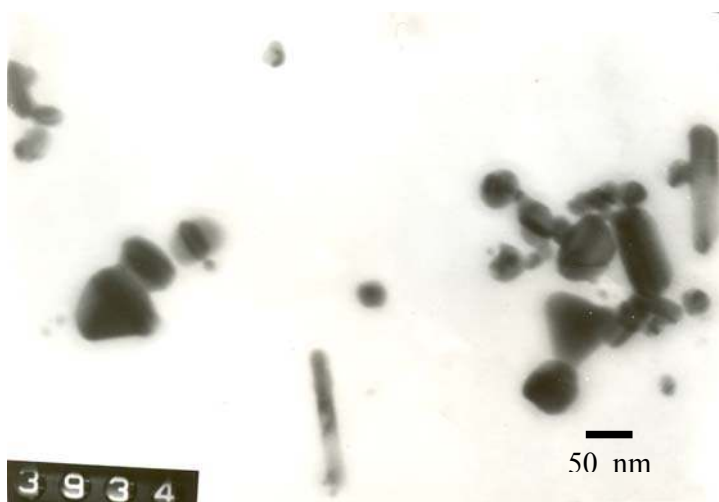


Fig. 3.22 TEM image of gold nanoparticles covered by 16-mercaptohexadecanoic acid after dialysis.

An attempt to stabilize the gold nanoparticles has been performed by adding 16-mercaptohexadecanoic acid to the solution. The 16-mercaptohexadecanoic acid will cover the gold nanoparticles, and is expected to give more stable gold

---

nanoparticles. Fig 3.22 is TEM image of the gold nanoparticles which is covered by 16-mercaptohexadecanoic acid (the gold nanoparticles solution is purified by dialysis technique before adding the 16-mercaptohexadecanoic acid). The average size of the covered gold nanoparticles is bigger than the uncovered nanoparticles. The size of the covered gold nanoparticles is estimated about 20 nm – 100 nm.

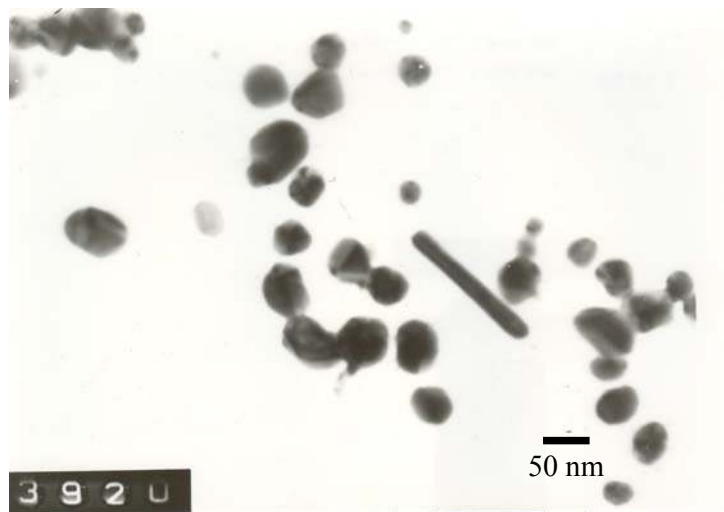


Fig. 3.23 TEM image of silver nanoparticles before dialysis.

Fig 3.23 is TEM image of the silver nanoparticles before dialysis. The size of silver nanoparticles is estimated about 50 nm that is bigger than gold nanoparticles which are produced with the same methods. After dialysis process to get more stable silver nanoparticles, the average size of silver nanoparticles becomes smaller. Figure 3.24 demonstrates the size of the silver nanoparticles after dialysis that is estimated about 20 nm. The decreasing size of the silver nanoparticles probably is caused by precipitation of the large silver nanoparticles during dialysis, while the small particles remain in the solution.

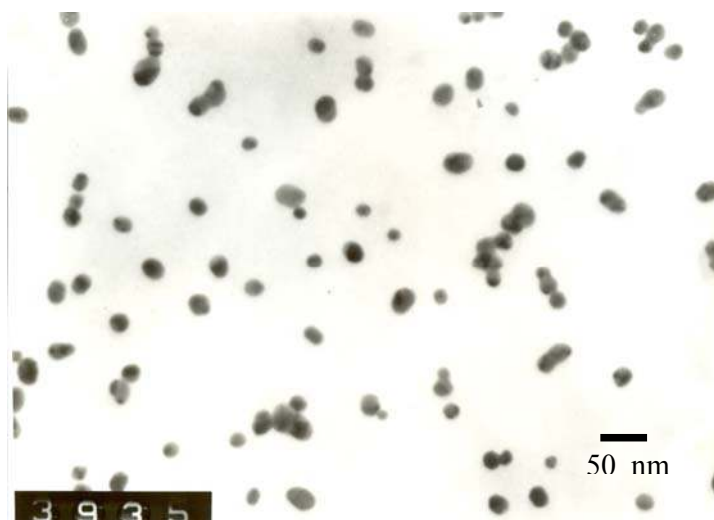


Fig. 3.24 TEM image of the silver nanoparticles after dialysis.

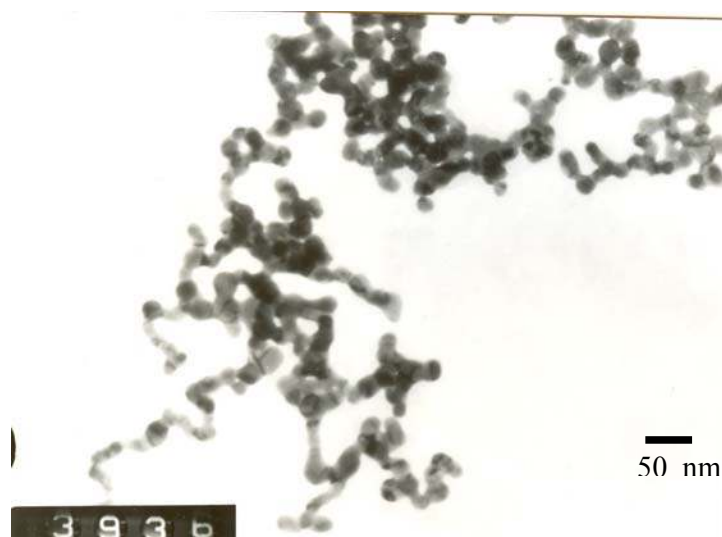


Fig. 3.25 TEM image of silver nanoparticles after dialysis that is covered by 16-mercaptohexadecanoic acid.

Addition of 16-mercaptohexadecanoic acid into the purified silver nanoparticles is performed. Fig 3.25 shows the silver nanoparticles which are covered by 16-mercaptohexadecanoic acid. The average size of the silver nanoparticles is estimated 20 nm that has similar size with the uncovered silver nanoparticles. But the most interesting part, the silver nanoparticles demonstrate the formation of the wire shape.

### **3.5 Detection of glucose**

A number of industrial, medical and biotechnological applications demand a simple technique for analysis of sugars. The developed methods include traditional methods of quantitative analyses (silver mirror reaction), as well as polarometry<sup>175</sup>, IR spectroscopy<sup>176</sup>, affinity sensors based on phenylboronic acid<sup>177-179</sup> and lectins<sup>180,181</sup> and enzymatic biosensors<sup>182,183</sup>. Some of these approaches are not selective others (affinity sensors with lectins, enzymatic biosensors) give detailed information on molecular types of sugars. The most perspective for routine applications are considered to be biosensors based on the corresponding oxidases or other enzymes. Such sensors are highly selective, sensitive, fast and reversible. However, many applications demand such a sensor which is stable being exposed to high temperature, aggressive chemicals, heavy metals and other enzyme inhibitors; which can be cleaned in hard conditions, dried and stored for a long time and does not need to be calibrated often. Such a sensor can be based on non-enzymatic electrochemical oxidation of glucose. The advantages and disadvantages of enzymatic and non-enzymatic sensors for glucose are discussed in<sup>184</sup>.

The most appropriate electrode for electrochemical oxidation of glucose was considered the platinum one<sup>185</sup>. However, low sensitivity, poisoning by adsorbed intermediates and chloride and poor selectivity<sup>184</sup> were the reasons to search for another electrode surface providing selective electrochemical activity towards glucose. Modifications of platinum electrode by Ti, Pb, Bi and WO<sub>3</sub> were studied<sup>186</sup>. However, a high affinity of platinum to the most of organic compounds leading to fast poisoning of the electrocatalytical surface, low sensitivity and toxicity of heavy metals hinder a further development in this field.

Another promising material for development of non-enzymatic electrochemical sensors for glucose is gold. The mechanism of electrochemical oxidation of glucose on gold electrodes was studied in<sup>187</sup>. It was demonstrated that the oxidation is a multistep process, and the first step includes a formation of catalytically active gold hydroxide. The glucose oxidation starts at the electrode potential of - 0.75 V vs SCE and becomes fast after increasing the potential up to -0.35 V vs SCE. A further increase of the electrode potential leads to the blocking of the glucose oxidation,

probably due to formation of gold oxide<sup>187</sup>. An essential improvement of electrocatalytical properties of gold electrodes can be reached by oxidative treatment of the gold surface<sup>188-190</sup>. Glucose oxidation was also studied at several metal adlayers (Hg, Cu, Ag, Ru, Pt, Pd and Cd) deposited on gold surfaces<sup>191,192</sup>. The role of the catalytically active adlayers (Ag and Hg) was related either to the shift of the pzc of the electrode or to the formation of catalytically active metal hydroxide sites. The latter process occurs at less positive potentials for silver<sup>192</sup> or results in a larger amount of adsorbed OH<sup>-</sup> for mercury<sup>191</sup>. Another approach for development of gold-based glucose sensors is the immobilization of gold nanoparticles on a conductive carrying substrate. First attempts for using this approach were recently reported<sup>193,194</sup> but no difference was detected in the voltammetric response for glucose oxidation at the Au-nanoparticles modified and gold-plate electrodes<sup>194</sup>. The present investigation presents another attempt to use gold nanoparticles immobilized on gold electrodes for voltammetric detection of glucose.

### ***Preparation of gold electrodes modified by gold nanoparticles***

The gold electrodes consisted of a thin gold layer sputtered onto a glass or silicone support with adhesive chromium sublayer. The electrodes had a disk-shaped gold pad with a macroscopic area of 0.385 mm<sup>2</sup> and connected to a contact pad by a contact line of 8 mm length and 10 μm width. Deposition of nanoparticles was performed by LbL (Layer-by-Layer) technique<sup>195</sup>: the gold electrode was immersed into the freshly prepared 0,2% solution of polyacrylic acid (pH 10) for 30 minutes, rinsed in water, immersed into the suspension of gold nanoparticles for 15 minutes, and rinsed with water again. This cycle was repeated three times. The quality of the electrode surface was controlled by optical microscopy. *Surface plasmon resonance* (SPR) monitoring of deposition of gold nanoparticles was performed by SPR-reflectometer Biosuplar-3 from Analytical μ-Systems ([www.biosuplar.com](http://www.biosuplar.com)). The experiments were performed in slope mode (i.e. as measurement of the intensity of the reflected light at fixed incident angle). Gold coated SPR-slides were used for the LbL deposition in these measurements



### *Measurement condition*

*Electrochemical measurements* were performed by AUTOLAB PGSTAT-13 electrochemical workstation (EcoChemie, The Netherlands). A standard three-electrode electrochemical cell was used. The electrode assembly consisted of a bare or modified Au electrode as the working electrode, a Pt wire as counter electrode, and Ag/AgCl (sat) as the reference electrode. The potential in all figures are indicated relative this reference electrode. The measurements were performed in 0.1 M NaOH at 22° C. And other properties of electrode during detection of glucose also have been observed using impedance spectroscopy.

### *Results and discussion*

Modified gold nanoparticles were obtained using LbL procedure. The gold/polymer layers deposited on the surface of gold electrode using three-cycle and characterized by SEM ; the mean size of the gold nanoparticles was estimated to be about 14 nm (Fig. 3.26).

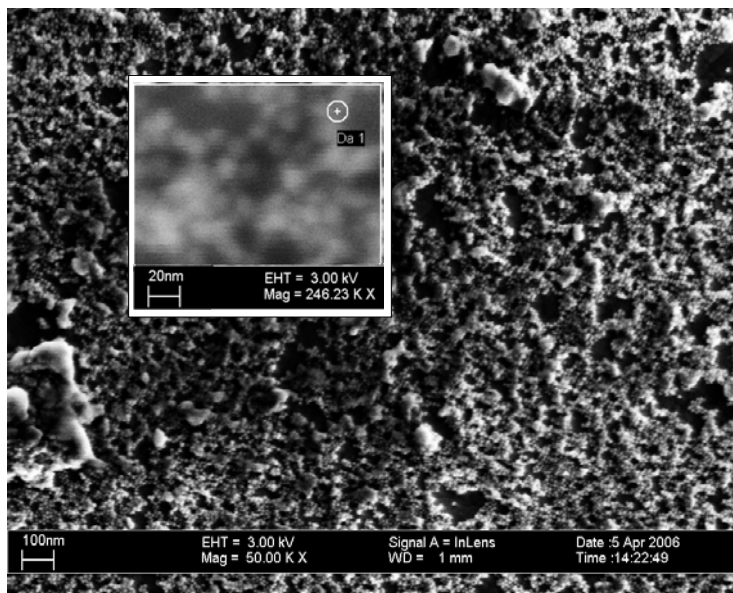


Fig 3.26 SEM image of gold electrodes coated by gold nanoparticles and polymer. The circle in the inset (corresponding approximately to the size of the nanoparticles) is 14 nm in diameter.

Identification of the polymer in the SEM images was performed by destroying using focused electron beam; also samples without gold nanoparticles, without polymer as

well as uncoated gold electrodes were studied. The figure shows that LbL deposition resulted in the formation of a rough polymer layer impregnated by gold nanoparticles.

The procedure of LbL deposition was optimized by using surface plasmon resonance monitoring. Typical results for the SPR shift at different steps of the LbL deposition procedure are shown in fig.3.27.

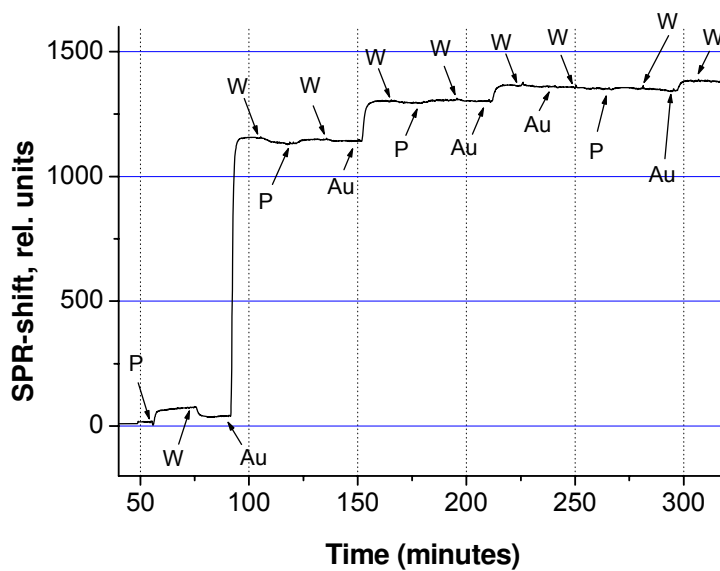


Fig. 3.27. Surface plasmon resonance (SPR) monitoring of the formation of nanocomposite layer from polyacrilic acid and gold nanoparticles on the gold surface. The letters W, P and Au indicate the beginning of perfusion of the SPR cell with water (W), polyacrilic acid (P) and suspension of gold nanoparticles (Au).

Optimization of the deposition demonstrated, that it is not necessary to use  $\omega$ -terminated thiolated compounds to get defined surface charge of the gold surface: an immersion of the uncoated gold electrode in polyacrilic acid in alkaline pH at open circuit potential provides irreversible adsorption of this polymer. Probably, the surface charge of the gold is positive at such conditions. This explains also the next step of the deposition - very strong adsorption of gold nanoparticles on the polymer coated gold surface. A further rinsing with water demonstrated that this adsorption is also irreversible. This cycle of subsequent deposition of the polymer and nanoparticles was repeated several times, the SPR effect was less and less pronounced for each consecutive cycle. One has to take into account that because of very high signal

changes, the relation between reflecting light and shift of SPR angle was not linear, which lead to about 50% decrease of sensitivity at high signal values. However, this non-linearity has no influence on the qualitative conclusion drawn above. It is also important to stress that no gold deposition was observed if the polyacrilic acid deposition step was omitted in the LbL deposition cycle.

After optimization of the nanoparticles deposition procedure by means of SPR monitoring, the same procedure was used for coating of thin layer gold electrodes fabricated on the surface of oxidized silicon wafer. Three cycles of the deposition of polyacrilic acid and gold nanoparticles led to the formation of characteristic gold luster on the surface of oxidized silicon. With a microscope, it was possible to see optical changes also on the surface of the gold electrode (Fig. 3.28). An increase of the number of cycles till eight led to the formation of visually perfect gold layer on the surface of silicon oxide; a high electrical conductivity of this layer in lateral direction was measured. However, because of decreasing of stability at increasing number of layers, gold electrodes modified by three cycles of deposition of gold nanoparticles and polyacrilic acid were used in the electrochemical part of our work.

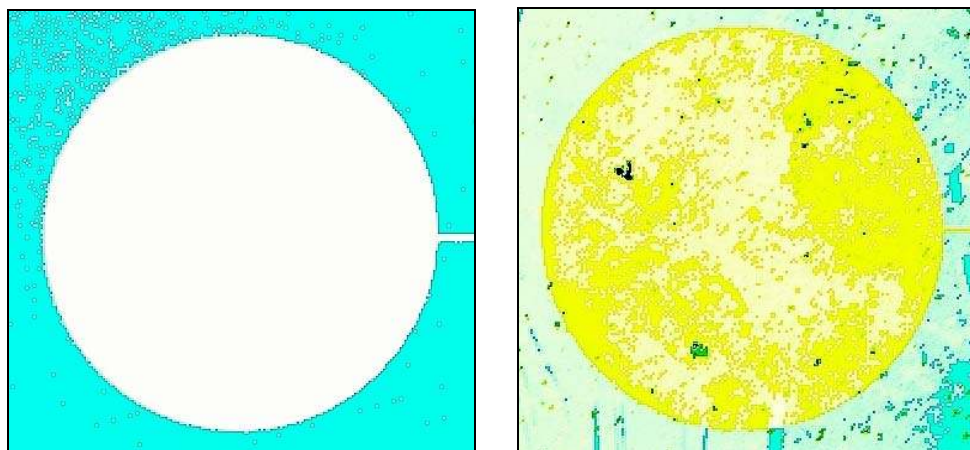


Fig. 3.28. Thin layer of gold (a circle and a 10  $\mu\text{M}$  wide connection wire) on the surface of oxidized silicon wafer before (left) and after (right) three deposition cycles including consecutive adsorption of polyacrilic acid and immobilization of gold nanoparticles. See text for details.

***Electrochemical oxidation of glucose on electrodes coated by gold nanoparticles.***

The voltammetric curve of bare gold electrode measured in 0.1 M NaOH (Fig. 3.29, curve 1) demonstrated typical gold oxidation/reduction behavior usually associated to formation and reduction of gold oxide<sup>185</sup>. Very similar voltammetric curve but with a higher current was observed for the gold electrodes coated by gold nanoparticles (Fig. 3.29, curve 3). In the presence of glucose, an additional oxidation starting at 0.2 V appeared (Fig. 3.29, curve 2). The same curve measured with gold nanoparticles coated electrode (Fig. 3.29, curve 4), showed much more pronounced glucose oxidation currents.

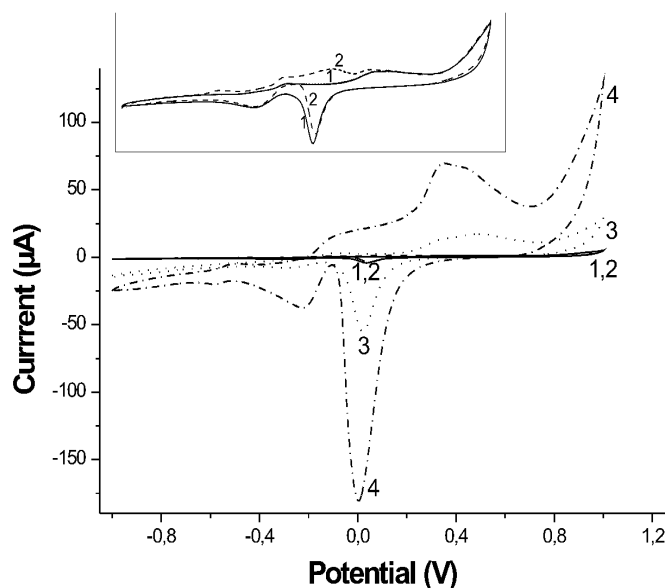


Fig. 3.29. Voltammograms of uncoated gold electrodes (curves 1, 3) and gold electrodes coated by a layer consisting from polyacrylic acid and gold nanoparticles (curves 2, 4) in 0.1 M NaOH in the absence (curves 1, 2) and in the presence (curves 3,4) of 0.5 mM glucose. Sweep rate: 20 mV/s. Inset: curves 1 and 2 with magnification of the current scale.

It was further observed that the application of the potential sweep between -1.0 V and +1.0 V leads to irreversible changes in voltammograms. Therefore, the

potential sweep was limited to the range from  $-0.1$  V to  $+0.4$  V. The voltammetric signals observed at such conditions were essentially different. Potential sweep to the anodic direction resulted in oxidation peak at about  $+0.24$  -  $+0.28$  V. No negative reduction peak was observed during the potential sweep in the cathodic direction. Instead, a second positive peak at the potential of about  $+0.12$  V was observed. The concentration dependence of electrochemical signals associated with glucose oxidation (Fig. 3.30) was studied in the medically important concentration range between  $0.5$  mM and  $8$  mM with  $0.5$  mM step. The heights of both peaks were found to be linearly dependent on the glucose concentration (Fig. 3.31), the correlation coefficients being  $0,987$  and  $0,989$  for the peaks at anodic and cathodic directions of the potential scans correspondingly. These linear dependencies can be used as calibrations for analytical applications.

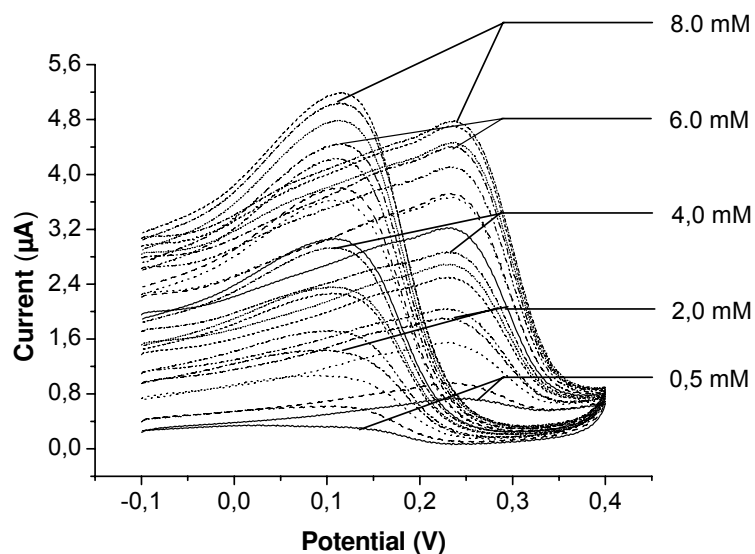


Fig. 3.30. Cyclic voltammograms of the gold electrodes coated by gold nanoparticles measured in  $0.1$  M NaOH with concentrations of glucose varying from  $0.5$  mM to  $8$  mM with a step of  $5$  mM. Sweep rate:  $50$  mV/s

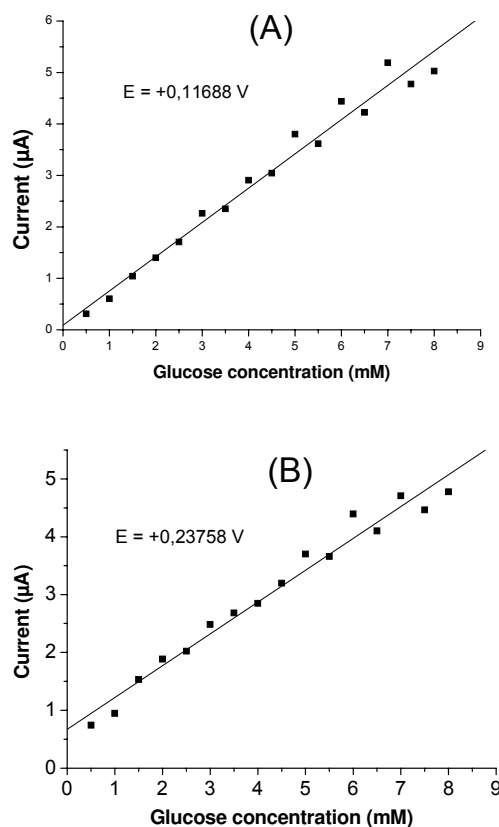


Fig 3.31. Dependence of the currents measured at cathodic direction of the potential sweep at the potential +0.117 V (A) and at the anodic direction of the potential sweep at the potential +0.238 V (B). The measurement conditions are indicated in Fig. 3.27.

### ***Potentially dependent current blockage***

The physical reason for the appearance of oxidation peak during cathodic direction of the potential sweep can be in the electrical blockage of the electrode surface by not-conductive gold oxide forming at potentials higher than +0.3 V. This insulating layer leads also to the decrease of the oxidation current during the potential sweep to anodic direction. Such effect was discussed earlier for glucose oxidation on bare gold electrodes<sup>187</sup>. In the case of gold electrodes coated by gold nanoparticles, this effect may be much more significant: electrons should tunnel not only through oxide layer on the electrolyte-metal interface but also through oxide layer of about double thickness between nanoparticles and metal (Fig. 3.32).

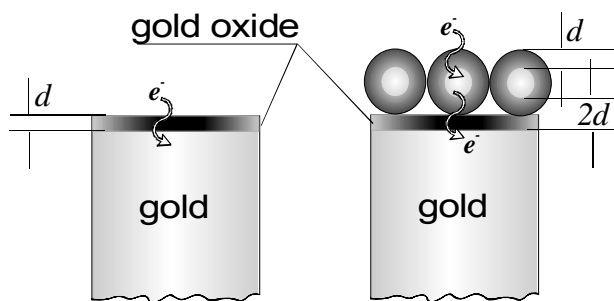


Fig. 3.32. Formation of insulating gold oxide on all gold surfaces leads to longer tunneling distance and therefore to higher resistance increase for the gold electrodes coated by gold nanoparticles.

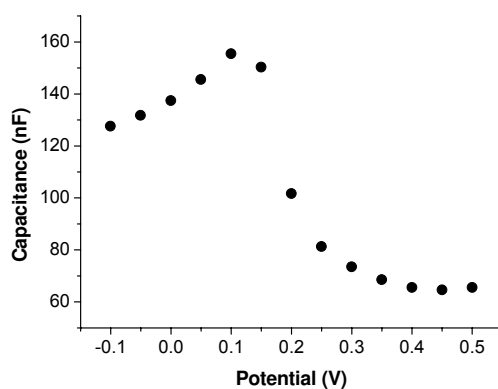
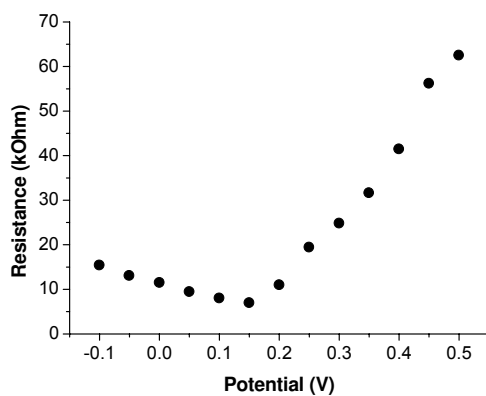


Fig. 3.33. Dependence of the resistance (left) and capacitance (right) of the gold electrodes coated by polyacrylic acid and nanoparticles on the electrode potential.

The blocking effect of anodic potential was studied directly, by impedance spectroscopy. To exclude a complicated analysis of equivalent circuits and numerous assumptions required for such analysis, we suggested that the active component of the current at 5 Hz is caused by the electrode resistance while the reactive component at 10 kHz is caused by the electrode capacitance. The results of such simplified analysis are presented in Fig. 3.33. Increase of the electrode resistance and decrease of the electrode capacitance indicate to the formation of insulating layer on the electrode surface. Most probably this layer consists of gold oxide.

### ***Selectivity aspects***

Glucose analysis in biological liquids is performed mainly in blood or urine. Most physiological components of these liquids are not electrochemically active in the potential range used in the glucose sensor (-0.1 - +0.4 V); the only exceptions are probably glucose and uric acid. Because of this reason, the electrochemical activity of uric acid on the gold nanoparticles modified gold electrodes was studied and compared with the electrochemical activity of glucose. Changes of voltammograms induced by introduction of glucose or uric acid are presented in fig. 3.34. The electrochemical signal of uric acid has usual monotonous shape; the current is almost zero if the electrode potential does not exceed +0.15 V. The concentrations of glucose in blood and urea are respectively 3 - 8 mM and below 0.5 mM while these values for urine are respectively below 0.65 mM and 1.2 - 6 mM<sup>196</sup>. Comparing these values with the experimental data (Fig. 3.34), we conclude that uric acid should not interfere the measurements in blood. Oppositely, the measurements of glucose in urine by this method seem not to be appropriate due to strong interference of uric acid. Possible influence of non-biological substances (drugs, food additives, etc.) which can be also presented in blood demand a further investigation.

The peak of glucose oxidation observed at the cathodic direction of the potential sweep is especially interesting for analytical applications. First, it is observed at very low potentials thus decreasing the number of possible interferents. Second, the current at the peak potential is about zero in the absence of glucose



(Fig. 3.31A). This makes possible the application of the techniques of standard additions for glucose analysis.

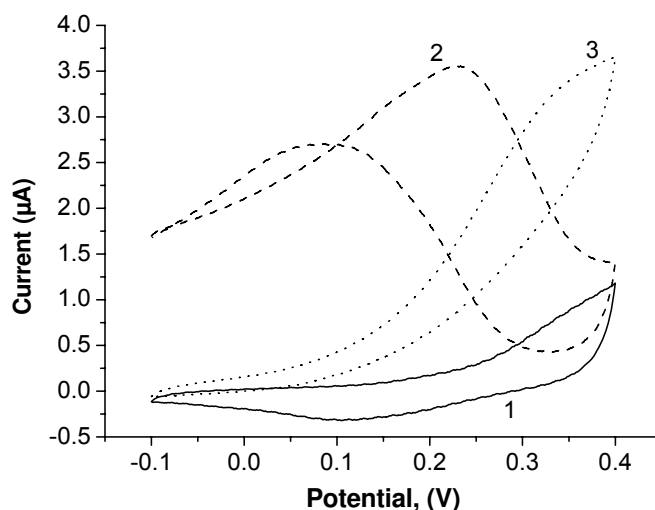


Fig. .3.34. Cyclic voltammograms of the gold electrodes coated by gold nanoparticles measured in 0.1 M NaOH (1), in 0.1 M NaOH in the presence of 3 mM glucose (2) and in 0.1 M NaOH in the presence of 3 mM uric acid (3). Sweep rate: 50 mV / s.

### 3.6 Detection of dopamine

Dopamine belongs to the group of catecholamine and plays an important role in the function of central nervous, renal, hormonal and cardiovascular systems<sup>197,198</sup>. Its deficiency can lead to brain disorders such as Parkinson's disease or schizophrenia<sup>199-201</sup>. The development of methods for dopamine quantification in blood and biological fluids has received much attention in recent investigations. Different attempts have been made to develop electrochemical detection of dopamine using electrodes with various types of surface modification: chemically modified electrodes<sup>202-209</sup>, electroactive polymer modified electrodes<sup>210-221</sup> and nanoparticles modified electrodes<sup>221-226</sup>. The testing of various modified electrodes for the dopamine oxidation reaction relates to the following problems:(a) fouling of the surface of conventional electrodes due to the absorption of oxidation products which results in poor reproducibility, (b) interfering reactions due to the co-existence of other analytes and mainly of ascorbic acid in the biological fluids which undergo

oxidation in a similar potential range, and (c) high concentration of the interfering analytes in comparison to dopamine (e.g. the concentration of ascorbic acid is about 1000 times higher than that of dopamine), resulting in poor selectivity and sensitivity for dopamine detection.

The detection of dopamine in the presence of excess of ascorbic acid and the development of a sensor with good selectivity, sensitivity and reproducibility is still a challenging task in the electroanalytical research. In this work, we report on the use of gold nanoparticles modified electrode for detection of dopamine in the presence of ascorbic acid in aqueous solutions. In the previous work on dopamine detection by means of gold nanoparticles modified electrodes the nanoparticles immobilization was performed by means of amine<sup>222</sup> or sulfhydryl<sup>223</sup> terminated self assembled monolayer, by embedding in a poly(3,4-ethylenedioxythiophene)<sup>221</sup> or poly-(4-aminothiophenol)<sup>224</sup> films or by mixing in a carbon paste<sup>226</sup>.

In our investigation gold nanoparticles are deposited on the surface of a gold electrode using the Layer by Layer technique. The general idea was to incorporate the gold nanoparticles into a negatively charged matrix<sup>205</sup> thus combining fast electron transfer kinetics on the surface of the gold nanoparticles<sup>227</sup>, electrostatic discrimination of negatively charged species (e.g. ascorbate ions) and increase in the local concentration of the positively charged analyte (dopamine) near the sensor surface. A similar approach was attempted by embedding gold nanoparticles into a conducting polymer matrix with hydrophilic (charged) and hydrophobic (neutral) regions<sup>221</sup>. However, the intrinsic electroactivity of conductive polymers is in the origin of high pseudocapacitive current which may affect the sensitivity of these materials. In our investigation this problem is overcome by using an inert polymeric material without intrinsic electroactivity.

### ***Procedure of the experiment***

Hydrogen tetrachloroaurate(III) hydrate was obtained from Chem Pur. Polyacrylic acid (M.W.500 - 1000 kD) and Nafion-117 solution (5%, in the mixture of lower aliphatic alcohols and water) were from Fluka. Sodium citrate, dopamine, sodium acetate, acetic acid, monosodium hydrogen phosphate, and disodium

hydrogen phosphate were from Merck, ascorbic acid and other chemicals were from Sigma-Aldrich. All reagents were of analytical grade. Deionized water was purified using Millipore Milli-Qsystem (18.2 M $\Omega$ ) and used in all preparations.

The preparation of gold nanoparticles was performed according to the classical procedure<sup>17</sup>. Shortly, 1 mL of 1% sodium citrate is added into 10 mL of boiled 1 mM aqueous solution of HAuCl<sub>4</sub> under intensive stirring. In several minutes the color of the solution changes from yellow to colorless, then dark blue, dark red and finally red wine color; at this moment the solution was cooled. The obtained suspension of nanoparticles was stored at room temperature and used within several days. The optical absorbance of the gold plasmon band in the suspension is about 1.5 at the spectral maximum (519 nm). A UV-vis spectrophotometer CARY 50 Bio was used for this measurement. Scanning electron microscopy (SEM) was performed by LEOSUPRA 35.

The gold electrodes were prepared by RF-sputtering on a glass or silicone support with adhesive chromium sub-layer resulting in about 250 nm thick gold layers. The electrodes were disk-shaped with a macroscopic area of 0.385 mm<sup>2</sup> connected to a contact pad by a contact line of 8 mm length and 10  $\mu$ m width. Other details are described in<sup>228</sup>. The deposition of gold nanoparticles was performed by Layer by layer (LbL) technique: the gold electrode was immersed into the freshly prepared 0.2% (w/w) solution of polyacrylic acid (pH 10) for 30 minutes, rinsed in water, immersed into the suspension of the gold nanoparticles for 15 minutes, and rinsed with water again. This cycle was repeated three times. The quality of the electrode surface was controlled by optical microscopy. Further in the text these electrodes will be termed nano-Au electrodes.

Most of the electrochemical measurements were performed by an AUTOLAB PGSTAT-13 electrochemical workstation (Eco Chemie, The Netherlands); the measurements at fast sweep rate were performed by a CH Instruments (USA) potentiostat 602 A. Standard three electrode electrochemical cell was used. The electrode assembly consisted of a bare or modified Au electrode as working electrode, a Pt wire as counter electrode, and Ag/AgCl (sat) as reference electrode. The potentials are indicated relative to this reference electrode. The measurements were performed in 0.1 M phosphate buffer, pH 7 or 0.2 M acetate buffer, pH 4 at

22°C. Before use the electrodes were cleaned electrochemically in the buffer solution by applying of a single potential scan from -0.1 V to 3 V with 50 mV/s.

Surface plasmon resonance (SPR) monitoring of the gold surface was performed by a SPR-reflectometer Biosuplar-321 from Mivitec GmbH / Analytical  $\mu$ -System ([www.biosuplar.com](http://www.biosuplar.com)) in the tracking mode; the laser wavelength was 650 nm. The SPR signals were recalculated into changes of refractive index; calibration with KCl solutions was used. Gold-coated SPR slides were connected to the potentiostat for simultaneous SPR spectroscopy and cyclic voltammetry; the potential applied to the gold coated SPR-slide was cycled from -0.1 V to 0.4 V in the phosphate buffer (pH 7.0) or from 0.0 V to 0.5 V in the acetate buffer (pH 4.0) with sweep rate of 5 mV/s.

Nafion deposition was performed from a mixture of Nafion-117 solution (5%) with isopropanol (1:2 v/v) by setting a droplet on the nano-Au electrode. After evaporation, the Nafion film was treated first at 80°C for 12 h, then at 130°C for 30 min. The thickness of the Nafion layer, estimated by the shift of the focus plane of visual microscope, was about 1  $\mu$ m.

### ***Results and discussion***

#### ***a. Electrochemical behavior at neutral pH***

Fig. 3.35 shows consecutive voltammetric curves obtained by means of the nano-Au electrode in the presence of dopamine in phosphate buffer at pH=7. The gradual inhibition in both oxidation and reduction reactions indicates the loss of electroactivity of the investigated electrode. The initial voltammetric curve could not be recovered even after transfer of this electrode back into phosphate buffer (in the absence of dopamine) and continuous cycling. Usual electrochemical methods to clean the electrode surface by high cathodic (-1 V) or high anodic (+2 V) potentials did also not help the electrode recovery.

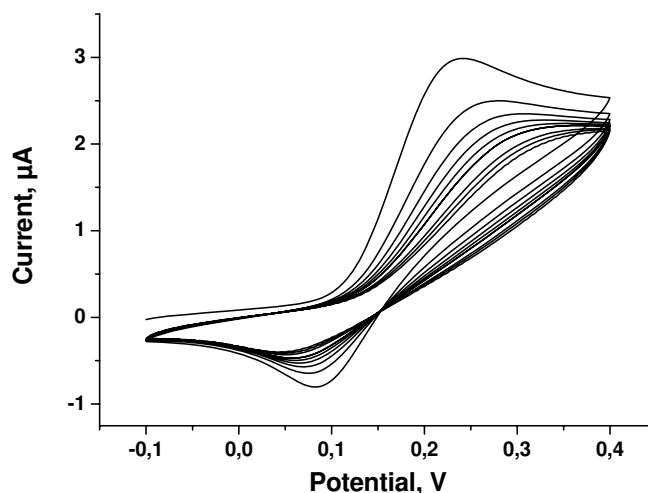


Fig. 3.35. Ten cycles of cyclic voltammograms measured with a gold electrode modified by gold nanoparticles. Electrolyte: 2 mM dopamine in 0.1 M phosphate buffer, pH 7. The curve with the highest reduction and oxidation currents was observed during the first cycle; in each next cycle the current was smaller.

The irreversible behavior of the nano-Au electrode can be due either to some changes in the multilayer structure (for example, desorption and loss of gold nanoparticles) or to irreversible adsorption of dopamine oxidation products on the gold surface. This question was addressed by means of simultaneous SPR and voltammetric measurements, performed on a gold-coated SPR slide in the presence of dopamine. For synchronization of the devices, the sweep rate was decreased to 5 mV/s. The results demonstrated irreversible changes in the SPR signal (Fig. 3.36), corresponding to an increase in the refractive index near the surface by  $2.9 \cdot 10^{-3}$  units in the first cycle. To calculate the thickness of the adsorbed layer, data on its refractive index are needed. Assuming that the layer's refractive index is close to the typical values for dopamine, phenol polyphenol and pyrocatechines (1.55 - 1.63), the layer thickness is estimated to be about 1 -2 nm. (The calculation is performed according to<sup>229</sup> ). The estimation of the adsorbed layer's thickness based on the oxidation charge, by assuming one electron per one oxidized dopamine molecule and 1 g/mL density<sup>230</sup> , gives a value for the thickness of about 50 nm. The difference in these two values can be explained by the following reasons: (i) only a small

amount (few percent) of the primary dopamine oxidation products forms the insulating film, (ii) the formation of the insulating film from the primary dopamine oxidation product is an oxidation process resulting in the release of additional electrons, therefore the total stoichiometry can be much higher than one. The formation of an insulating layer due to dopamine oxidation was suggested earlier for other types of electrodes<sup>219,220</sup>, but the application of simultaneous SPR- and electrochemical measurements allowed us to observe this process directly and to make quantitative characterization of this layer.

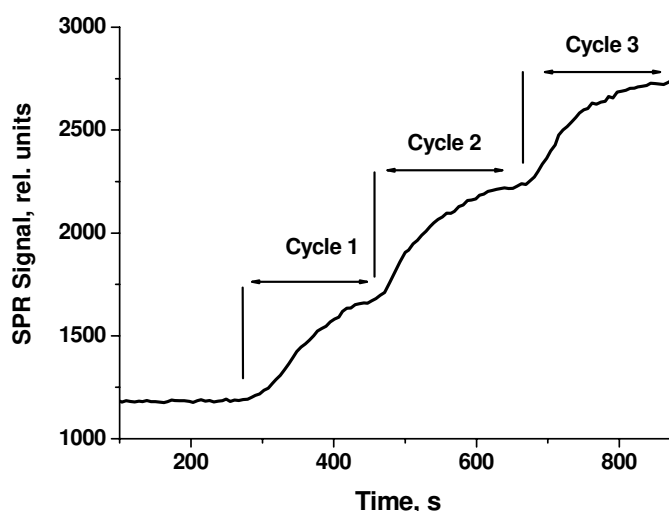


Fig. 3.36. Changes in the surface plasmon resonance signal monitored during the cycling of a non-modified gold electrode in the presence of 2 mM dopamine in 0.1 M phosphate buffer solution at pH 7.

The irreversible behavior, observed in the course of the dopamine oxidation, diminishes in each subsequent voltammetric cycle. Electrode conditioning, performed by means of 5 cycles, decreases the signal loss to 1.4% per cycle. A deposition of a Nafion is often considered as an almost universal coating against undesirable adsorption. However, a coating of nano-Au electrode by Nafion did not lead to any decrease in the fouling. Moreover, this coating resulted in essential loss of electrocatalytical activity, shift of the dopamine oxidation peak to higher anodic potentials and disappearance of the corresponding reductive peak. The loss of the activity of the Nafion coated electrode is presented in Fig. 3.37 (squares), the effect

was 57% signal loss for the first 10 cycles, and 2.8% signal loss per cycle after the 5-th cycle. An effective way to diminish the electrode fouling is the increasing in the sweep rate<sup>231</sup>. This approach turned out to be effective also for the nano-Au electrodes (Fig. 3.37, triangles) - the loss of the signal during the first 10 cycles was below 23%. For the electrode which was conditioned by 5 cycles, the loss of the signal was below 0.8% per cycle. Such loss of the sensor activity can be tolerated in the most biological applications. One can expect that further increase in the sweep rate can exclude the irreversible behavior of the nano-Au electrode almost completely.

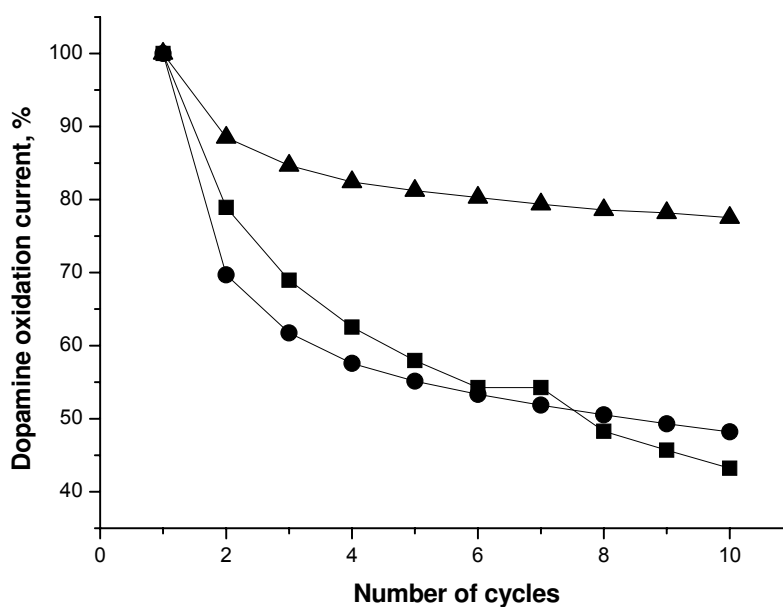


Fig. 3.37. Decrease of the dopamine oxidation current in ten subsequent cycles of potential sweep. The current values correspond to oxidation peaks, the current of the first cycle was considered as 100%. The measurements were performed in the presence of 2 mM dopamine in 0,1 M phosphate at pH 7.0 for the electrodes with gold nanoparticles immobilized by LbL deposition with polyacrylic acid without coating (● and ▲) and with coating by Nafion (■) at sweep rate of 50 mV/s (● and ■) or 10 V/s (▲).

**b. Electrochemical behavior at pH 4**

Fig. 3.38 shows voltammograms measured on the nano-Au electrode in the presence of dopamine in acetate buffer at pH 4. In contrast to the measurements at pH 7 (Fig. 3.35), the consecutive voltammetric cycles are almost coinciding and show that no fouling of the electrode surface occurs in this solution. Both oxidation and reduction peaks are well resolved and can be used for quantitative electroanalytical determination of dopamine in electrolytes.

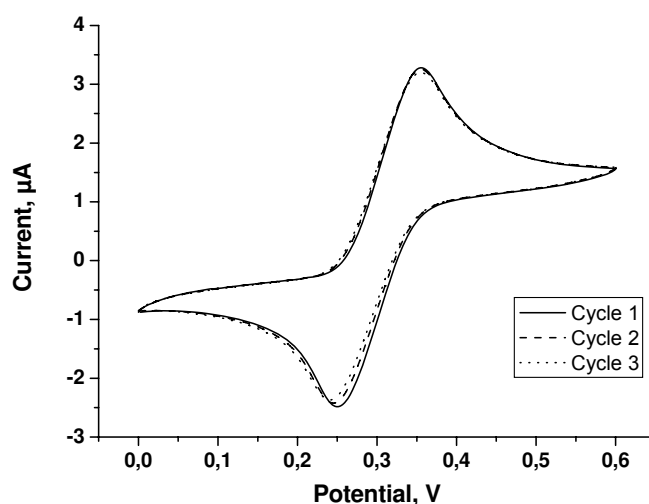


Fig. 3.38. Cyclic voltammograms measured by gold electrode modified by gold nanoparticles in the presence of 2 mM dopamine in 0.2 M acetate buffer solution, pH 4.

The absence of fouling effects on the gold surface during the dopamine oxidation at pH 4 was also confirmed by SPR measurements. The SPR signal (Fig. 3.39) measured in the course of potentiodynamic cycling in 0.2 M acetate buffer on a gold-coated SPR slide indicates a reversible electrochemical process. The magnitude of the irreversible component per cycle is about 100 times smaller than at pH 7; an estimation of the mean effective thickness of the layer of the oxidized dopamine species on the electrode surface, based on the same assumption as for pH 7, gives a value for the adsorbed layer's thickness of only 10 pm per cycle. Thus, in this case almost no poisoning of the gold surface occurs: the electrochemical measurements



do not indicate the formation of an insulating film and the SPR measurements do not indicate the formation of a layer with refractive index different from water.

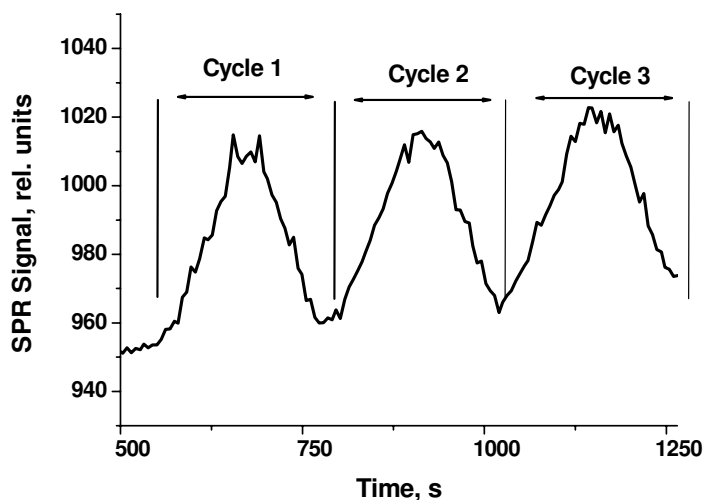


Fig. 3.39. Changes in the surface plasmon resonance signal monitored during the cycling of a non-modified gold electrode in the presence of 2 mM dopamine in 0,2 M acetate buffer at pH 4.

### ***c. Comparison of bare gold electrodes and gold electrodes modified by gold nanoparticles.***

The electrocatalytical behavior of a given electrode material can be observed as a decrease in the reaction polarization (decrease in the overvoltage) or as an increase in the reaction current. The behavior of the latter type was observed in the case of dopamine oxidation at the nano-Au electrode. In such a case a comparison of the electrode areas with and without catalyst becomes critical. In order to estimate the catalyst surface, the nano-Au electrodes were studied by SEM. The results demonstrated that the surface density of gold nanoparticles on the electrode surface is  $3.3 \cdot 10^{15}/\text{m}^2$  and the mean diameter is 14 nm. Taking into account the total surface of the gold nanoparticles, the electrode surface area should be increased by a factor of two. However, the nanoparticles are distributed along the polymer chains which are several thousands times longer than the size of nanoparticles, but only the nanoparticles which are placed within the electron tunneling distance from the electrode surface ( $< 0.5$  nm) can be electrochemically active. Also, due to the contacting of the nanoparticles to the macroscopic gold electrode substrate, some

part of their surface gets lost for the oxidation reaction. Additionally, adsorption of the inert non-conductive polymer on the surfaces of the gold nanoparticles and the macroscopic gold electrode, leads to further decrease in the electrochemically active surface. This discussion demonstrates that only a decrease in the electrochemically active electrode area after the LbL deposition of the gold nanoparticles should be expected.

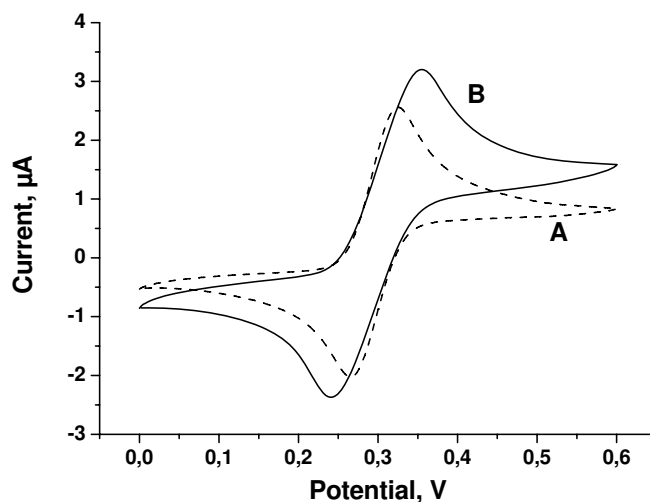


Fig. 3.40. Voltammograms measured in presence of 2 mM dopamine in 0,2 M acetate buffer at pH 4 using non-modified gold electrode (A) and gold electrode modified by gold nanoparticles (B).

Fig. 3.40 shows voltammetric curves measured in the presence of dopamine by non-modified gold electrodes and by nano-Au electrodes. The higher oxidation currents, observed on the Au-nano electrode, should be attributed to the effect of the catalytically active gold atoms<sup>228</sup> on the surface of the nanoparticles. An additional effect contributing to the higher electrochemical activity of the nano-Au electrode is an electrostatic interaction between the positively charged dopamine species and the slightly negatively charged polyacrylic matrix resulting in an increase in local concentration of dopamine near the electrode surface.

One of the main substances interfering with the electrochemical detection of dopamine is ascorbic acid. For that reason further experiments were performed to test electrochemical activity of the nano-Au electrode with respect to the oxidation of this analyte. Comparison of the voltammetric curves (Fig. 3.41), measured in the

presence of ascorbic acid on the macroscopic gold electrode and the nano-Au electrode shows almost no difference between the performances of these electrodes. In fact, the oxidation currents measured on the pristine Au electrode are slightly higher in the almost entire potential window for both forward and reverse scans. Therefore, the electrocatalytic effect of the gold nanoparticle either does not occur for oxidation of ascorbic acid or there is an additional effect inhibiting its oxidation on the nano-Au electrode. Considering the charge distribution on the electrode surface consisting of the gold nanoparticles and the negatively charged polymer (polyacrylic acid) and bearing in mind that the ascorbate anion is also negatively charged, an electrostatic repulsion and thus a limited access of this interferent to the surface of the gold nanoparticles is expected. The same mechanism was earlier suggested for exclusion of anionic interferents by coating with Nafion<sup>232</sup>.

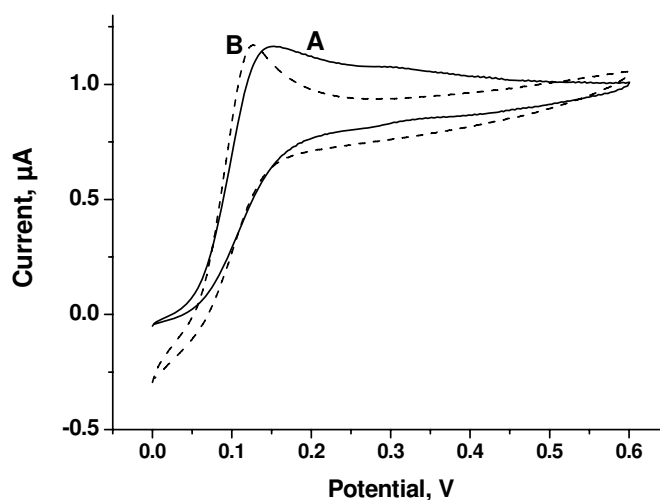


Fig. 3.41. Voltammograms measured in presence of 2 mM ascorbic acid in 0,2 M acetate buffer at pH 4 using non-modified (A) gold electrode and gold electrode modified by gold nanoparticles (B).

#### ***d. Selectivity of dopamine detection.***

A comparison of the voltammetric scans measured in 2 mM solutions of ascorbic acid (Fig. 3.41) and of dopamine (Fig. 3.40) shows that the oxidation peaks due to both analytes are resolved by about 240 mV. At equal concentrations of both substances the dopamine oxidation peak is about three times higher than the oxidation peak of the ascorbic acid. It is to note that a reduction peak on nano-Au

electrode is observed only for the dopamine reaction and therefore it can be also used (instead of the corresponding oxidation peak) for quantitative detection of dopamine in the presence of ascorbic acid.

Fig. 3.43 shows voltammograms measured by the gold electrodes modified by gold nanoparticles at various concentrations of dopamine in the absence of ascorbic acid. The oxidation currents (measured at  $E=0.36$  V) and the reduction currents (measured at  $E=0.24$  V) are plotted against dopamine concentration (Fig. 3.44 and fig 3.45 respectively). Both signals demonstrate linear concentration dependence in the whole studied concentration range (4-40  $\mu$ M).

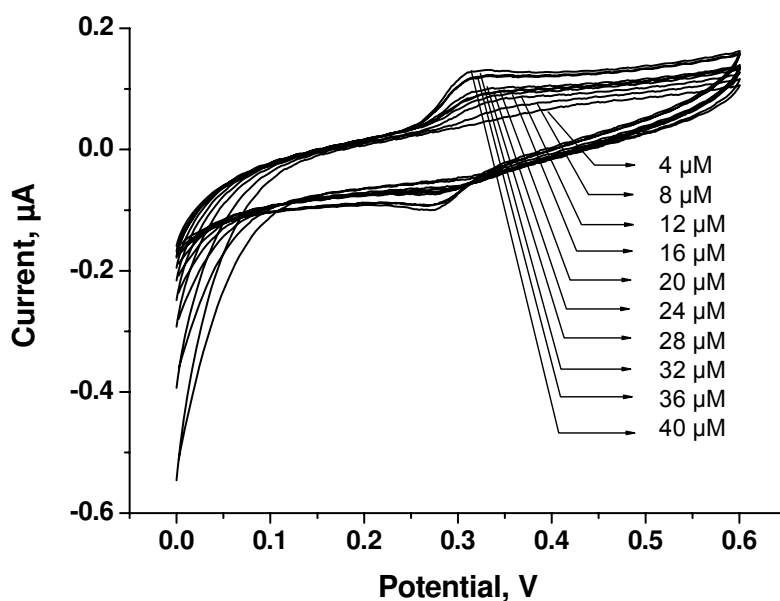


Fig. 3.43. Voltammograms measured on the gold electrodes modified by gold nanoparticles at various concentrations of dopamine in 0,2 M acetate buffer at pH 4 in the absence of ascorbic acid.

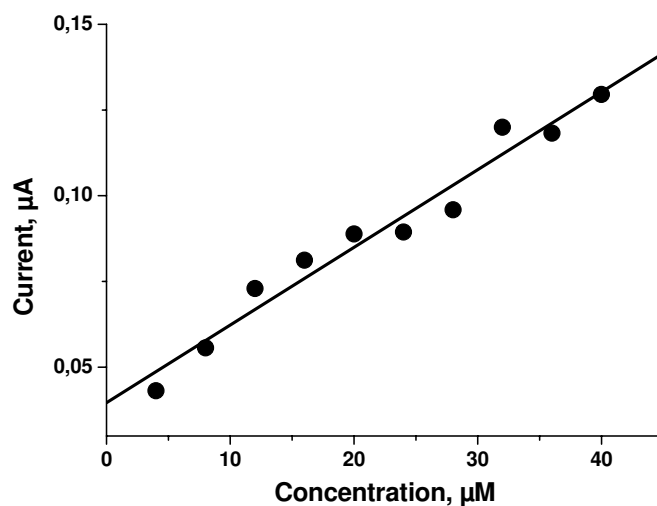


Fig. 3.44. Concentration dependence of the dopamine oxidation peak measured at 0.36 V in 0,2 M acetic buffer at pH 4 in the absence of ascorbic acid (data from fig. 3.43).

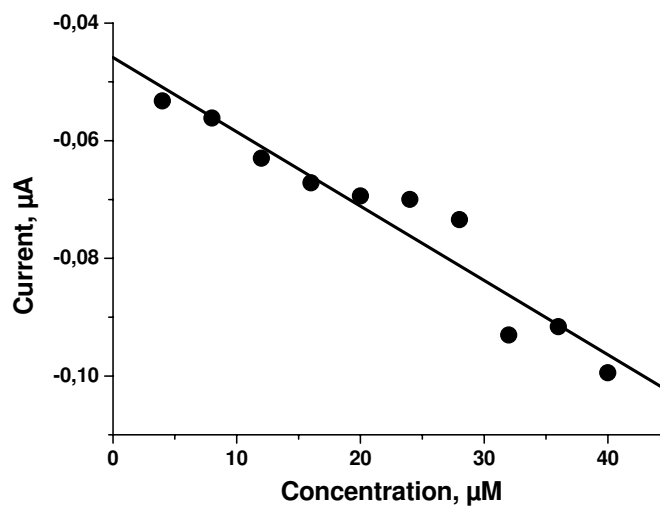


Fig. 3.45. Concentration dependence of the dopamine oxidation peak measured at 0.24 V in 0,2 M acetic buffer at pH 4 in the absence of ascorbic acid (data from fig. 3.43).

A similar series of voltammetric measurements was performed at various concentrations of dopamine (from 4 to 40  $\mu\text{M}$ ) in the presence of 1 mM ascorbic acid (Fig. 3.46). The mechanism of the inhibition of ascorbic acid oxidation by much smaller concentrations of dopamine is not clear but this process does not affect the electrochemical activity of dopamine. The plots of the dopamine oxidation (at  $E=0.36$  V) and reduction (at  $E=0.24$  V) currents against dopamine concentration (Fig. 3.47 and fig 3.48 respectively) show linear concentration dependences in the whole studied concentration range (4-40  $\mu\text{M}$ ).

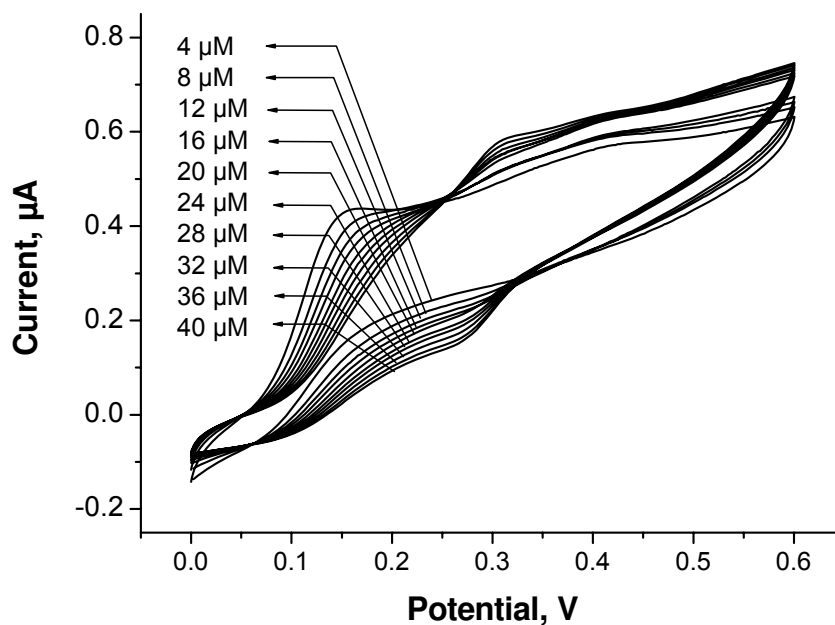


Fig. 3.46. Voltammograms of gold electrodes modified with gold nanoparticles measured in 0,2 M acetic buffer at pH 4 in the presence of 1 mM of ascorbic acid at various concentrations of dopamine.

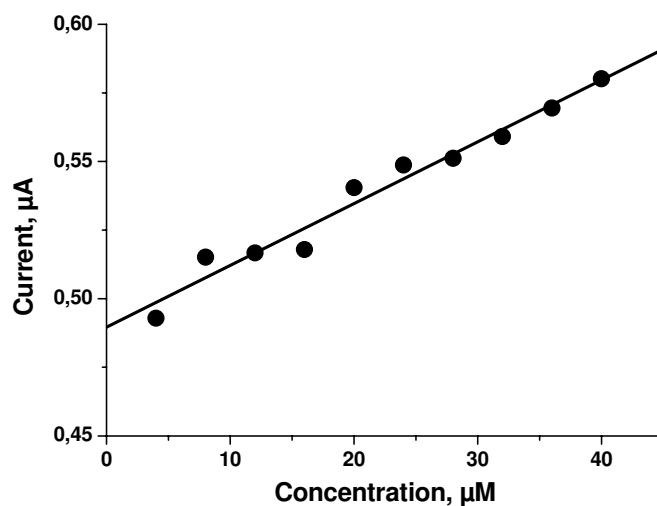


Fig. 3.47. Concentration dependence of the dopamine oxidation peak measured at 0.36 V in the presence of 1 mM ascorbic acid in 0,2 M acetic buffer at pH 4 (data from Fig. 12).

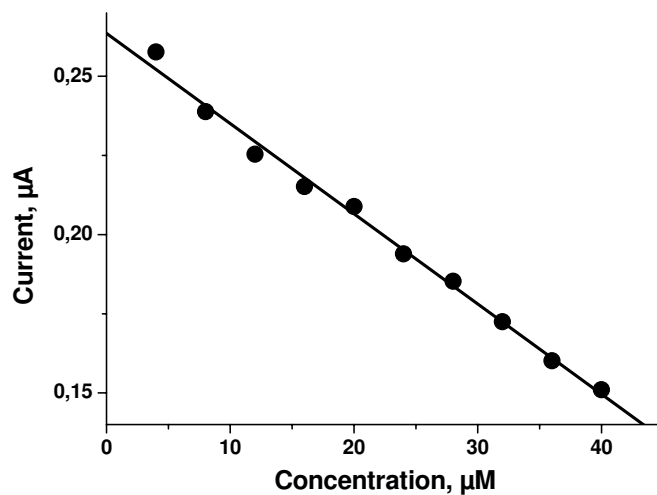


Fig. 3.48. Concentration dependence of the dopamine reduction peak measured at 0.24 V in the presence of 1 mM ascorbic acid in 0,2 M acetic buffer pH 4 (data from Fig. 12).

### **3.7 Nanoparticles as nucleation centers for protein crystallization**

Biochemical functions of proteins are closely related to their molecular structure. Common techniques for determination of the protein structure include X-ray crystallography and NMR spectroscopy. These methods provide atomic resolution of the protein molecules in solid and liquid state, respectively. Before analysis, proteins need to be crystallized, and exactly this step is the main barrier for analysis of a number of proteins by X-ray crystallography techniques. Additionally, crystallization is a way to obtain ultrapure protein samples, it makes this approach important for different fields of biological science and biotechnology.

Crystallization of proteins includes nucleation and crystal growth. During the nucleation stage, the solute protein molecules dispersed in the solvent start to gather into clusters and form stable nuclei. These clusters are stable only if they reached some critical size; smaller clusters tend to dissolve. This size depends on physical conditions, such as temperature<sup>233,234</sup> and pressure<sup>235</sup>, and on protein concentration. Once the critical size is reached, the protein crystal is growing spontaneously so long as the solution is in the supersaturated state. Different aspects of protein crystallization have been studied. For examples, an influence of temperature gradient<sup>233,234</sup>, ultrasonic treatment<sup>236,237</sup>, magnetic<sup>238,239</sup> or electric fields<sup>237,239,240</sup> were studied. Other efforts were focused on the search for a suitable nucleant in order to reduce the nucleation energy barrier<sup>241,242</sup>. However, no effective nucleation agent for crystallization of different types of proteins was suggested so far.

In the present work we demonstrated for the first time that gold nanoparticles are effective nucleants for crystallization of proteins. This system was tested with two model proteins of very different structure: Hen-Egg-White Lysozyme (HEWL) and ferritin in apo- and holo- form. Last years gold nanoparticles were used for different applications<sup>13</sup> including (electro)catalysis<sup>243</sup>, development of chemical sensors<sup>228</sup>, amplification of signals in bioanalytics<sup>244,245</sup> or generation of plasmonic effects<sup>246,247</sup>. This paper describes a new application of this system.



**Result**

Preliminary semi-quantitative experiments using the droplet method showed a drastic increase of the nucleation number of HEWL in the presence of gold nanoparticles. No lysozyme crystals were observed if HEWL crystallization solution (25 mg/mL) is incubated for 30 days at 20°C in the absence of gold nanoparticles. The presence of gold nanoparticles leads to the formation of about 40 crystals/cm<sup>2</sup> at the same condition. Similar results were obtained with ferritin. The crystals of lysozyme and ferritin formed in the presence of uncoated gold nanoparticles are presented in the Fig. 3.49.

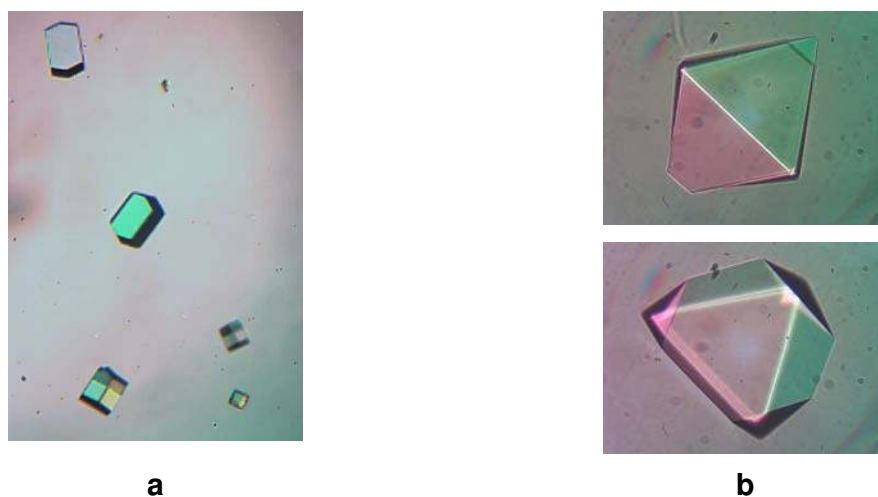


Figure 3.49 . Images of lysozyme (a) and ferritin (b) crystals formed from supersaturated aqueous solutions in the presence of uncoated gold nanoparticles. The images were obtained by differential interference contrast microscopy.

Crystallization with double pulse technique<sup>234,237</sup> confirmed quantitatively that uncoated gold nanoparticles as well as nanoparticles coated by alkylthiol with COOH – terminated groups increased significantly the nucleation number of HEWL: the number of crystals was increased from about 180 crystals/cm<sup>2</sup> in the absence of gold nanoparticles until 230 - 280 crystals/cm<sup>2</sup> in the presence of these types of gold nanoparticles (Table 3.1). An incorporation of macroscopic pieces of gold wire into

the cell does not induce HEWL nucleation, therefore the nucleation effect is caused by some peculiarities of the nanoparticles surface.

Table 3.1. Influence of gold nanoparticles on the nucleation and growth of lysozyme crystals.

experimental technique	number of lysozyme crystals, n/cm <sup>2</sup>		
	without nanoparticles	In the presence of gold nanoparticles	
		uncoated	with –COOH terminated groups
Initial metastable conditions	0	41	47
double pulse technique	180	230	280

The results suggest that namely the gold nanoparticles induce lysozyme and ferritin crystallization. It is well known that a heterogeneous nucleation is thermodynamically much more favourable than the homogeneous one<sup>248</sup>. Probably, proteins form a monomolecular layer on the surface of gold nanoparticles introduced into protein solution. For uncoated nanoparticles this process may be driven by formation of Au-S bonds between thiol groups of methionin of the proteins and gold atoms on the surface of the nanoparticles. For nanoparticles with COOH-terminated coating, such a process can be explained by electrostatic interaction of negatively charged carboxy-groups and some positively charged aminoacids. The difference between gold nanoparticles and macroscopic gold wires may be in the much higher curvature of the nanoparticle surface leading to additional surface energy of bound molecules of the protein monolayer.

Gold atoms are much heavier than the atoms of protein molecules (C, N, S, H, O) and this gives a possibility to observe gold nanoparticles included in or attached to the HEWL crystals. Typically not single gold nanoparticles but aggregates of these

## RESULTS AND DISCUSSIONS

---

nanoparticles were trapped in the smallest protein crystals (Fig.3.50). Also chains of gold nanoparticles were often observed on the surface of HEWL crystals. This confirms the conclusion that the gold nanoparticles or their aggregates effect on nucleation and growth of the lysozyme crystals.

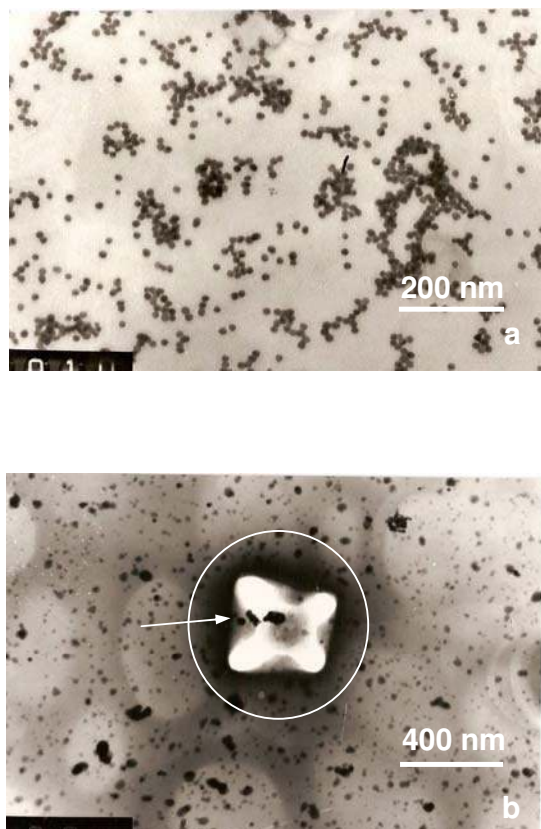


Figure 3.50. TEM images of gold nanoparticles deposited from aqueous suspension (a) and of the nanoparticle inside partially melted lysozyme nanocrystal (marked by by the circle).(b).

To distinguish gold nanoparticles on the surface of the protein crystals, an Energy-Dispersive X-Ray (EDX) investigation was performed (Fig.3.51). The signals of Na and Cl arises from the salt crystallization, the signal of sulfur indicate on the presence of protein.

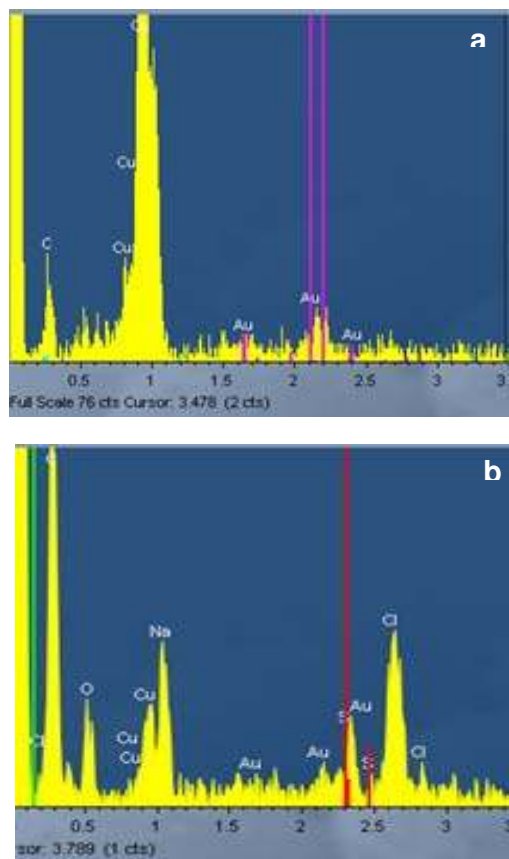


Figure 3.51. EDX analysis of gold nanoparticles deposited from aqueous solution on metal holder (a) and of lysozyme crystallized by gold nanoparticles (b). The presence of Au peaks in (a) and (b) confirm the presence of gold nanoparticles and their aggregates in both probes. Besides the higher Au peaks, peaks of Na and Cl arising from the precipitation agent (NaCl), and S from the protein are observed in (b).

### ***Condition of the experiment***

Most of the experiments have been performed with tetragonal HEWL crystals (50 mM acetate buffer, pH = 4.5) following standard prescriptions. Briefly, the solutions were mixed to obtain 25 mg/ml of lysozyme in 0.5 M NaCl and 70  $\mu\text{g}/\text{mL}$  gold nanoparticles. Similar experiments with ferritin were performed at 0.5 mg/ml of ferritin, 1.6% (w/v)  $\text{CdSO}_4$ , 200 mM acetate buffer, pH=5. The preparation of gold nanoparticles was performed according to the classical procedure<sup>17</sup>. Shortly, 1 mL of 1% sodium citrate is added into 10 mL of boiled aqueous solution of  $\text{HAuCl}_4$  (1 mM)

under intensive stirring. In several minutes the color of the solution changes from yellow to colorless, then to dark blue, dark red and finally to the red wine color; at this moment the reaction was stopped by fast cooling of the solution. The obtained suspension was dialyzed against Millipore water three times each for 24 h at the volume ratio of 1:250. The suspension of gold nanoparticles was stored at room temperature and used within several days. The optical absorbance of the gold plasmon band in the suspension is about 1.5 at the spectral maximum (519 nm), UV Vis spectrophotometer CARY 50 Bio was used. The mean diameter of nanoparticles determined by SEM (LEOSUPRA 35) is about 14 nm; similar values were obtained by dynamic light scattering (Zeta-Sizer from Malvern was used).

Preliminary experiments have been performed in the batch sitting droplet configuration with both HEWL and ferritin crystallization. A direct comparison of the number of the grown protein crystals in the two probes were performed under the same conditions in the presence and absence of the gold nanoparticles. Smaller crystals in the presence of gold nanoparticles are more stable in vacuum environment so they can be easier analyzed by TEM. For this characterization, we performed an experiment by sitting droplet technique directly on the surface of a Formvar film at 13°C for 10 min to obtain small crystals (from 0,1 to 5 µm). The rest of the solution has been removed by filter paper prior to TEM characterization. Similar procedure but with a microscope object holder instead of the Formvar film was used for SEM analyses.

A quantitative study of the crystal nucleation in the presence of gold nanoparticles has been performed in the quasi-two-dimensional glass cells. The nucleation of HEWL crystals takes place in thin (typically 100 µm thick) solution layer that is confined between two glass plates of the cell (Fig.3.52). This cell has a small volume and allows excellent microscopic observations and easy cleaning. Two series of experiments were performed with HEWL in these cells: investigations under metastable conditions (at 20°C) when no nucleation without gold nanoparticles was observed as well as with the classical double-thermal-pulse technique. This technique provides time separation of the nucleation and growth stages. The experiments were started with metastable HEWL solutions at room temperature, 20°C<sup>249</sup>. Then the temperature was fast decreased down to 10°C, which corresponds

to the supersaturated state, and HEWL start nucleate. Then the temperature was increased up to 20°C, this blocks formation of new HEWL nuclei but allows the existing nuclei to grow. In 21 days, the number of the nucleated and grown crystals was counted. The experiments performed in the quasi-two-dimensional glass cells without and with gold nanoparticles were also performed in the presence of three gold wires of 100 µm diameter and 2,8 cm length.

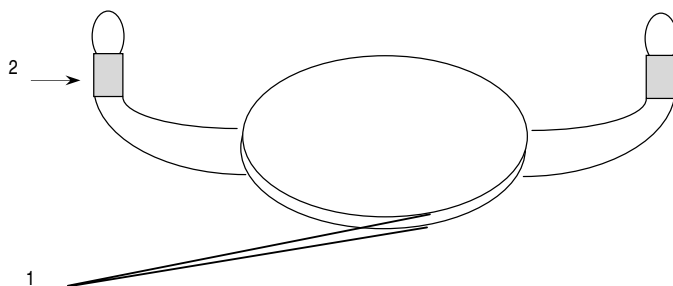


Figure 3.52. The quasi two-dimensional cell for investigation of crystallization consists of two optically parallel glass plates (1); a protein solution was injected through inlet (2) into the gap between the plates.

The protein crystals were characterized using Scanning Electron Microscopy (SEM, JEOL, JSM 6390), Energy Dispersive Spectroscopy (EDS) and Transmission Electron Microscopy (TEM, JEOL-TEM 100B). Indeed, the electron microscopy encounters some difficulties during observation of the protein crystals, both due to the vacuum environment extracting water from the crystals, and due to heating by the electron beam. (HEWL crystals burn or melt at 80 kV TEM for 10 s). The detection of the gold nanoparticles incorporated in protein crystals (near the crystal surface) can be done easily using EDS.

### **3.8 Localized Surface Plasmon Resonance**

Greater understandings of nanoscience and nanoscale phenomena are vital for the development of devices based on nanotechnology. Relevant to this work, the potential to develop highly sensitive and specific sensors for biological targets motivates a portion of the research in this field. Nanoscale development, termed the

Localized Surface Plasmon Resonance (LSPR) nanosensor, is a refractive index based sensing device that relies on the extraordinary optical properties of gold nanoparticles. It is well established that the maximum extinction wavelength,  $\lambda_{\max}$ , of the LSPR is dependent upon the composition, size, shape, and interparticle spacing of the nanoparticles as well as the dielectric properties of their local environment (i.e. substrate, solvent, and surface-confined molecules). The basic idea of this technique is based on the following Mie equation.

$$\sigma_{\text{ext}}(\omega) = 9 \frac{\omega}{c} \epsilon_{3/2} V_0 \frac{\epsilon_2(\omega)}{[\epsilon_1(\omega) + 2\epsilon_m]^2 + \epsilon_2(\omega)^2}$$

Where  $V_0 = (4\pi/3)R^3$ ,  $\omega$  is the angular frequency of the exciting radiation  $\epsilon_m$  is the electric function of the medium surrounding (or the embedding) the metallic nanoparticles and  $\epsilon_1$  and  $\epsilon_2$  are the real and imaginary part of the dielectric function of the metallic nanoparticles, respectively. Even it is well known but, only a few papers in this technique had been published.

The following is one of the experiment about the effect of the medium surrounding gold nanoparticles by Mulvaney<sup>250</sup>

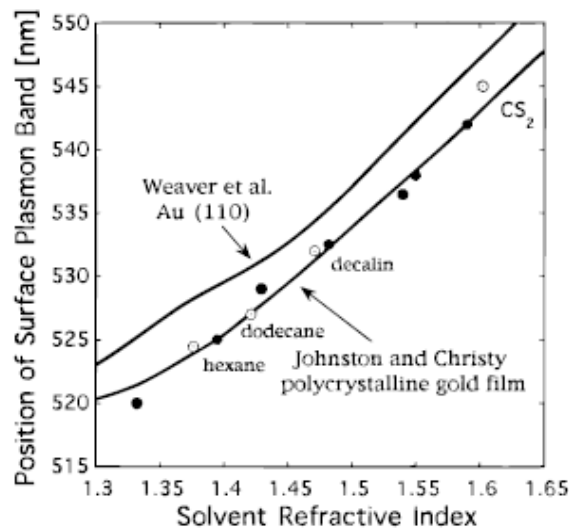


Figure 3.53 Position of the plasmon band of gold nanoparticles in numerous solvents which have different refractive index.

Figure 3.53 demonstrates the correlation between the refractive index of the solvent against the peak position of surface plasmon band. It shows poor sensitivity because every 0.5 of refractive index units gives only 2 nm differences in the surface plasmon band.

Various glucose concentrations (i.e. 1, 2, 3, 4, and 5 %) in constant gold nanoparticles solution are measured using UV-Vis spectrophotometer. The spectrums are analyzed. The difference of the refractive index between 1% and 5% glucose solution is 0.008 unit<sup>251</sup>. Based on fig 3.53, that difference of the refractive index will influence only 0.032 at the plasmon band difference.

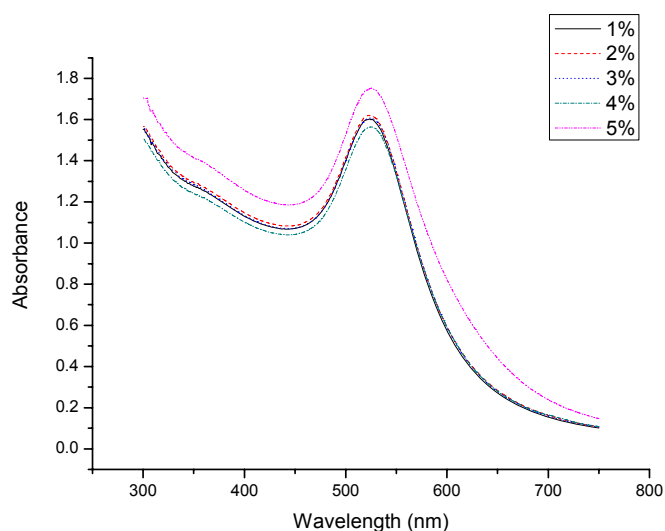


Fig. 3.54 Gold nanoparticles plasmon band (1 mM) in various concentration of glucose

Fig 3.54 demonstrates the spectrums of the gold nanoparticles in various concentrations of glucose. Normalization of the spectrums is performed (Fig 3.55) to minimize the random error. Normalization of the spectrums is performed by dividing all the points with the maximum its peak value. Most of the spectrums are almost identical because the shifting of the plasmon band is very small. Magnification of the slope of the spectrum is also performed (Fig 3.56) to see the dependencies more precisely. Fig 3.56 demonstrates the spectrums have shifted to the right for higher glucose concentrations. That shifting indicates that LSPR work for glucose analysis,



but this technique unfortunately has poor sensitivity. It becomes clear that an exploiting of this technology required special optical techniques designed for detection of small spectral changes, for example differential double wavelength measurements.

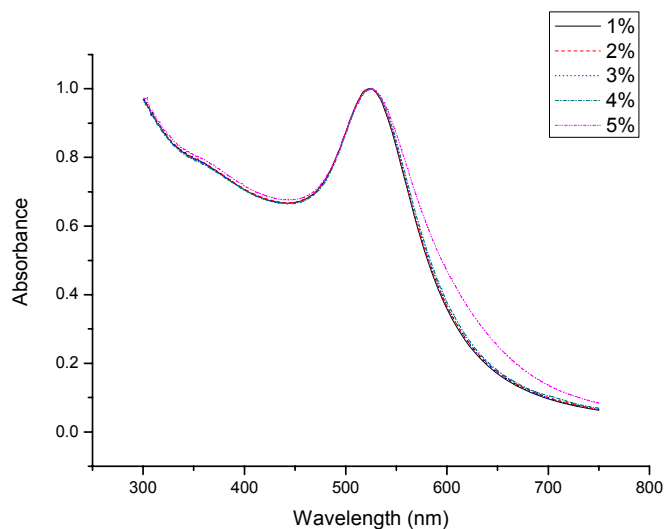


Fig 3.55. Normalization curve of gold nanoparticles plasmon band (1 mM) in various concentration of gold nanoparticles

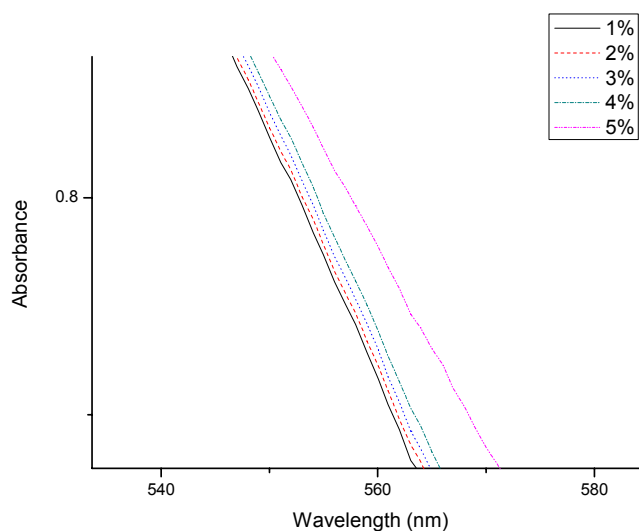


Fig 3.56 Magnification of the slope from fig. 3.55

### 3.9 Freezing indicator

This part of the work is industrial project. Gold nanoparticles can change its color irreversibly when the solution become frozen ( $0^{\circ}\text{C} \pm 0.5$ ), is one of the interesting property (Fig 3.57). This property is used for the development of freezing indicator. This indicator may be useful for specific application. An example, If we would like to store vaccine, WHO recommends that oral poliovirus vaccine should be stored either at between  $0^{\circ}\text{C}$  and  $8^{\circ}\text{C}$ . Maintaining the vaccine in correct temperature is an essential part of a successful immunization program, but in developed countries faulty procedures may occur more commonly than is generally believed. A survey was conducted in a health district in central Italy to assess the methods of vaccine transportation and storage. From 52 primary vaccination offices inspected, 39 (76.5%) had a refrigerator for vaccine storage but only 17 (33.3%) kept records of received and stored doses. None of the seven main offices selected for monitoring had a maximum and minimum thermometer and none monitored the internal temperature of the refrigerator<sup>252</sup>.

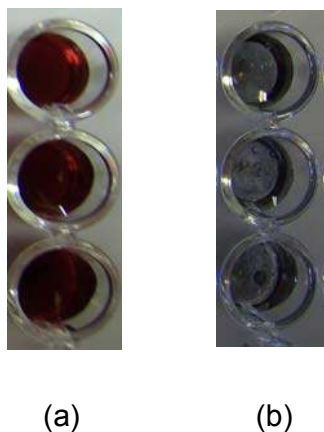


Fig. 3.57 Color of gold nanoparticles, before (a), and after (b) freezing.

Mathias<sup>253</sup> reported that between 14% and 35% of refrigerators or transport shipments were found to have exposed vaccine to freezing temperatures, while in studies that examined all segments of distribution, between 75% and 100% of the vaccine shipments were exposed. More rigorous study designs were associated with

higher levels of freeze exposure. As more expensive, freeze-sensitive vaccines are introduced into immunization schedules, freeze prevention will become increasingly critical for ensuring that the world's children are receiving fully potent vaccine.

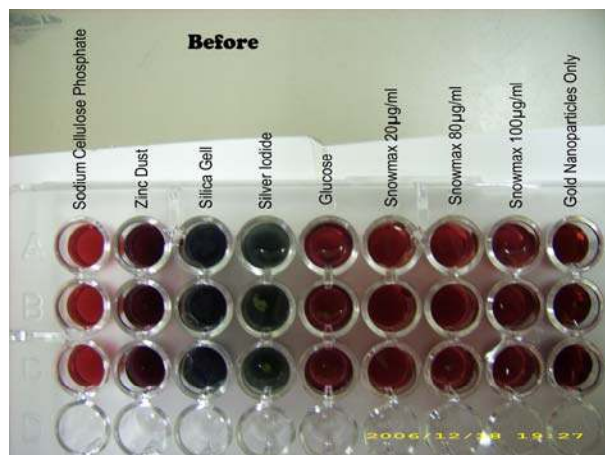
Gold nanoparticles can be proposed as a new alternative for freezing indicator. The suggestion is to stick the freezing indicator on the each packaging of the vaccine. Once the freezing indicator change color to colorless, that indicates that the vaccine has been exposed to freezing state.

An attempt to stabilize nanoparticles has been performed by adding some additives. It is expected that the additives will give longer storage time or faster respond to temperature change. The list of the additives used can be seen in the table 3.2

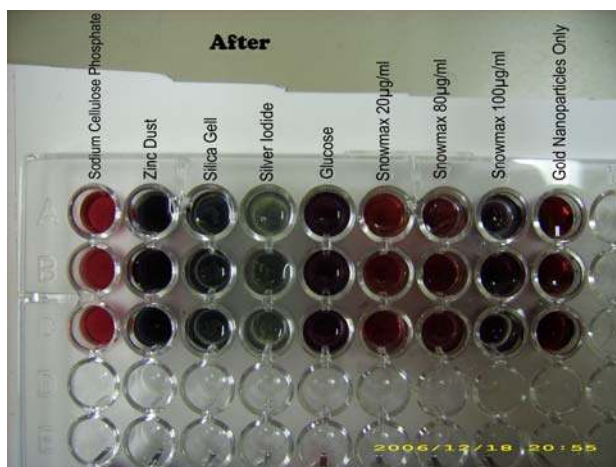
Table 3.2 Name of additives

No	Name of additives
1	Sodium cellulose phosphate
2	Zinc Dust
3	Silica Gel
4	Silver Iodide (home made, without purification)
5	Glucose
6	Snowmax 20 $\mu$ g/ml
7	Snowmax 80 $\mu$ g/ml
8	Snowmax 100 $\mu$ g/ml
9	No additive

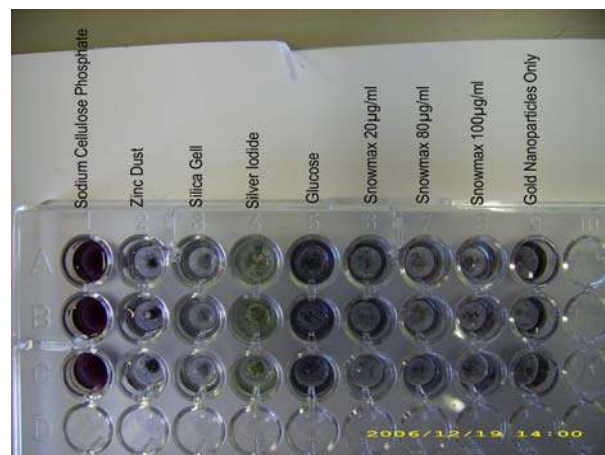
The result of the test demonstrates at fig 3.58. It shows that zinc dust, silica gel, silver iodide (home made, without purification) affect instability of the gold nanoparticles solution. The color of gold nanoparticles changes after addition of the additives in room temperature (Fig. 3.58a). Snowmax 100  $\mu$ g/ml is considered to be the one of the fast additives that can change color (Fig 3.58b). After the gold nanoparticles is frozen completely, all the solution become colorless (Fig 3.58c)



(a)



(b)



(c)

Fig. 3.58 Gold nanoparticles with the additives at room temperature (a), near the freezing point (b), after completely freezing then defrosted

Another attempt to improve the stability of the gold nanoparticles in the solution also has been performed as the following procedure.

***The procedure of the experiment***

The solution of gold nanoparticles is prepared using reduction of sodium citrate reaction as described before, and purified by dialysis process. Some amounts of this solution are sampled, and different additives are added into them, and then sealed in the glass ampules (Table 3.3). Every type and concentration of the additives is repeated 3 times. The ampules are heated in the thermostat oven at 85<sup>0</sup>C. The state of the samples is observed within 47 days. The picture of each ampules is taken when necessary (Table. 3.4). The samples which become colorless during test period are deleted from the experiment. The rest amount of the solutions is characterized by UV-Vis spectrophotometer.



Tabel 3.3 Types of Additive added into the gold nanoparticles solution.

Type of chemicals (R)	Concentrations of additives (J)		
	1	2	3
A Triton X-114	0.1 %	0.01%	0.001%
B sodium decyl sulfate	0.1 %	0.01%	0.001%
C cetyl pyridinium bromide	0.1 %	0.01%	0.001%
D 16-mercaptohexanedecanoic acid	5·10 <sup>-4</sup> M	5·10 <sup>-5</sup> M	5·10 <sup>-6</sup> M
E 6-mercapto-1-propanol	5·10 <sup>-4</sup> M	5·10 <sup>-5</sup> M	5·10 <sup>-6</sup> M
F 3-mercaptopropionic acid	5·10 <sup>-4</sup> M	5·10 <sup>-5</sup> M	5·10 <sup>-6</sup> M
G 11-mercapto-1-undecanol	5·10 <sup>-4</sup> M	5·10 <sup>-5</sup> M	5·10 <sup>-6</sup> M
H 4-aminophenol	5·10 <sup>-4</sup> M	5·10 <sup>-5</sup> M	5·10 <sup>-6</sup> M
X –blank solution (without heating)	-	-	-
X +blank solution (with heating)	-	-	-

Codes of the ampule : RJ-number of repetition

## RESULTS AND DISCUSSIONS

Table 3.4. Color changes of the gold nanoparticles solutions.

day) date	A Triton X-114	B sodium decyl sulfate	C cetyl pyridinium bromide	D 16-mercaptohexadecanoic acid
1) 14.09.06	no change	no change		no change
2) 15.09.06		no change	no change	
3) 16.09.06		no change		
4) 17.09.06		no change		
5) 18.09.06	no change	no change	no change	no change
6) 19.09.06	no change	no change	no change	no change
7) 20.09.06	no change	no change	no change	no change
8) 21.09.06				
10) 23.09.06				
12) 25.09.06				
14) 27.09.06				

## RESULTS AND DISCUSSIONS



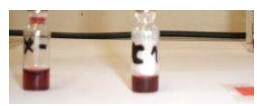

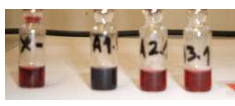
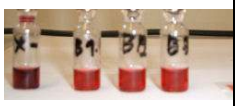



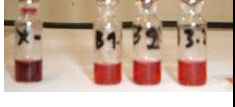


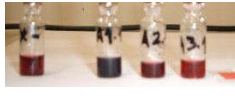
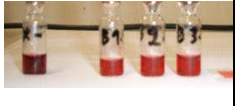







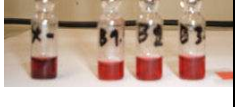







17) 30.09.06				
19) 2.10.06				
22) 5.10.06				
26) 9.10.6				
32) 15.10.06				
47) 30.10.06				

Table 3.4 (continued)

day) date	E 6-mercapto-1- propanol	F 3- mercaptopropionic acid	G 11-mercapto-1- undecanol	H 4-aminophenol
1) 14.09.06	no change	no change	no change	
2) 15.09.06	no change	no change		no change
3) 16.09.06	no change	no change		
4) 17.09.06	no change	no change	no change	no change

## RESULTS AND DISCUSSIONS

5) 18.09.06	no change	no change	no change	no change
6) 19.09.06	no change	no change	no change	no change
7) 20.09.06	no change	no change	no change	no change
8) 21.09.06				
10) 23.09.06				
12) 25.09.06				
14) 27.09.06				No change
17) 30.09.06				
19) 2.10.06				
22) 5.10.06				
26) 9.10.06				



## RESULTS AND DISCUSSIONS

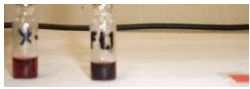





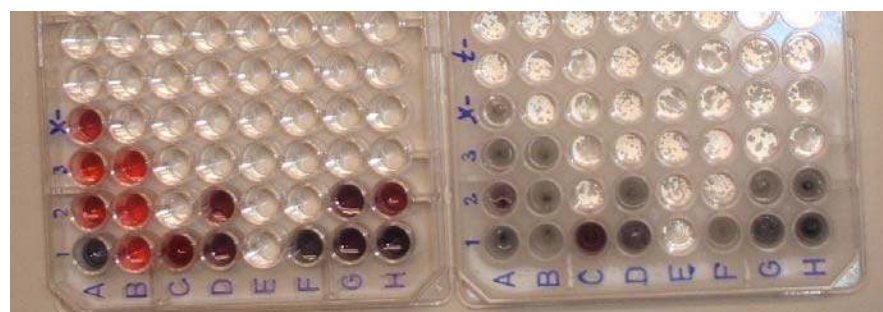
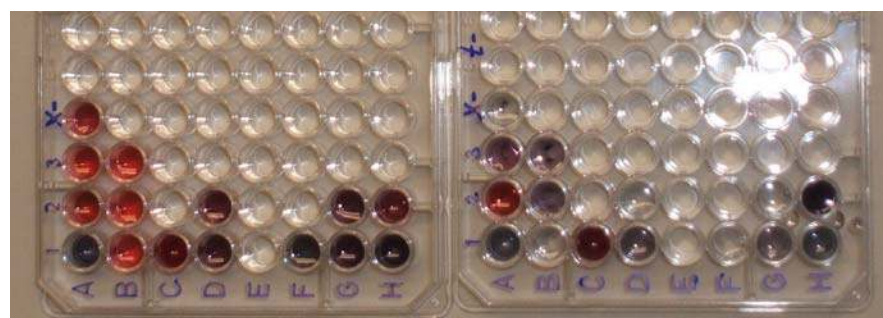
32) 15.10.06	no change			
47) 30.10.06	no change			

Table 3.4 demonstrates that the color of gold nanoparticles containing sodium decyl sulfate does not change until the end of the experiment (47 days). The gold nanoparticles solution with 6-mercapto-1-propanol, in all concentration examined undergo aggregation after 32 days. Some others samples of the gold nanoparticles solution also undergo aggregation (Table 3.4). The rest of the samples then are tested by freezing them (Fig. 3.59) and also analyzed using UV-VIS spectrophotometer (Fig 3.60)



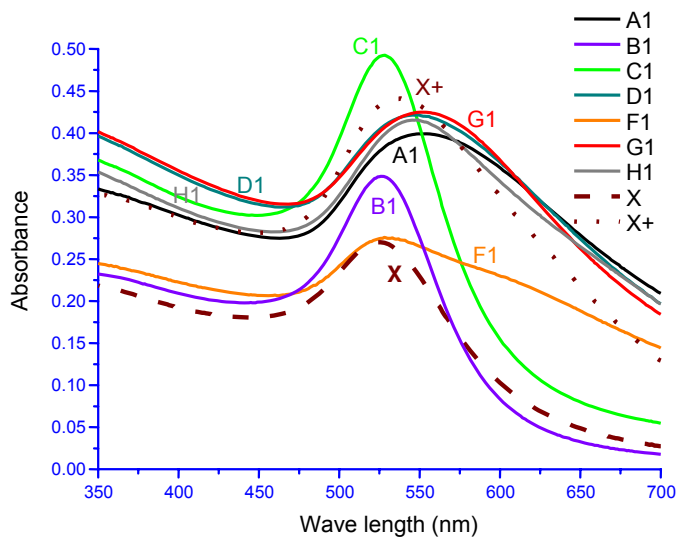
(a)



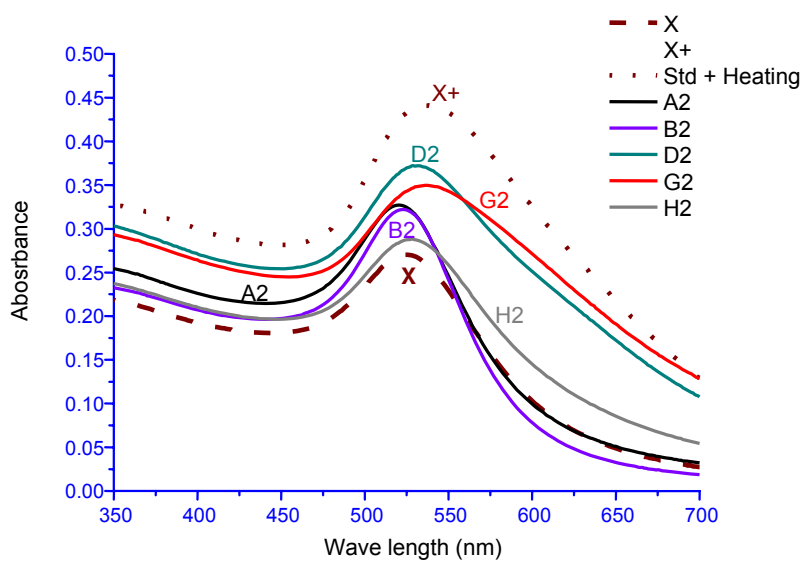
(b)

Fig 5.59 Gold nanoparticles solution, initial state (a) and (b) left, frozen state (a) right, defrosted state (b) right.

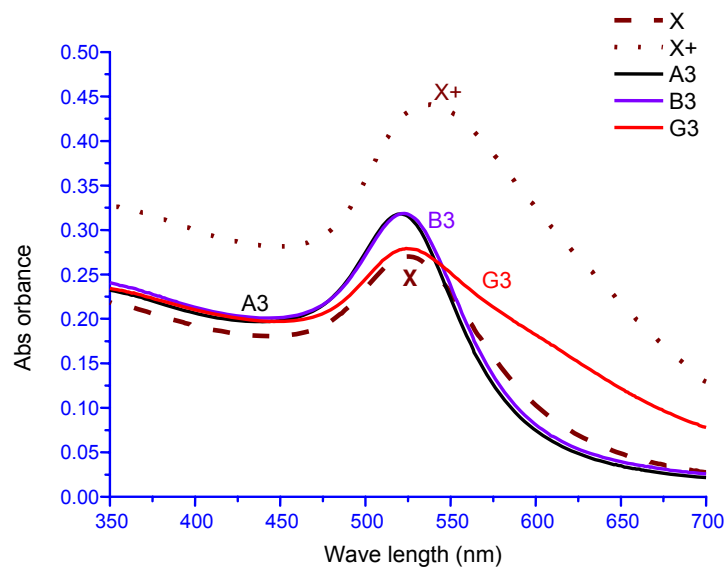
Fig 5.59 demonstrates that Triton X-114 and cetyl pyridinium bromide can not be used for additive of the gold nanoparticles solution as freezing indicator because the color change is reversible after defrosting (Fig. 5.59b right sample A2 and C1 respectively).



(a)



(b)



(c)

Figure 3.60 The UV Vis spectrums of the remaining samples of gold nanoparticles solution.

Fig 3.60 demonstrates UV-Vis spectrums of the sample B1, B2, B3 and C1 are the most stable, because they have the highest plasmon band intensity when the intensity of the spectrum is measured from the based line. They also have the same peak with the standard (spectrum X) at 523 nm. Even though sample C1 is almost as stable as sample B, but sample C1 shows an increasing intensity of the based line. Other additives also show increasing intensity on all the part of the wavelength like sample C1. That increasing intensity of the based line probably is caused by the formation of bigger particles in the solution.

### 3.10. Automation of Layer-by-Layer deposition.

The aim of the work in this part is to suggest an automation deposition for industrial purpose. Automated deposition of defined amount of conductive polymer onto solid surface can be simply performed by Layer- by Layer (LbL) in flow mode. The LbL deposition developed by Decher<sup>254</sup> is widely used as a simple technique for fabrication of multilayered structures for a broad area of scientific and technological

applications. This approach can be used for formation of mixed cationic/anionic films from polyelectrolytes<sup>254</sup> including films containing biomolecules<sup>255</sup>, conducting polymers<sup>256-261</sup> or nanoparticles<sup>228</sup>. Some applications of LbL formed films require a large number of the deposited layers. This reason as well as commercial fabrication of these structures is a motivation for automation of LbL technique. One of the recently suggested automated approaches is based on deposition of sprayed polyelectrolyte multilayer; this method can be used for industrial coating of large areas<sup>262</sup>. Other automation techniques are based on the development of mechanical robot for alternative dipping of the sample into solutions of cationic and anionic electrolytes<sup>263</sup>.

We suggest here another technology which is much more simple and cheap and has such additional advantages as a control of gaseous environment near the sample and excluding of its possible exposure to dust, light or other physical and chemical factors. The technology is based on dynamic adsorption of polyelectrolyte from the flow of diluted polyelectrolyte solution. The alteration of electrolytes is performed simply by switching of electromagnetic valve controlled by low frequency pulse generator. Formation of thin film consisting of alternating layers of polyaniline (PANI) and polystyrenesulfonate (PSS) are used as a model system providing simple electrochemical determination of amount of deposited electroactive polymer.

PANI is synthesized by oxidation of 0.1 M aniline in 0.5 M sulfuric acid with 0.1 M ammonium persulfate. The dipping solution of PANI in water is prepared according to Cheung et al<sup>264</sup>. The concentrations of PANI and PSS in dipping solution recalculated to the concentrations of monomers are 1 mM and 10 mM respectively.

The principle of the new technology for automation LbL deposition is shown in the fig. 3.61. The set-up is very simple and consists of two reservoirs with diluted anionic and anionic polyelectrolytes (or other materials suitable for LbL deposition), electromagnetic valve controlled by a square pulse generator and flow cell with a solid support which should be coated, and peristaltic pump. There is no special requirement in the used equipment. For deposition of PANI-PSS films, a flow rate of 0,915 ml/min, a flow cell with the volume of about 20  $\mu$ L and duration of each adsorption cycle of 4 min is selected. Longer time of the adsorption cycle is also tested, but the results are identical.

Electrochemical analysis of the formed films is performed with Autolab PGSTAT-13 electrochemical workstation (EcoChemie, The Netherlands) using three electrode configuration with a gold working electrode ( $S = 0,25 \text{ mm}^2$ ), SCE reference and Pt-wire counter electrode.

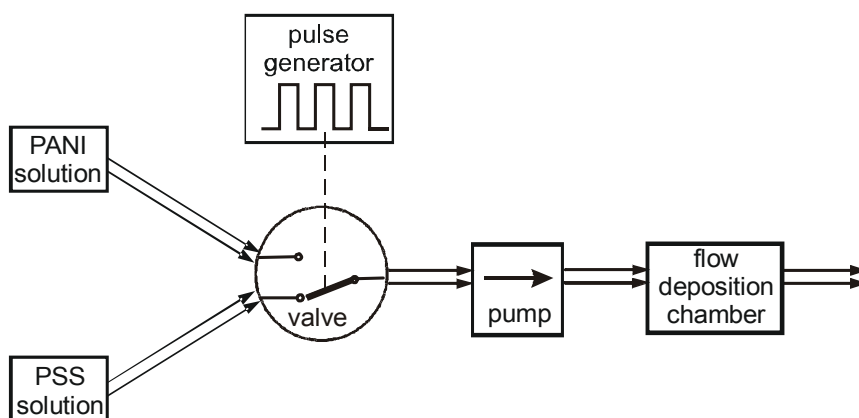


Fig. 3.61. Scheme of the automated set-up for PANI – PSS multilayer deposition.

The new approach has been tested with a deposition of up to 45 bi-layers of PANI – PSS. Cyclic voltammetry has been performed after deposition of each fifth bi-layer. Typical PANI voltammograms (Fig. 3.62) are observed. The increase of the current is associated with the increase of the amount of polyaniline adsorbed on the surface at each step of the deposition procedure (Fig. 3.63). The results obtained by the automated deposition show good reproducibility and linear increase of the anodic peak current for a large number of deposited bi-layers.

In view of possible electroanalytical application, the obtained PANI – PSS multilayer coatings are tested for electrooxidation of ascorbic acid. Fig. 3.64 shows the electrochemical redox activity of the layer in neutral media and the voltammetric response due to ascorbic acid oxidation. By means of potentiostatic measurements, the concentration dependence of the AA oxidation currents is studied in the 0,05 – 0,8 mM range. A linear current versus concentration plot (Fig. 3.65) is obtained.

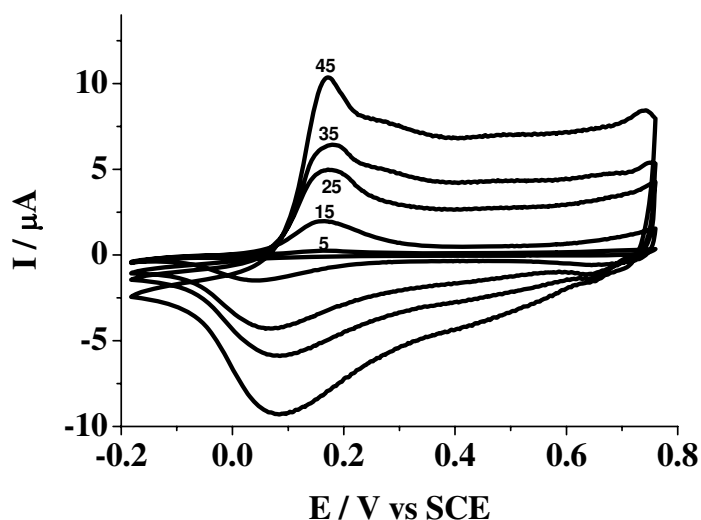


Fig. 3.62. PANI – PSS voltammogram in the presence of 0.5 M  $H_2SO_4$ , recorded at  $100 \text{ mV} \cdot \text{s}^{-1}$  after 5, 15, 25, 35 and 45 cycle of the automated LbL deposition.

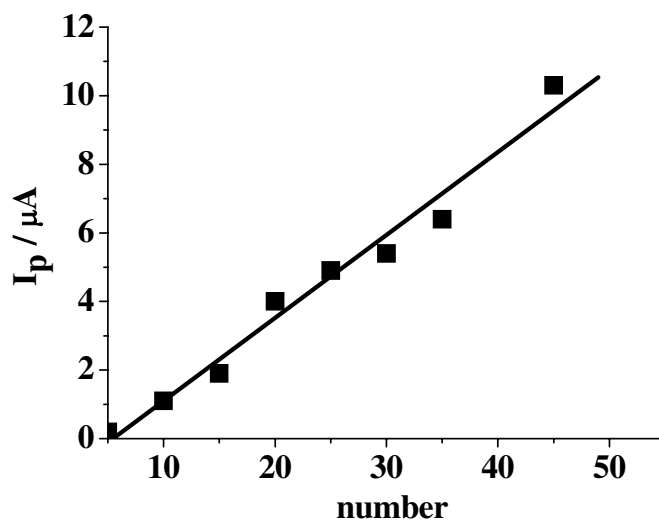


Fig. 3.63. Dependence of the first anodic peak current versus layer number obtained by cyclic voltammetry (■).

The data for electrocatalytic activity of the self assembled PANI/PSS coatings are compared with electrochemically deposited 'self doped' PANI<sup>265</sup>, PANI/PSS<sup>266</sup>

and PANI/polyvinylsulfonate<sup>267</sup>. The comparison shows that PANI/PSS LbL structure is active in the sub-millimolar range and have a very low detection limit (0,05 mM AA), whereas the electrochemically obtained layers have about one order higher of detection limits magnitude and are mostly investigated at millimolar AA concentrations.

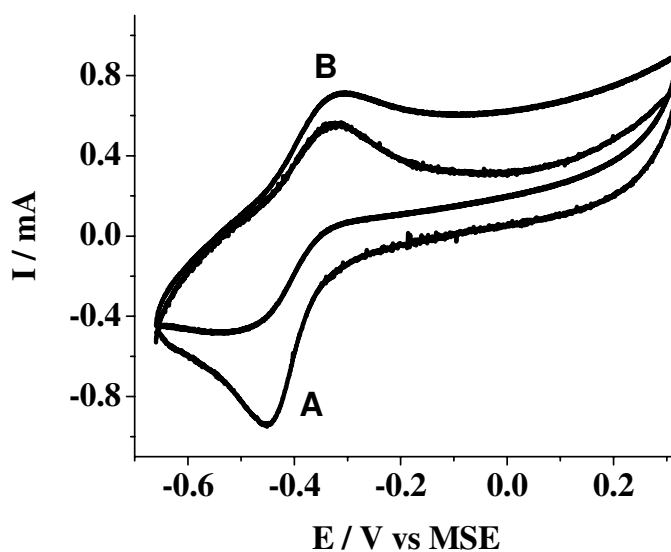


Fig. 3.64. Voltamogram of PANI – PSS layers measured at 100 mV/s in PBS buffer pH 7 (A) and in 1 mM ascorbic acid (B).

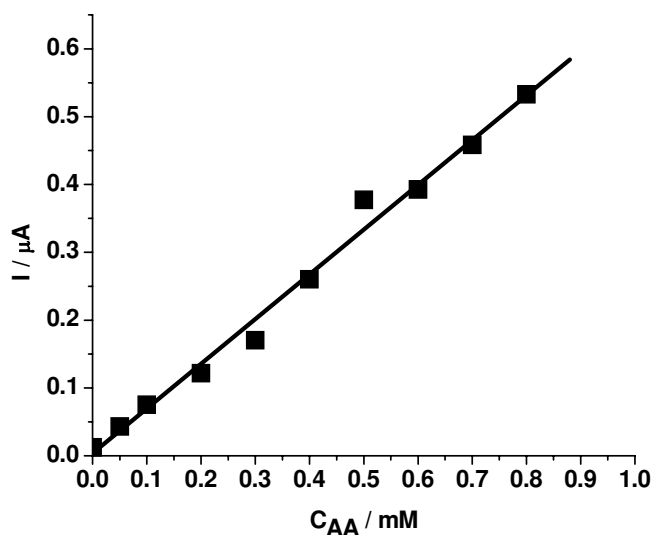


Fig. 3.65. AA oxidation current measured at  $E=0.4$  V at different AA concentrations.

#### **4. SUMMARY**

The work includes improvements of surface technology, new analytical applications of metallic nanoparticles and optimization of technological steps for production of different types of metallic nanoparticles in discrete and continuous modes. The technology of LbL deposition was optimized and applied for immobilization of metallic nanoparticles. SPR detection was used for the determination of optimal deposition conditions and on-line monitoring of the deposition process. Simple approach for automation of LbL deposition allowing one to deposit up to hundreds of layers was developed. The technology was proved by electrochemical analysis for deposition of electrochemically active polymers. A new diffusion based semi-quantitative assay for detection of sugars was suggested.

Electrochemical oxidation of glucose and dopamine on electrodes modified with gold nanoparticles was studied. Conditions for electrochemical analysis of these substances in the presence of typical natural interferences were evaluated. A combination of voltammetry and impedance spectroscopy was used to demonstrate a formation of insulating layer on gold surface, this resulted in explanation of anomalous shape of voltammetric curves. A combination of electrochemical and SPR measurements demonstrated directly a formation of an insulating layer on the electrode surface and was used for optimization of the assay conditions. The results indicate a possibility to develop an enzyme free sensors for glucose and dopamine.

It was discovered that gold nanoparticles are effective nucleating agents for protein crystallization. Nanoparticles induce protein crystallization at lower supersaturation and increase the number of protein crystals formed at higher supersaturation. The fact that this technology works with so different proteins as lysozyme and ferritin allows one to suggest that it may be also applied for many other proteins including the ones which are reluctant to crystallization by known technologies.

Irreversible freezing indicators based on gold nanoparticles were developed. The filling suspension containing nanoparticles, nucleation and stabilization agents were optimized in sense of stability and irreversibility of color changes. A large scale production of this indicator will be started in spring 2008.



## 5. ZUSAMMENFASSUNG

Die Arbeit umfasst Verbesserungen der Oberfläche Technologie, neue analytische Anwendungen von metallischen Nanopartikeln und Optimierung der technologischen Schritte für die Herstellung von verschiedenen Arten von metallischen Nanopartikeln in diskreter und kontinuierlicher Art. Die Technologie der LbL Deposition wurde für die Immobilisierung von metallischen Nanopartikeln optimiert. SPR-Messungen wurden für die Bestimmung der optimalen Bedingungen der Deposition und der on-line Überwachung des Depositionsprozesses verwendet. Ein einfaches Verfahren für die Automatisierung der LbL Deposition wurde entwickelt, so dass bis zu Hunderte von Schichten abgeschieden werden können. Die Technologie wurde anhand der Abscheidung elektrochemisch aktiver Polymere durch elektrochemische Analyse geprüft. Ein neuer semi-quantitativer auf Diffusion basierender Assay für die Erkennung von Zuckern wurde vorgeschlagen.

Die elektrochemische Oxidation von Glucose und Dopamin mittels Gold-Nanopartikeln modifizierten Elektroden wurde untersucht. Die Bedingungen für die elektrochemische Analyse dieser Stoffe in der Anwesenheit von typischen natürlichen Interferenzen wurden ausgewertet. Eine Kombination von Voltammetrie- und Impedanz-Spektroskopie wurde verwendet, um die Bildung einer isolierenden Schicht auf der Gold-Oberfläche zu demonstrieren. Dies führte zu einer anomalen Form der Voltammogramme. Eine Kombination von elektrochemischen und SPR-Messungen hat direkt die Bildung einer Isolierschicht auf der Elektrodenoberfläche gezeigt und wurde für die Optimierung der Test-Bedingungen verwendet. Die Ergebnisse zeigen die Möglichkeit zur Entwicklung eines Enzym-freien Sensors für Glucose und Dopamin.

Es wurde entdeckt, dass Gold-Nanopartikel wirksame Keimbildner für die Protein Kristallisation sind. Nanopartikel induzieren die Protein Kristallisation bei niedriger Übersättigung und erhöhen die Anzahl der erzeugten Protein-Kristalle bei höherer Übersättigung. Die Tatsache, dass diese Technologie mit so verschiedenen Proteinen wie Lysozym und Ferritin funktioniert erlaubt es vorzuschlagen, dass sie möglicherweise auch für viele andere Proteine, einschließlich derjenigen, die keine Kristallisation bei bei bekannten Technologien zeigen, anwendbar ist.

Irreversibel Frostindikatoren, wurden auf der Grundlage von Gold-Nanopartikeln entwickelt. Die verwendete Suspension beinhaltet Nanopartikel, Keimbildner und Stabilisatoren, die im Sinne der Stabilität und der Irreversibilität der Farbänderung optimiert wurden. Eine groß angelegte Produktion von diesen Indikatoren wird im Frühjahr 2008 begonnen.

**6. KESIMPULAN**

Penelitian yang dilakukan meliputi pengembangan teknologi permukaan, aplikasi analitik baru dari nanopartikel logam serta optimisasi teknologi untuk pembuatan berbagai jenis nanopartikel secara diskrit dan kontinyu. Optimisasi teknologi deposisi LbL dilakukan, dan digunakan untuk imobilisasi nanopartikel logam. Pengukuran menggunakan SPR, dipakai dalam penentuan kondisi optimal dan pengamatan secara on-line dari deposisi yang dilakukan. Telah dikembangkan pendekatan sederhana deposisi otomatis secara LbL, yang memungkinkan seseorang mendeposisi sampai ratusan lapis. Teknologi ini dibuktikan secara elektrokimia dari polimer aktif yang di deposisikan. Suatu uji semi kuantitatif berdasarkan prinsip difusi untuk analisis gula telah pula di ajukan.

Oksidasi glukosa dan dopamin pada permukaan elektroda yang telah dimodifikasi dengan nanopartikel emas telah dipelajari. Kondisi untuk analisis secara elektrokimia dari senyawa-senyawa tersebut dalam ion pengganggu alaminya juga telah di pelajari. Kombinasi voltametri dan impedans spektroskopi digunakan untuk menunjukkan pembentukan lapisan insulator pada permukaan emas, yang kemudian dapat dipakai menjelaskan bentuk anomali dari voltamogram yang dihasilkan. Kombinasi pengukuran elektrokimia dan SPR menunjukkan secara langsung pembentukan lapisan insulator tersebut pada permukaan elektroda, sekaligus pula digunakan untuk optimasi kondisi pengukuran. Hasil menunjukkan adanya kemungkinan untuk mengembangkan sensor bebas enzim bagi glukosa dan dopamin

Gold nanopartikel juga diketahui merupakan agen nukleasi yang efektif untuk kristalisasi protein. Nanopartikel memicu kristalisasi protein pada kondisi supersaturasi rendah, dan meningkatkan jumlah kristal protein yang terbentuk pada supersaturasi tinggi. Terbukti bahwa teknik ini bekerja pada protein yang berbeda seperti lysozyme dan ferritin, yang mungkin mengilhami seseorang bahwa hal tersebut dapat juga di gunakan pada protein lain, termasuk pada protein yang tidak bisa dikristalisasi dengan teknik yang ada sekarang.

Indikator titik beku yang tidak balik berbahan dasar nanopartikel emas telah dikembangkan. Suspensi dari indikator ini berisi nanopartikel, agen nukleasi dan

stabilisator, dan telah di optimisasi untuk memperoleh kestabilan dan perubahan warna yang tidak dapat balik. Produksi skala besar dari indikator ini, direncanakan dibuat pada musim semi 2008.

---

## 8. REFERENCES

1. Kostoff, R. N.; Koytcheff, R. G.; Lau, C. G. Y. Structure of the nanoscience and nanotechnology applications literature. *The Journal of Technology Transfer*, 1-13.
2. Andrievskii, R. A. Directions in Current Nanoparticle Research. *Powder Metallurgy and Metal Ceramics* **2003**, 42 (11), 624-629.
3. Liz-Marzan, L. M. Nanometals: Formation and color. *Materials Today* **2004**, 7 (2), 26-31.
4. Roco, M. C. Nanoparticles and Nanotechnology Research. *Journal of Nanoparticle Research* **1999**, 1 (1), 1-6.
5. Reibold, M.; Paufler, P.; Levin, A. A.; Kochmann, W.; Patzke, N.; Meyer, D. C. Materials: Carbon nanotubes in an ancient Damascus sabre. *Nature* **2006**, 444 (7117), 286.
6. Perttula, J. Reproduced wootz Damascus steel. *Scandinavian Journal of Metallurgy* **2001**, 30 (2), 65-68.
7. Kochmann, W.; Reibold, M.; Goldberg, R.; Hauffe, W.; Levin, A. A.; Meyer, D. C.; Stephan, T.; Muller, H.; Belger, A.; Paufler, P. Nanowires in ancient Damascus steel. *Journal of Alloys and Compounds* **2004**, 372 (1-2), L15-L19.
8. Sherby, O. D.; Wadsworth, J. Ancient blacksmiths, the Iron Age, Damascus steels, and modern metallurgy. *Journal of Materials Processing Technology* **2001**, 117 (3), 347-353.
9. Perttula, J. Wootz Damascus steel of ancient orient. *Scandinavian Journal of Metallurgy* **2004**, 33 (2), 92-97.
10. Lee, B. I.; Qi, L.; Copeland, T. NANOPARTICLES FOR MATERIALS DESIGN: PRESENT & FUTURE. *Journal of Ceramic Processing & Research* **2005**, 6 (1), 31-40.
11. Wiederrecht, G. P. Near-field optical imaging of noble metal nanoparticles. *The European Physical Journal Applied Physics* **2004**, 28 (1), 3-18.
12. Schmidt, J. J.; Montemagno, C. D. Using machines in cells. *Drug Discovery Today* **2002**, 7 (9), 500-503.
13. Katz, E.; Willner, I. Integrated nanoparticle-biomolecule hybrid systems: synthesis, properties, and applications. *Angew. Chem. Int. Ed* **2004**, 43, 6042-6108.
14. Mamalis, A. G. Recent advances in nanotechnology. *Journal of Materials Processing Technology* **2007**, 181 (1-3), 52-58.

15. Ahmadi, T. S.; Wang, Z. L.; Green, T. C.; Henglein, A.; El-Sayed, M. A. Shape-Controlled Synthesis of Colloidal Platinum Nanoparticles. *Science* **1996**, *272* (5270), 1924-1925.
16. Harriman, A.; Millward, G. R.; Neta, P.; Richoux, M. C.; Thomas, J. M. Interfacial electron-transfer reactions between platinum colloids and reducing radicals in aqueous solution. *The Journal of Physical Chemistry* **1988**, *92* (5), 1286-1290.
17. Turkevich, J.; Stevenson, P. C.; Hillier, J. The Formation of Colloidal Gold. *The Journal of Physical Chemistry* **1953**, *57* (7), 670-673.
18. Narayanan, R.; El-Sayed, M. A. Catalysis with Transition Metal Nanoparticles in Colloidal Solution: Nanoparticle Shape Dependence and Stability. *J. Phys. Chem. B* **2005**, *109* (26), 12663-12676.
19. Sun, Y.; Xia, Y. Shape-Controlled Synthesis of Gold and Silver Nanoparticles. *Science* **2002**, *298* (5601), 2176-2179.
20. Xiulan, S.; Xiaolian, Z.; Jian, T.; Zhou, J.; Chu, F. S. Preparation of gold-labeled antibody probe and its use in immunochromatography assay for detection of aflatoxin B1. *International Journal of Food Microbiology* **2005**, *99* (2), 185-194.
21. Wilson, O. M.; Hu, X.; Cahill, D. G.; Braun, P. V. Colloidal metal particles as probes of nanoscale thermal transport in fluids. *Physical Review B* **2002**, *66* (22), 224301.
22. Mayer, A. B. R.; Mark, J. E. Colloidal gold nanoparticles protected by water-soluble homopolymers and random copolymers. *European Polymer Journal* **1998**, *34* (1), 103-108.
23. Teranishi, T.; Hosoe, M.; Tanaka, T.; Miyake, M. Size Control of Monodispersed Pt Nanoparticles and Their 2D Organization by Electrophoretic Deposition. *J. Phys. Chem. B* **1999**, *103* (19), 3818-3827.
24. Hostetler, M. J.; Wingate, J. E.; Zhong, C. J.; Harris, J. E.; Vachet, R. W.; Clark, M. R.; Londono, J. D.; Green, S. J.; Stokes, J. J.; Wignall, G. D.; Glish, G. L.; Porter, M. D.; Evans, N. D.; Murray, R. W. Alkanethiolate Gold Cluster Molecules with Core Diameters from 1.5 to 5.2 nm: Core and Monolayer Properties as a Function of Core Size. *Langmuir* **1998**, *14* (1), 17-30.
25. Pillai, Z. S.; Kamat, P. V. What Factors Control the Size and Shape of Silver Nanoparticles in the Citrate Ion Reduction Method? *J. Phys. Chem. B* **2004**, *108* (3), 945-951.

- 
26. Cassagneau, T.; Fendler, J. H. Preparation and Layer-by-Layer Self-Assembly of Silver Nanoparticles Capped by Graphite Oxide Nanosheets. *J. Phys. Chem. B* **1999**, *103* (11), 1789-1793.
  27. Richter, R. S. Nanoscale Palladium Metallization of DNA. *Advanced Materials* **2000**, *12* (7), 507-510.
  28. Lin, C. S.; Khan, M. R.; Lin, S. D. Platinum states in citrate sols by EXAFS. *Journal of Colloid and Interface Science* **2005**, *287* (1), 366-369.
  29. Schmid, G. Large clusters and colloids. Metals in the embryonic state. *Chem. Rev.* **1992**, *92* (8), 1709-1727.
  30. Keating, C. D.; Kovaleski, K. M.; Natan, M. J. Protein:Colloid Conjugates for Surface Enhanced Raman Scattering: Stability and Control of Protein Orientation. *J. Phys. Chem. B* **1998**, *102* (47), 9404-9413.
  31. Chen, Y. H.; Nickel, U. Superadditive catalysis of homogeneous redox reactions with mixed silver-gold colloids. *Journal of the Chemical Society, Faraday Transactions* **1993**, *89* (14), 2479-2485.
  32. Christopher Roos, M. S. J. E. F. B. B. D. J. W. Design and Synthesis of Molecular Reactors for the Preparation of Topologically Trapped Gold Cluster. *Advanced Materials* **1999**, *11* (9), 761-766.
  33. Kamat, P. V.; Shanghavi, B. Interparticle Electron Transfer in Metal/Semiconductor Composites. Picosecond Dynamics of CdS-Capped Gold Nanoclusters. *J. Phys. Chem. B* **1997**, *101* (39), 7675-7679.
  34. Bright, R. M.; Walter, D. G.; Musick, M. D.; Jackson, M. A.; Allison, K. J.; Natan, M. J. Chemical and Electrochemical Ag Deposition onto Preformed Au Colloid Monolayers: Approaches to Uniformly-Sized Surface Features with Ag-Like Optical Properties. *Langmuir* **1996**, *12* (3), 810-817.
  35. Brown, K. R.; Natan, M. J. Hydroxylamine Seeding of Colloidal Au Nanoparticles in Solution and on Surfaces. *Langmuir* **1998**, *14* (4), 726-728.
  36. Freeman, R. G.; Hommer, M. B.; Grabar, K. C.; Jackson, M. A.; Natan, M. J. Ag-Clad Au Nanoparticles: Novel Aggregation, Optical, and Surface-Enhanced Raman Scattering Properties. *J. Phys. Chem.* **1996**, *100* (2), 718-724.
  37. Buining, P. A.; Humbel, B. M.; Philipse, A. P.; Verkleij, A. J. Preparation of Functional Silane-Stabilized Gold Colloids in the (Sub)nanometer Size Range. *Langmuir* **1997**, *13* (15), 3921-3926.
-

- 
38. Johnson, S. R.; Evans, S. D.; Brydson, R. Influence of a Terminal Functionality on the Physical Properties of Surfactant-Stabilized Gold Nanoparticles. *Langmuir* **1998**, *14* (23), 6639-6647.
  39. Badia, A.; Gao, W.; Singh, S.; Demers, L.; Cuccia, L.; Reven, L. Structure and Chain Dynamics of Alkanethiol-Capped Gold Colloids. *Langmuir* **1996**, *12* (5), 1262-1269.
  40. Brust, M.; Walker, M.; Bethell, D.; Schiffrin, D. J.; Whyman, R. Synthesis of thiol-derivatised gold nanoparticles in a two-phase Liquid-Liquid system. *Journal of the Chemical Society, Chemical Communications* **1994**, *1994* (7), 801-802.
  41. Esumi, K.; Suzuki, A.; Aihara, N.; Usui, K.; Torigoe, K. Preparation of Gold Colloids with UV Irradiation Using Dendrimers as Stabilizer. *Langmuir* **1998**, *14* (12), 3157-3159.
  42. Xuping Sun, X. J. S. D. E. W. One-Step Synthesis and Size Control of Dendrimer-Protected Gold Nanoparticles: A Heat-Treatment-Based Strategy. *Macromolecular Rapid Communications* **2003**, *24* (17), 1024-1028.
  43. Hussain, I.; Graham, S.; Wang, Z.; Tan, B.; Sherrington, D. C.; Rannard, S. P.; Cooper, A. I.; Brust, M. Size-Controlled Synthesis of Near-Monodisperse Gold Nanoparticles in the 1-4 nm Range Using Polymeric Stabilizers. *J. Am. Chem. Soc.* **2005**, *127* (47), 16398-16399.
  44. Otsuka, H.; Nagasaki, Y.; Kataoka, K. PEGylated nanoparticles for biological and pharmaceutical applications. *Advanced Drug Delivery Reviews* **2003**, *55* (3), 403-419.
  45. Mayer, A.; Antonietti, M. Investigation of polymer-protected noble metal nanoparticles by transmission electron microscopy: control of particle morphology and shape. *Colloid & Polymer Science* **1998**, *276* (9), 769-779.
  46. Martin Möller, J. P. S. Gold nanoparticles in micellar poly(styrene)-b-poly(ethylene oxide) films - size and interparticle distance control in monoparticulate films. *Advanced Materials* **1996**, *8* (4), 337-340.
  47. Zhang, Z.; Patel, R. C.; Kothari, R.; Johnson, C. P.; Friberg, S. E.; Aikens, P. A. Stable Silver Clusters and Nanoparticles Prepared in Polyacrylate and Inverse Micellar Solutions. *J. Phys. Chem. B* **2000**, *104* (6), 1176-1182.
  48. Bharathi, S.; Fishelson, N.; Lev, O. Direct Synthesis and Characterization of Gold and Other Noble Metal Nanodispersions in Sol-Gel-Derived Organically Modified Silicates. *Langmuir* **1999**, *15* (6), 1929-1937.
-



- 
49. Bharathi, S.; Lev, O. Direct synthesis of gold nanodispersions in sol-gel derived silicate sols, gels and films. *Chemical Communications* **1997**, 1997 (23), 2303-2304.
  50. Porter, L. A.; Ji, D.; Westcott, S. L.; Graupe, M.; Czernuszewicz, R. S.; Halas, N. J.; Lee, T. R. Gold and Silver Nanoparticles Functionalized by the Adsorption of Dialkyl Disulfides. *Langmuir* **1998**, 14 (26), 7378-7386.
  51. Ahmadi, T. S.; Wang, Z. L.; Green, T. C.; Henglein, A.; El-Sayed, M. A. Shape-Controlled Synthesis of Colloidal Platinum Nanoparticles. *Science* **1996**, 272 (5270), 1924-1925.
  52. Lahiri, D.; Bunker, B.; Mishra, B.; Zhang, Z.; Meisel, D.; Doudna, C. M.; Bertino, M. F.; Blum, F. D.; Tokuhira, A. T.; Chattopadhyay, S.; Shibata, T.; Terry, J. Bimetallic Pt-Ag and Pd-Ag nanoparticles. *Journal of Applied Physics* **2005**, 97 (9), 094304-094308.
  53. Jana, L. G. Seed-Mediated Growth Approach for Shape-Controlled Synthesis of Spheroidal and Rod-like Gold Nanoparticles Using a Surfactant Template. *Advanced Materials* **2001**, 13 (18), 1389-1393.
  54. Alivisatos, A. P. Semiconductor Clusters, Nanocrystals, and Quantum Dots. *Science* **1996**, 271 (5251), 933-937.
  55. Hickey, S. G.; Riley, D. J. Photoelectrochemical Studies of CdS Nanoparticle-Modified Electrodes. *J. Phys. Chem. B* **1999**, 103 (22), 4599-4602.
  56. Nakanishi, T.; Ohtani, B.; Uosaki, K. Fabrication and Characterization of CdS-Nanoparticle Mono- and Multilayers on a Self-Assembled Monolayer of Alkanedithiols on Gold. *J. Phys. Chem. B* **1998**, 102 (9), 1571-1577.
  57. Zhu, J.; Liu, S.; Palchik, O.; Koltypin, Y.; Gedanken, A. A Novel Sonochemical Method for the Preparation of Nanophasic Sulfides: Synthesis of HgS and PbS Nanoparticles. *Journal of Solid State Chemistry* **2000**, 153 (2), 342-348.
  58. Eugenii Katz, I. W. J. W. Electroanalytical and Bioelectroanalytical Systems Based on Metal and Semiconductor Nanoparticles. *Electroanalysis* **2004**, 16 (1-2), 19-44.
  59. Gao, F.; Lu, Q.; Zhao, D. Controllable Assembly of Ordered Semiconductor Ag<sub>2</sub>S Nanostructures. *Nano Lett.* **2003**, 3 (1), 85-88.
  60. Kryukov, A. I.; Stroyuk, A. L.; Zin'chuk, N. N.; Korzhak, A. V.; Kuchmii, S. Ya. Optical and catalytic properties of Ag<sub>2</sub>S nanoparticles. *Journal of Molecular Catalysis A: Chemical* **2004**, 221 (1-2), 209-221.
  61. Lifshitz, E.; Dag, I.; Litvin, I.; Hodes, G.; Gorer, S.; Reisfeld, R.; Zelner, M.; Minti, H. Optical properties of CdSe nanoparticle films prepared by
-

- 
- chemical deposition and sol-gel methods. *Chemical Physics Letters* **1998**, 288 (2-4), 188-196.
62. Talapin, E. V. S. A New Approach to Crystallization of CdSe Nanoparticles into Ordered Three-Dimensional Superlattices. *Advanced Materials* **2001**, 13 (24), 1868-1871.
63. Bessekhoud, Y.; Robert, D.; Weber, J. V. Synthesis of photocatalytic TiO<sub>2</sub> nanoparticles: optimization of the preparation conditions. *Journal of Photochemistry and Photobiology A: Chemistry* **2003**, 157 (1), 47-53.
64. Li, X.; Chen, W.; Bian, C.; He, J.; Xu, N.; Xue, G. Surface modification of TiO<sub>2</sub> nanoparticles by polyaniline. *Applied Surface Science* **2003**, 217 (1-4), 16-22.
65. Steigerwald, M. L.; Alivisatos, A. P.; Gibson, J. M.; Harris, T. D.; Kortan, R.; Muller, A. J.; Thayer, A. M.; Duncan, T. M.; Douglass, D. C.; Brus, L. E. Surface derivatization and isolation of semiconductor cluster molecules. *J. Am. Chem. Soc.* **1988**, 110 (10), 3046-3050.
66. Li, X.; Fryer, J. R.; Cole-Hamilton, D. J. A new, simple and versatile method for the production of nano-scale particles of semiconductors. *Journal of the Chemical Society, Chemical Communications* **1994**, 1994 (14), 1715-1716.
67. Murray, C. B.; Norris, D. J.; Bawendi, M. G. Synthesis and characterization of nearly monodisperse CdE (E = sulfur, selenium, tellurium) semiconductor nanocrystallites. *J. Am. Chem. Soc.* **1993**, 115 (19), 8706-8715.
68. Chen, C. C. Y. Large-Scale Catalytic Synthesis of Crystalline Gallium Nitride Nanowires. *Advanced Materials* **2000**, 12 (10), 738-741.
69. Azuma, M. S. Synthesis of Monodisperse Ultrapure Gallium Nitride Nanoparticles by MOCVD. *Chemical Vapor Deposition* **2004**, 10 (1), 11-13.
70. Takagi, M.; Maki, T.; Miyahara, M.; Mae, K. Production of titania nanoparticles by using a new microreactor assembled with same axle dual pipe. *Chemical Engineering Journal* **2004**, 101 (1-3), 269-276.
71. Zhang, D.; Qi, L.; Ma, J.; Cheng, H. Formation of crystalline nanosized titania in reverse micelles at room temperature. *Journal of Materials Chemistry* **2002**, 12 (12), 3677-3680.
72. Kruis, F. E.; Fissan, H.; Peled, A. Synthesis of nanoparticles in the gas phase for electronic, optical and magnetic applications--a review. *Journal of Aerosol Science* **1998**, 29 (5-6), 511-535.
-

- 
73. Hahn, H. Gas phase synthesis of nanocrystalline materials. *Nanostructured Materials* **1997**, *9* (1-8), 3-12.
  74. Ullmann, M.; Friedlander, S. K.; Schmidt-Ott, A. Nanoparticle Formation by Laser Ablation. *Journal of Nanoparticle Research* **2002**, *4* (6), 499-509.
  75. Simakin, A. V.; Voronov, V. V.; Kirichenko, N. A.; Shafeev, G. A. Nanoparticles produced by laser ablation of solids in liquid environment. *Applied Physics A: Materials Science & Processing* **2004**, *79* (4), 1127-1132.
  76. Jensen, T. R.; Schatz, G. C.; Van Duyne, R. P. Nanosphere lithography: surface plasmon resonance spectrum of a periodic array of silver nanoparticles by ultraviolet-visible extinction spectroscopy and electrodynamic modeling. *J. Phys. Chem. B* **1999**, *103* (13), 2394-2401.
  77. Hultheen, J. C.; Treichel, D. A.; Smith, M. T.; Duval, M. L.; Jensen, T. R.; Van Duyne, R. P. Nanosphere lithography: size-tunable silver nanoparticle and surface cluster arrays. *J. Phys. Chem. B* **1999**, *103* (19), 3854-3863.
  78. Kim, S. S.; Nah, Y. C.; Noh, Y. Y.; Jo, J.; Kim, D. Y. Electrodeposited Pt for cost-efficient and flexible dye-sensitized solar cells. *Electrochimica Acta* **2006**, *51* (18), 3814-3819.
  79. Reetz, M. T.; Winter, M.; Dumpich, G.; Lohau, J.; Friedrichowski, S. Fabrication of Metallic and Bimetallic Nanostructures by Electron Beam Induced Metallization of Surfactant Stabilized Pd and Pd/Pt Clusters. *J. Am. Chem. Soc.* **1997**, *119* (19), 4539-4540.
  80. Saurakhiya, N.; Zhu, Y. W.; Cheong, F. C.; Ong, C. K.; Wee, A. T. S.; Lin, J. Y.; Sow, C. H. Pulsed laser deposition-assisted patterning of aligned carbon nanotubes modified by focused laser beam for efficient field emission. *Carbon* **2005**, *43* (10), 2128-2133.
  81. Moriguchi, I.; Shibata, F.; Teraoka, Y.; Kagawa, S. Control of Size of CdS Formed in Organized Molecular Assembly Films by Molecular Structure and Film Orderliness. *Chemistry Letters* **1995**, *24* (9), 761-762.
  82. Panyam, J.; Labhasetwar, V. Biodegradable nanoparticles for drug and gene delivery to cells and tissue. *Advanced Drug Delivery Reviews* **2003**, *55* (3), 329-347.
  83. Ma, J.; Wong, H.; Kong, L. B.; Peng, K. W. Biomimetic processing of nanocrystallite bioactive apatite coating on titanium. *Nanotechnology* **2003**, *14* (6), 619-623.
  84. O'Neal, D. P.; Hirsch, L. R.; Halas, N. J.; Payne, J. D.; West, J. L. Photo-thermal tumor ablation in mice using near infrared-absorbing nanoparticles. *Cancer Letters* **2004**, *209* (2), 171-176.
-

- 
85. Molday, R. S.; Mackenzie, D. Immunospecific ferromagnetic iron-dextran reagents for the labeling and magnetic separation of cells. *Journal of Immunological Methods* **1982**, *52* (3), 353-367.
  86. Parak, R. B. Cell Motility and Metastatic Potential Studies Based on Quantum Dot Imaging of Phagokinetic Tracks. *Advanced Materials* **2002**, *14* (12), 882-885.
  87. Sato, M.; Webster, T. J. Nanobiotechnology: implications for the future of nanotechnology in orthopedic applications. *Expert Rev. Med. Devices* **2004**, *1* (1), 105-114.
  88. Adamopoulos, O.; Papadopoulos, T. Nanostructured bioceramics for maxillofacial applications. *Journal of Materials Science: Materials in Medicine* **2007**, *18* (8), 1587-1597.
  89. Roy, I.; Ohulchanskyy, T. Y.; Pudavar, H. E.; Bergey, E. J.; Oseroff, A. R.; Morgan, J.; Dougherty, T. J.; Prasad, P. N. Ceramic-Based Nanoparticles Entrapping Water-Insoluble Photosensitizing Anticancer Drugs: A Novel Drug-Carrier System for Photodynamic Therapy. *J. Am. Chem. Soc.* **2003**, *125* (26), 7860-7865.
  90. Pankhurst, Q. A.; Connolly, J.; Jones, S. K.; Dobson, J. Applications of magnetic nanoparticles in biomedicine. *Journal of Physics D: Applied Physics* **2003**, *36* (13), R167-R181.
  91. Reich, D. H.; Tanase, M.; Hultgren, A.; Bauer, L. A.; Chen, C. S.; Meyer, G. J. Biological applications of multifunctional magnetic nanowires (invited). *Journal of Applied Physics* **2003**, *93* (10), 7275-7280.
  92. Salata, O. V. Applications of nanoparticles in biology and medicine. *feedback* **2004**.
  93. Andrey, L. G. Enzyme-catalyzed direct electron transfer: Fundamentals and analytical applications. *Electroanalysis* **1997**, *9* (9), 661-674.
  94. Maye, M. M.; Lou, Y.; Zhong, C. J. Core-Shell Gold Nanoparticle Assembly as Novel Electrocatalyst of CO Oxidation. *Langmuir* **2000**, *16* (19), 7520-7523.
  95. Tang, J. L.; Cheng, S. F.; Hsu, W. T.; Chiang, T. Y.; Chau, L. K. Fiber-optic biochemical sensing with a colloidal gold-modified long period fiber grating. *Sensors and Actuators B: Chemical* **2006**, *119* (1), 105-109.
  96. Mena, M. L.; Yanez-Sedeno, P.; Pingarron, J. M. A comparison of different strategies for the construction of amperometric enzyme biosensors using gold nanoparticle-modified electrodes. *Analytical Biochemistry* **2005**, *336* (1), 20-27.
-

- 
97. Andrey, L. G. Enzyme-catalyzed direct electron transfer: Fundamentals and analytical applications. *Electroanalysis* **1997**, *9* (9), 661-674.
  98. Brown, K. R.; Fox, A. P.; Natan, M. J. Morphology-Dependent Electrochemistry of Cytochrome c at Au Colloid-Modified SnO<sub>2</sub> Electrodes. *J. Am. Chem. Soc.* **1996**, *118* (5), 1154-1157.
  99. Jia, J.; Wang, B.; Wu, A.; Cheng, G.; Li, Z.; Dong, S. A Method to Construct a Third-Generation Horseradish Peroxidase Biosensor: Self-Assembling Gold Nanoparticles to Three-Dimensional Sol-Gel Network. *Anal. Chem.* **2002**, *74* (9), 2217-2223.
  100. Wang, L.; Wang, E. Direct electron transfer between cytochrome c and a gold nanoparticles modified electrode. *Electrochemistry Communications* **2004**, *6* (1), 49-54.
  101. Gu, H. Y.; Yu, A. M.; Chen, H. Y. Direct electron transfer and characterization of hemoglobin immobilized on a Au colloid-cysteamine-modified gold electrode. *Journal of Electroanalytical Chemistry* **2001**, *516* (1-2), 119-126.
  102. Yi, X.; Huang-Xian, J.; Hong-Yuan, C. Direct Electrochemistry of Horseradish Peroxidase Immobilized on a Colloid/Cysteamine-Modified Gold Electrode. *Analytical Biochemistry* **2000**, *278* (1), 22-28.
  103. Songqin Liu, H. J. Electrocatalysis via Direct Electrochemistry of Myoglobin Immobilized on Colloidal Gold Nanoparticles. *Electroanalysis* **2003**, *15* (18), 1488-1493.
  104. Agui, L.; Manso, J.; Yanez-Sedeno, P.; Pingarron, J. M. Amperometric biosensor for hypoxanthine based on immobilized xanthine oxidase on nanocrystal gold-carbon paste electrodes. *Sensors and Actuators B: Chemical* **2006**, *113* (1), 272-280.
  105. Han, X.; Cheng, W.; Zhang, Z.; Dong, S.; Wang, E. Direct electron transfer between hemoglobin and a glassy carbon electrode facilitated by lipid-protected gold nanoparticles. *Biochimica et Biophysica Acta (BBA) - Bioenergetics* **2002**, *1556* (2-3), 273-277.
  106. Zhang, J.; Oyama, M. Gold nanoparticle-attached ITO as a biocompatible matrix for myoglobin immobilization: direct electrochemistry and catalysis to hydrogen peroxide. *Journal of Electroanalytical Chemistry* **2005**, *577* (2), 273-279.
  107. Shumyantseva, V. V.; Carrara, S.; Bavastrello, V.; Jason Riley, D.; Bulko, T. V.; Skryabin, K. G.; Archakov, A. I.; Nicolini, C. Direct electron transfer between cytochrome P450<sub>scc</sub> and gold nanoparticles on screen-printed rhodium-graphite electrodes. *Biosensors and Bioelectronics* **2005**, *21* (1), 217-222.
-

- 
108. Tang, D.; Yuan, R.; Chai, Y.; Fu, Y.; Dai, J.; Liu, Y.; Zhong, X. New amperometric and potentiometric immunosensors based on gold nanoparticles/tris(2,2'-bipyridyl)cobalt(III) multilayer films for hepatitis B surface antigen determinations. *Biosensors and Bioelectronics* **2005**, *21* (4), 539-548.
  109. Shihong Chen, R. Y. Y. C. L. X. N. W. X. L. L. Z. Amperometric Hydrogen Peroxide Biosensor Based on the Immobilization of Horseradish Peroxidase (HRP) on the Layer-by-Layer Assembly Films of Gold Colloidal Nanoparticles and Toluidine Blue. *Electroanalysis* **2006**, *18* (5), 471-477.
  110. Hoshi, T.; Sagae, N.; Daikuhara, K.; Takahara, K.; Anzai, J. i. Multilayer membranes via layer-by-layer deposition of glucose oxidase and Au nanoparticles on a Pt electrode for glucose sensing. *Materials Science and Engineering: C* **2007**, *27* (4), 890-894.
  111. Yang, W.; Wang, J.; Zhao, S.; Sun, Y.; Sun, C. Multilayered construction of glucose oxidase and gold nanoparticles on Au electrodes based on layer-by-layer covalent attachment. *Electrochemistry Communications* **2006**, *8* (4), 665-672.
  112. Payne, G. F.; Raghavan, S. R. Chitosan: a soft interconnect for hierarchical assembly of nano-scale components. *Soft Matter* **2007**, *3* (5), 521-527.
  113. Luo, X. L.; Xu, J. J.; Du, Y.; Chen, H. Y. A glucose biosensor based on chitosan-glucose oxidase-gold nanoparticles biocomposite formed by one-step electrodeposition. *Analytical Biochemistry* **2004**, *334* (2), 284-289.
  114. Xu, Q.; Mao, C.; Liu, N. N.; Zhu, J. J.; Sheng, J. Direct electrochemistry of horseradish peroxidase based on biocompatible carboxymethyl chitosan-gold nanoparticle nanocomposite. *Biosensors and Bioelectronics* **2006**, *22* (5), 768-773.
  115. Lin, J.; Qu, W.; Zhang, S. Disposable biosensor based on enzyme immobilized on Au-chitosan-modified indium tin oxide electrode with flow injection amperometric analysis. *Analytical Biochemistry* **2007**, *360* (2), 288-293.
  116. Joseph, W. Towards Genoelectronics: Electrochemical Biosensing of DNA Hybridization. *Chemistry - A European Journal* **1999**, *5* (6), 1681-1685.
  117. Justin, G. Electrochemical DNA Hybridization Biosensors. *Electroanalysis* **2002**, *14* (17), 1149-1156.
  118. M.T.Castañeda, S. A. Electrochemical Sensing of DNA Using Gold Nanoparticles. *Electroanalysis* **2007**, *19* (7-8), 743-753.
-

- 
119. Wang, J.; Xu, D.; Kawde, A. N.; Polsky, R. Metal Nanoparticle-Based Electrochemical Stripping Potentiometric Detection of DNA Hybridization. *Anal. Chem.* **2001**, *73* (22), 5576-5581.
120. Authier, L.; Grossiord, C.; Brossier, P.; Limoges, B. Gold Nanoparticle-Based Quantitative Electrochemical Detection of Amplified Human Cytomegalovirus DNA Using Disposable Microband Electrodes. *Anal. Chem.* **2001**, *73* (18), 4450-4456.
121. Wang, J.; Polsky, R.; Xu, D. Silver-Enhanced Colloidal Gold Electrochemical Stripping Detection of DNA Hybridization. *Langmuir* **2001**, *17* (19), 5739-5741.
122. Wang, J.; Xu, D.; Polsky, R. Magnetically-induced solid-state electrochemical detection of DNA hybridization. *J. Am. Chem. Soc* **2002**, *124* (4208), 140.
123. Pumera, M.; Castaneda, M. T.; Pividori, M. I.; Eritja, R.; Merkoci, A.; Alegret, S. Magnetically Triggered Direct Electrochemical Detection of DNA Hybridization Using Au<sub>67</sub> Quantum Dot as Electrical Tracer. *Langmuir* **2005**, *21* (21), 9625-9629.
124. Cai, H.; Wang, Y.; He, P.; Fang, Y. Electrochemical detection of DNA hybridization based on silver-enhanced gold nanoparticle label. *Analytica Chimica Acta* **2002**, *469* (2), 165-172.
125. Rochelet-Dequaire, M.; Limoges, B.; Brossier, P. Subfemtomolar electrochemical detection of target DNA by catalytic enlargement of the hybridized gold nanoparticle labels. *The Analyst* **2006**, *131* (8), 923-929.
126. Wang, J.; Li, J.; Baca, A. J.; Hu, J.; Zhou, F.; Yan, W.; Pang, D. W. Amplified Voltammetric Detection of DNA Hybridization via Oxidation of Ferrocene Caps on Gold Nanoparticle/Streptavidin Conjugates. *Anal. Chem.* **2003**, *75* (15), 3941-3945.
127. Wang, H.; Zhang, C.; Li, Y.; Qi, H. Electrogenated chemiluminescence detection for deoxyribonucleic acid hybridization based on gold nanoparticles carrying multiple probes. *Analytica Chimica Acta* **2006**, *575* (2), 205-211.
128. Liang, R.; Qiu, J.; Cai, P. A novel amperometric immunosensor based on three-dimensional sol-gel network and nanoparticle self-assemble technique. *Analytica Chimica Acta* **2005**, *534* (2), 223-229.
129. Tang, D. P.; Yuan, R.; Chai, Y. Q.; Zhong, X.; Liu, Y.; Dai, J. Y.; Zhang, L. Y. Novel potentiometric immunosensor for hepatitis B surface antigen using a gold nanoparticle-based biomolecular immobilization method. *Analytical Biochemistry* **2004**, *333* (2), 345-350.
-

- 
130. Dequaire, M.; Degrand, C.; Limoges, B. An Electrochemical Metalloimmunoassay Based on a Colloidal Gold Label. *Anal. Chem.* **2000**, *72* (22), 5521-5528.
131. Chu, X.; Fu, X.; Chen, K.; Shen, G. L.; Yu, R. Q. An electrochemical stripping metalloimmunoassay based on silver-enhanced gold nanoparticle label. *Biosensors and Bioelectronics* **2005**, *20* (9), 1805-1812.
132. Liao, K. T.; Huang, H. J. Femtomolar immunoassay based on coupling gold nanoparticle enlargement with square wave stripping voltammetry. *Analytica Chimica Acta* **2005**, *538* (1-2), 159-164.
133. Chen, J.; Tang, J.; Yan, F.; Ju, H. A gold nanoparticles/sol-gel composite architecture for encapsulation of immunoconjugate for reagentless electrochemical immunoassay. *Biomaterials* **2006**, *27* (10), 2313-2321.
134. Jin Chen, F. Y. F. T. H. J. Gold Nanoparticles Doped Three-Dimensional Sol-gel Matrix for Amperometric Human Chorionic Gonadotrophin Immunosensor. *Electroanalysis* **2006**, *18* (17), 1696-1702.
135. Tang, H.; Chen, J.; Nie, L.; Kuang, Y.; Yao, S. A label-free electrochemical immunoassay for carcinoembryonic antigen (CEA) based on gold nanoparticles (AuNPs) and nonconductive polymer film. *Biosensors and Bioelectronics* **2007**, *22* (6), 1061-1067.
136. Zhang, S.; Huang, F.; Liu, B.; Ding, J.; Xu, X.; Kong, J. A sensitive impedance immunosensor based on functionalized gold nanoparticle-protein composite films for probing apolipoprotein A-I. *Talanta* **2007**, *71* (2), 874-881.
137. Das, J.; Aziz, M. A.; Yang, H. A Nanocatalyst-Based Assay for Proteins: DNA-Free Ultrasensitive Electrochemical Detection Using Catalytic Reduction of p-Nitrophenol by Gold-Nanoparticle Labels. *J. Am. Chem. Soc.* **2006**, *128* (50), 16022-16023.
138. Penner, R. M.; Martin, C. R. Preparation and electrochemical characterization of ultramicroelectrode ensembles. *Anal. Chem.* **1987**, *59* (21), 2625-2630.
139. Escorcia, A.; Dhirani, A. A. Electrochemical properties of ferrocenylalkane dithiol-gold nanoparticle films prepared by layer-by-layer self-assembly. *Journal of Electroanalytical Chemistry* **2007**, *601* (1-2), 260-268.
140. Tian, R. h.; Zhi, J. f. Fabrication and electrochemical properties of boron-doped diamond film-gold nanoparticle array hybrid electrode. *Electrochemistry Communications* **2007**, *9* (5), 1120-1126.
141. Ding, L.; Hao, C.; Xue, Y.; Ju, H. A Bio-Inspired Support of Gold Nanoparticles-Chitosan Nanocomposites Gel for Immobilization and
-



- Electrochemical Study of K562 Leukemia Cells. *Biomacromolecules* **2007**, 8 (4), 1341-1346.
142. Tominaga, M.; Shimazoe, T.; Nagashima, M.; Taniguchi, I. Electrocatalytic oxidation of glucose at gold nanoparticle-modified carbon electrodes in alkaline and neutral solutions. *Electrochemistry Communications* **2005**, 7 (2), 189-193.
143. Lu, L. P.; Wang, S. Q.; Lin, X. Q. Fabrication of layer-by-layer deposited multilayer films containing DNA and gold nanoparticle for norepinephrine biosensor. *Analytica Chimica Acta* **2004**, 519 (2), 161-166.
144. Raj, C. R.; Okajima, T.; Ohsaka, T. Gold nanoparticle arrays for the voltammetric sensing of dopamine. *Journal of Electroanalytical Chemistry* **2003**, 543 (2), 127-133.
145. Su, L.; Mao, L. Gold nanoparticle/alkanedithiol conductive films self-assembled onto gold electrode: Electrochemistry and electroanalytical application for voltammetric determination of trace amount of catechol. *Talanta* **2006**, 70 (1), 68-74.
146. Wang, L.; Bai, J.; Huang, P.; Wang, H.; Zhang, L.; Zhao, Y. Self-assembly of gold nanoparticles for the voltammetric sensing of epinephrine. *Electrochemistry Communications* **2006**, 8 (6), 1035-1040.
147. Wang, J.; Wang, F.; Zou, X.; Xu, Z.; Dong, S. Surface plasmon resonance and electrochemistry for detection of small molecules using catalyzed deposition of metal ions on gold substrate. *Electrochemistry Communications* **2007**, 9 (2), 343-347.
148. Bikash Kumar Jena, C. R. R. Enzyme-Free Amperometric Sensing of Glucose by Using Gold Nanoparticles. *Chemistry - A European Journal* **2006**, 12 (10), 2702-2708.
149. Dominguez Renedo, O.; rcos Martinez, M. J. Anodic stripping voltammetry of antimony using gold nanoparticle-modified carbon screen-printed electrodes. *Analytica Chimica Acta* **2007**, 589 (2), 255-260.
150. Yue-Shian Song, G. M. Y.-Z. C. C.-C. L. J.-M. Z. Screen Printed Carbon Electrode Modified with Poly(L-Lactide) Stabilized Gold Nanoparticles for Sensitive As(III) Detection. *Electroanalysis* **2006**, 18 (18), 1763-1770.
151. Xuan Dai, R. G. Gold Nanoparticle Modified Electrodes Show a Reduced Interference by Cu(II) in the Detection of As(III) Using Anodic Stripping Voltammetry. *Electroanalysis* **2005**, 17 (14), 1325-1330.

- 
152. Milsom, E. V.; Novak, J.; Oyama, M.; Marken, F. Electrocatalytic oxidation of nitric oxide at TiO<sub>2</sub>-Au nanocomposite film electrodes. *Electrochemistry Communications* **2007**, *9* (3), 436-442.
153. Yu, A.; Liang, Z.; Cho, J.; Caruso, F. Nanostructured Electrochemical Sensor Based on Dense Gold Nanoparticle Films. *Nano Lett.* **2003**, *3* (9), 1203-1207.
154. Zhang, J.; Oyama, M. Gold nanoparticle arrays directly grown on nanostructured indium tin oxide electrodes: Characterization and electroanalytical application. *Analytica Chimica Acta* **2005**, *540* (2), 299-306.
155. Jena, B. K.; Raj, C. R. Ultrasensitive Nanostructured Platform for the Electrochemical Sensing of Hydrazine. *J. Phys. Chem. C* **2007**, *111* (17), 6228-6232.
156. Parak, W. J.; Gerion, D.; Pellegrino, T.; Zanchet, D.; Micheel, C.; Williams, S. C.; Boudreau, R.; Gros, M. A. L.; Larabell, C. A.; Alivisatos, A. P. Biological applications of colloidal nanocrystals. *Nanotechnology* **2003**, *14* (7), R15-R27.
157. Han, M.; Gao, X.; Su, J. Z.; Nie, S. Quantum-dot-tagged microbeads for multiplexed optical coding of biomolecules. *Nature Biotechnology* **2001**, *19*, 631-635.
158. Haes, A. J.; Van Duyne, R. P. A Nanoscale Optical Biosensor: Sensitivity and Selectivity of an Approach Based on the Localized Surface Plasmon Resonance Spectroscopy of Triangular Silver Nanoparticles. *J. Am. Chem. Soc.* **2002**, *124* (35), 10596-10604.
159. KIM, N. H.; BAEK, T. J.; PARK, H. G.; SEONG, G. H. Highly Sensitive Biomolecule Detection on a Quartz Crystal Microbalance Using Gold Nanoparticles as Signal Amplification Probes. *Analytical Sciences* **2007**, *23* (2), 177-181.
160. Aslan, K.; Zhang, J.; Lakowicz, J. R.; Geddes, C. D. Saccharide Sensing Using Gold and Silver Nanoparticles-A Review. *Journal of Fluorescence* **2004**, *14* (4), 391-400.
161. Hu, J.; Wang, Z.; Li, J. Gold Nanoparticles With Special Shapes: Controlled Synthesis, Surface-enhanced Raman Scattering, and The Application in Biodetection. *Sensors* **2007**, *7*, 3299-3311.
162. Aslan, K.; Lakowicz, J. R.; Geddes, C. D. Rapid deposition of triangular silver nanoplates on planar surfaces: Application to metal-enhanced fluorescence. *J. Phys. Chem. B* **2005**, *109* (13), 6247-6251.
163. Wang, J.; Liu, J.; Chen, L.; Lu, F. Highly Selective Membrane-Free, Mediator-Free Glucose Biosensor. *Anal. Chem.* **1994**, *66* (21), 3600-3603.
-

- 
164. Joseph, W. *Analytical Electrochemistry*; 3 ed.; VCH: 1994.
165. Mirabella, F. M.; Harrick, N. J. *Internal Reflection Spectroscopy: Review and Supplement*; Harrick Scientific Corporation Ossining, NY: 1985.
166. de Mello, A. J. *Surface Analytical Techniques for Probing Biomaterial Processes* ed J Davies; Boca Raton, FL: CRC Press: 1996; Vol. 1.
167. Swalen, J. D. Optical properties of Langmuir-Blodgett films. *Journal of Molecular Electronics* **1986**, 2, 155-181.
168. Kovacs, G. D. *In Electromagnetic Surface Modes (Boardman, AD, ed.)*; Wiley, New York: 1982.
169. Kretschmann, E. The determination of the optical constants of metals by excitation of surface plasmons. *Z. Phys* **1971**, 241 (4), 313.
170. Liedberg, B.; Nylander, C.; Lundstroem, I. Surface plasmon resonance for gas detection and biosensing. *SENSORS ACTUATORS*. **1983**, 4 (2), 299-304.
171. Jonsson, U.; Fagerstam, L.; Ivarsson, B.; Johnsson, B.; Karlsson, R.; Lundh, K.; Lofas, S.; Persson, B.; Roos, H.; Ronnberg, I. Real-time biospecific interaction analysis using surface plasmon resonance and a sensor chip technology. *Biotechniques* **1991**, 11 (5), 620-627.
172. Davies, J. *Surface Analytical Techniques for Probing Biomaterial Processes*; CRC Press: 1996.
173. Kumar, S.; Gandhi, K. S.; Kumar, R. Modeling of Formation of Gold Nanoparticles by Citrate Method. *Ind. Eng. Chem. Res.* **2007**, 46 (10), 3128-3136.
174. Brust, M.; Walker, M.; Bethell, D.; Schiffrin, D. J.; Whyman, R. Synthesis of thiol-derivatised gold nanoparticles in a two-phase Liquid-Liquid system. *Journal of the Chemical Society, Chemical Communications* **1994**, 1994 (7), 801-802.
175. Wijngaarden, R. J. Fast imaging polarimeter for magneto-optical investigations. *Review of Scientific Instruments* **2001**, 72 (6), 2661.
176. Sinnaeve, G.; Dardenne, P. Quantitative analysis of raw apple juices using near infrared, Fourier-transform near infrared and Fourier-transform infrared instruments: a comparison of their analytical performances. *J. Near Infrared Spectrosc* **1997**, 5, 1-17.
177. Takahashi, S.; Anzai, J. Phenylboronic Acid Monolayer-Modified Electrodes Sensitive to Sugars. *Langmuir* **2005**, 21 (11), 5102-5107.
-

- 
178. DiCesare, N.; Lakowicz, J. R. A new highly fluorescent probe for monosaccharides based on a donor–acceptor diphenyloxazole. *Chemical Communications* **2001**, 2001 (19), 2022-2023.
179. Kim, Y. S.; Liu, J.; Han, X. J.; Pervin, A.; Linhardt, R. J. Analysis of fluorescently labeled sugars by reversed-phase ion-pairing high-performance liquid chromatography. *J Chromatogr Sci* **1995**, 33 (4), 162-167.
180. Mikeska, R.; Wacker, R.; Arni, R.; Singh, T. P.; Mikhailov, A.; Gabdoulkhakov, A.; Voelter, W.; Betzel, C. protein structure communications. *logo* **2005**, 61 (Part 1), 17-25.
181. Duverger, E.; Frison, N.; Roche, A. C.; Monsigny, M. Carbohydrate-lectin interactions assessed by surface plasmon resonance. *Biochimie* **2003**, 85 (1-2), 167-179.
182. HIMURO, Y.; TAKAI, M.; Ishiharak, K. High Performance of Enzymatic Glucose Sensor with Polymeric Mediator for Blood Analysis. *Trans Mater Res Soc Jpn* **2005**, 30 (2), 417-420.
183. Derwinska, K.; Miecznikowski, K.; Koncki, R.; Kulesza, P. J.; Glab, S.; Malik, M. A. Application of Prussian Blue Based Composite Film with Functionalized Organic Polymer to Construction of Enzymatic Glucose Biosensor. *Electroanalysis* **2003**, 15 (2324), 1843-1849.
184. Park, S.; Boo, H.; Chung, T. D. Electrochemical non-enzymatic glucose sensors. *Analytica Chimica Acta* **2006**, 556 (1), 46-57.
185. Vassilyev, Y.; Khazova, O. A.; Nikolaeva, N. N. Kinetics and mechanism of glucose electrooxidation on different electrode-catalysts : Part I. Adsorption and oxidation on platinum. *Journal of Electroanalytical Chemistry* **1985**, 196 (1), 105-125.
186. Wittstock, G.; Strübing, A.; Szargan, R.; Werner, G. Glucose oxidation at bismuth-modified platinum electrodes. *Journal of Electroanalytical Chemistry* **1998**, 444 (1), 61-73.
187. Larew, A.; Johnson, D. C. Concentration dependence of the mechanism of glucose oxidation at gold electrodes in alkaline media. *Journal of Electroanalytical Chemistry* **1989**, 262 (1-2), 167-182.
188. Burke, L. D.; Nugent, P. F. Multicomponent hydrous oxide films grown on gold in acid solution. *Journal of Electroanalytical Chemistry* **1998**, 444 (1), 19-29.
189. Burke, L. D.; Nugent, P. F. The electrochemistry of gold. II. The electrocatalytic behaviour of the metal in aqueous media. *Gold Bull* **1998**, 31 (2), 39-50.
-

- 
190. Burke, L. D.; O'Connell, A. M.; O'Mullane, A. P. The role of defects, or active states, in surface electrochemistry with particular reference to gold in neutral solution. *Journal of Applied Electrochemistry* **2003**, *33* (12), 1125-1135.
191. Matsumoto, F.; Harada, M.; Koura, N.; Uesugi, S. Electrochemical oxidation of glucose at Hg adatom-modified Au electrode in alkaline aqueous solution. *Electrochemistry Communications* **2003**, *5* (1), 42-46.
192. Aoun, S. B.; Dursun, Z.; Koga, T.; Bang, G. S.; Sotomura, T.; Taniguchi, I. Effect of metal ad-layers on Au(1 1 1) electrodes on electrocatalytic oxidation of glucose in an alkaline solution. *Journal of Electroanalytical Chemistry* **2004**, *567* (2), 175-183.
193. Tominaga, M.; Shimazoe, T.; Nagashima, M.; Taniguchi, I. Electrocatalytic Oxidation of Glucose at Carbon Electrodes Modified with Gold and Gold-Platinum Alloy Nanoparticles in an Alkaline Solution. *Chemistry Letters* **2005**, *34* (2), 202-203.
194. Tominaga, M.; Shimazoe, T.; Nagashima, M.; Taniguchi, I. Electrocatalytic oxidation of glucose at gold nanoparticle-modified carbon electrodes in alkaline and neutral solutions. *Electrochemistry Communications* **2005**, *7* (2), 189-193.
195. N.Kotov *Multilayer Thin Film*; Willey-VCH, Weinheim, 2002.
196. W.Heil; R.Koberstein; B.Zawta *Reference Ranges for Adults and Children*; 1999.
197. Levesque, D.; Rouillard, C. Nur77 and retinoid X receptors: crucial factors in dopamine-related neuroadaptation. *Trends in Neurosciences* **2007**, *30* (1), 22-30.
198. Hayashi, K.; Iwasaki, Y.; Kurita, R.; Sunagawa, K.; Niwa, O.; Tate, A. The highly sensitive detection of catecholamines using a microfluidic device integrated with an enzyme-modified pre-reactor for interferent elimination and an interdigitated array electrode. *Journal of Electroanalytical Chemistry* **2005**, *579* (2), 215-222.
199. Mateos, J.; Lomeña, F.; Parellada, E.; Font, M.; Fernandez, E.; Pavia, J.; Prats, A.; Pons, F.; Bernardo, M. Decreased striatal dopamine transporter binding assessed with [<sup>123</sup>I] FP-CIT in first-episode schizophrenic patients with and without short-term antipsychotic-induced parkinsonism. *Psychopharmacology* **2005**, *181* (2), 401-406.
200. Marsden, C. A. Dopamine: the rewarding years. *Br J Pharmacol* **0 AD**, *147* (S1), S136-S144.
201. Hong, C. J.; Liu, H. C.; Liu, T. Y.; Liao, D. L.; Tsai, S. J. Association studies of the adenosine A2a receptor (1976T > C) genetic polymorphism in
-

- 
- Parkinson's disease and schizophrenia. *Journal of Neural Transmission* **2005**, *112* (11), 1503-1510.
202. Downard, A. J.; Roddick, A. D.; Bond, A. M. Covalent modification of carbon electrodes for voltammetric differentiation of dopamine and ascorbic acid. *Analytica Chimica Acta* **1995**, *317* (1-3), 303-310.
203. Sun, Y.; Ye, B.; Zhang, W.; Zhou, X. Simultaneous determination of dopamine and ascorbic acid at poly(neutral red) modified electrodes. *Analytica Chimica Acta* **1998**, *363* (1), 75-80.
204. Domenech, A.; Garcia, H.; Domenech-Carbo, M. T.; Galletero, M. S. 2,4,6-Triphenylpyrylium Ion Encapsulated into Zeolite Y as a Selective Electrode for the Electrochemical Determination of Dopamine in the Presence of Ascorbic Acid. *Anal. Chem.* **2002**, *74* (3), 562-569.
205. Vergheese, T. M.; Berchmans, S. Bio-inspired recognition of dopamine versus ascorbic acid. *Journal of Electroanalytical Chemistry* **2004**, *570* (1), 35-46.
206. Shahrokhian, S.; Karimi, M. Voltammetric studies of a cobalt(II)-4-methylsalophen modified carbon-paste electrode and its application for the simultaneous determination of cysteine and ascorbic acid. *Electrochimica Acta* **2004**, *50* (1), 77-84.
207. Chen, S. M.; Chzo, W. Y. Simultaneous voltammetric detection of dopamine and ascorbic acid using didodecyldimethylammonium bromide (DDAB) film-modified electrodes. *Journal of Electroanalytical Chemistry* **2006**, *587* (2), 226-234.
208. Ling Mei Niu, H. Q. L. N. B. L. Electrochemical Behavior of Dopamine at a Penicillamine Self-Assembled Gold Electrode and its Analytical Application. *Archiv der Pharmazie* **2006**, *339* (7), 356-360.
209. Shervedani, R. K.; Bagherzadeh, M.; Mozaffari, S. A. Determination of dopamine in the presence of high concentration of ascorbic acid by using gold cysteamine self-assembled monolayers as a nanosensor. *Sensors and Actuators B: Chemical* **2006**, *115* (2), 614-621.
210. Pihel, K.; Walker, Q. D.; Wightman, R. M. Overoxidized Polypyrrole-Coated Carbon Fiber Microelectrodes for Dopamine Measurements with Fast-Scan Cyclic Voltammetry. *Anal. Chem.* **1996**, *68* (13), 2084-2089.
211. Zhang, X.; Ogorevc, B.; Tavcar, G.; Švegl, I. G. Over-oxidized polypyrrole-modified carbon fibre ultramicroelectrode with an integrated silver/silver chloride reference electrode for the selective voltammetric measurement of dopamine in extremely small sample volumes. *The Analyst* **1996**, *121* (12), 1817-1822.
-

- 
212. Erdogdu, G.; Karagozler, A. E. Investigation and comparison of the electrochemical behavior of some organic and biological molecules at various conducting polymer electrodes. *Talanta* **1997**, *44* (11), 2011-2018.
213. GAO, Z.; YAP, D.; ZHANG, Y. Voltammetric Determination of Dopamine in a Mixture of Dopamine and Ascorbic Acid at a Deactivated Polythiophene Film Modified Electrode. *Analytical Sciences* **1998**, *14* (6), 1059-1063.
214. Mo, J. W.; Ogorevc, B. Simultaneous Measurement of Dopamine and Ascorbate at Their Physiological Levels Using Voltammetric Microprobe Based on Overoxidized Poly(1,2-phenylenediamine)-Coated Carbon Fiber. *Anal. Chem.* **2001**, *73* (6), 1196-1202.
215. Selvaraju, T.; Ramaraj, R. Simultaneous determination of ascorbic acid, dopamine and serotonin at poly(phenosafranin) modified electrode. *Electrochemistry Communications* **2003**, *5* (8), 667-672.
216. Selvaraju, T.; Ramaraj, R. Simultaneous determination of dopamine and serotonin in the presence of ascorbic acid and uric acid at poly(o-phenylenediamine) modified electrode. *Journal of Applied Electrochemistry* **2003**, *33* (8), 759-762.
217. Mathiyarasu, J.; Senthilkumar, S.; Phani, K. L. N.; Yegnaraman, V. Selective detection of dopamine using a functionalised polyaniline composite electrode. *Journal of Applied Electrochemistry* **2005**, *35* (5), 513-519.
218. Raoof, J. B.; Ojani, R.; Rashid-Nadimi, S. Voltammetric determination of ascorbic acid and dopamine in the same sample at the surface of a carbon paste electrode modified with polypyrrole/ferrocyanide films. *Electrochimica Acta* **2005**, *50* (24), 4694-4698.
219. Vasantha, V. S.; Chen, S. M. Electrocatalysis and simultaneous detection of dopamine and ascorbic acid using poly(3,4-ethylenedioxy)thiophene film modified electrodes. *Journal of Electroanalytical Chemistry* **2006**, *592* (1), 77-87.
220. Kumar, S.; Mathiyarasu, J.; Phani, K.; Yegnaraman, V. Simultaneous determination of dopamine and ascorbic acid on poly (3,4-ethylenedioxythiophene) modified glassy carbon electrode. *Journal of Solid State Electrochemistry* **2006**, *10* (11), 905-913.
221. Kumar, S. S.; Mathiyarasu, J.; Phani, K. L. Exploration of synergism between a polymer matrix and gold nanoparticles for selective determination of dopamine. *Journal of Electroanalytical Chemistry* **2005**, *578* (1), 95-103.
-

- 
222. Raj, C. R.; Okajima, T.; Ohsaka, T. Gold nanoparticle arrays for the voltammetric sensing of dopamine. *Journal of Electroanalytical Chemistry* **2003**, *543* (2), 127-133.
223. Zhang, L.; Jiang, X. Attachment of gold nanoparticles to glassy carbon electrode and its application for the voltammetric resolution of ascorbic acid and dopamine. *Journal of Electroanalytical Chemistry* **2005**, *583* (2), 292-299.
224. Gopalan, A. I.; Lee, K. P.; Manesh, K. M.; Santhosh, P.; Kim, J. H.; Kang, J. S. Electrochemical determination of dopamine and ascorbic acid at a novel gold nanoparticles distributed poly(4-aminothiophenol) modified electrode. *Talanta* **2007**, *71* (4), 1774-1781.
225. Bin Fang, G. W. W. Z. M. L. X. K. Fabrication of Fe<sub>3</sub>O<sub>4</sub> Nanoparticles Modified Electrode and Its Application for Voltammetric Sensing of Dopamine. *Electroanalysis* **2005**, *17* (9), 744-748.
226. Silvia A. Miscoria, G. D. B. G. A. R. Enzymatic Biosensor Based on Carbon Paste Electrodes Modified with Gold Nanoparticles and Polyphenol Oxidase. *Electroanalysis* **2005**, *17* (17), 1578-1582.
227. Welch, C.; Compton, R. The use of nanoparticles in electroanalysis: a review. *Analytical and Bioanalytical Chemistry* **2006**, *384* (3), 601-619.
228. Fredy Kurniawan; Vessela Tsakova; Vladimir M. Mirsky Gold Nanoparticles in Nonenzymatic Electrochemical Detection of Sugars. *Electroanalysis* **2006**, *18* (19-20), 1937-1942.
229. P. Cígler; V. Král; M. Kožíšek; J. Konvalinka; V. M. Mirsky Anomalous adsorptive properties of HIV protease: Indication of two-dimensional crystallization? *Coll. Surfaces* **2008**, *in press*.
230. Panasyuk, T. L.; Mirsky, V. M.; Piletsky, S. A.; Wolfbeis, O. S. Electropolymerized Molecularly Imprinted Polymers as Receptor Layers in Capacitive Chemical Sensors. *Anal. Chem.* **1999**, *71* (20), 4609-4613.
231. Robinson, D. L.; Venton, B. J.; Heien, M. L. A. V.; Wightman, R. M. Detecting Subsecond Dopamine Release with Fast-Scan Cyclic Voltammetry in Vivo. *Clinical Chemistry* **2003**, *49* (10), 1763.
232. Chen, Y.; Tan, T. C. Dopamine sensing and selectivity of Nafion-coated plant tissue powder sensors. *Talanta* **1995**, *42* (8), 1181-1188.
233. Adachi, H.; Niino, A.; Takano, K.; Matsumura, H.; Murakami, S.; Inoue, T.; Mori, Y.; Sasaki, T. Temperature-Screening System for Determining Protein Crystallization Conditions. *Japanese Journal of Applied Physics* **2005**, *44* (6A), 4080-4083.
-



- 
234. Penkova, A.; Dimitrov, I.; Nanev, C. Nucleation of Insulin Crystals in a Wide Continuous Supersaturation Gradient. *Ann NY Acad Sci* **2004**, *1027* (1), 56-63.
235. Suzuki, Y.; Miyashita, S.; Sazaki, G.; Nakada, T.; Sawada, T.; Komatsu, H. Effects of pressure on growth kinetics of tetragonal lysozyme crystals. *Journal of Crystal Growth* **2000**, *208* (1-4), 638-644.
236. Kakinouchi, K.; Adachi, H.; Matsumura, H.; Inoue, T.; Murakami, S.; Mori, Y.; Koga, Y.; Takano, K.; Kanaya, S. Effect of ultrasonic irradiation on protein crystallization. *Journal of Crystal Growth* **2006**, *292* (2), 437-440.
237. Nanev, C.; Penkova, A. Nucleation of lysozyme crystals under external electric and ultrasonic fields. *Journal of Crystal Growth* **2001**, *232* (1-4), 285-293.
238. Sazaki, G.; Yoshida, E.; Komatsu, H.; Nakada, T.; Miyashita, S.; Watanabe, K. Effects of a magnetic field on the nucleation and growth of protein crystals. *Journal of Crystal Growth* **1997**, *173* (1-2), 231-234.
239. Sazaki, G.; Moreno, A.; Nakajima, K. Novel coupling effects of the magnetic and electric fields on protein crystallization. *Journal of Crystal Growth* **2004**, *262* (1-4), 499-502.
240. Taleb, M.; Didierjean, C.; Jelsch, C.; Mangeot, J. P.; Capelle, B.; Aubry, A. Crystallization of proteins under an external electric field. *Journal of Crystal Growth* **1999**, *200*, 575-582.
241. Chayen, N. E.; Saridakis, E.; Sear, R. P. Experiment and theory for heterogeneous nucleation of protein crystals in a porous medium. *Proceedings of the National Academy of Sciences* **2006**, *103* (3), 597-601.
242. Georgieva, D. G.; Kuil, M. E.; Oosterkamp, T. H.; Zandbergen, H. W.; Abrahams, J. P. Heterogeneous nucleation of three-dimensional protein nanocrystals. *Acta Crystallographica Section D* **2007**, *63*, 564-570.
243. Wang, Y.; Wei, G.; Zhang, W.; Jiang, X.; Zheng, P.; Shi, L.; Dong, A. Responsive catalysis of thermoresponsive micelle-supported gold nanoparticles. *Journal of Molecular Catalysis A: Chemical* **2007**, *266* (1-2), 233-238.
244. Haizhen An, R. Y. D. T. Y. C. N. L. Dual-Amplification of Antigen-Antibody Interactions via Backfilling Gold Nanoparticles on (3-Mercaptopropyl) Trimethoxysilane Sol-Gel Functionalized Interface. *Electroanalysis* **2007**, *19* (4), 479-486.
245. Ye-Fu Wang, D.-W. P. Z.-L. Z. H.-Z. Z. J.-P. C. J.-T. S. Visual gene diagnosis of HBV and HCV based on nanoparticle probe amplification and silver
-

- staining enhancement. *Journal of Medical Virology* **2003**, *70* (2), 205-211.
246. László Bene, G. S. L. M. R.; Gáspár, S. D. Nanoparticle energy transfer on the cell surface. *Journal of Molecular Recognition* **2005**, *18* (3), 236-253.
247. Maier, M. L. B. Plasmonics - A Route to Nanoscale Optical Devices. *Advanced Materials* **2001**, *13* (19), 1501-1505.
248. Sear, R. P. Nucleation: theory and applications to protein solutions and colloidal suspensions. *Journal of Physics: Condensed Matter* **2007**, *19*, 033101.
249. Forsythe, E. L.; Judge, R. A.; Pusey, M. L. Tetragonal Chicken Egg White Lysozyme Solubility in Sodium Chloride Solutions. *J. Chem. Eng. Data* **1999**, *44* (3), 637-640.
250. Mulvaney, P. Surface Plasmon Spectroscopy of Nanosized Metal Particles. *Langmuir* **1996**, *12* (3), 788-800.
251. Liang, X.; Zhang, Q.; Jiang, H. Quantitative reconstruction of refractive index distribution and imaging of glucose concentration by using diffusing light. *Appl. Opt.* **2006**, *45* (32), 8360-8365.
252. Grasso, M.; Ripabelli, G.; Sammarco, M. L.; Manfredi, T. M.; Quaranta, A. Vaccine storage in the community: a study in central Italy. *Bull World Health Organ* **1999**, *77* (4), 352-354.
253. Matthias, D. M.; Robertson, J.; Garrison, M. M.; Newland, S.; Nelson, C. Freezing temperatures in the vaccine cold chain: A systematic literature review. *Vaccine* **2007**, *25* (20), 3980-3986.
254. Decher, G. Fuzzy Nanoassemblies: Toward Layered Polymeric Multicomposites. *Science* **1997**, *277* (5330), 1232-1237.
255. Cao, L.; Lin, H.; Mirsky, V. Detection of antibiotics in food: Extraction of fluoroquinolones by DNA. *Analytical and Bioanalytical Chemistry* **2007**, *388* (1), 253-258.
256. Baba, A.; Park, M. K.; Advincula, R. C.; Knoll, W. Simultaneous Surface Plasmon Optical and Electrochemical Investigation of Layer-by-Layer Self-Assembled Conducting Ultrathin Polymer Films. *Langmuir* **2002**, *18* (12), 4648-4652.
257. Tian, S.; Liu, J.; Zhu, T.; Knoll, W. Polyaniline doped with modified gold nanoparticles and its electrochemical properties in neutral aqueous solution. *Chemical Communications* **2003**, *2003* (21), 2738-2739.

- 
258. Tian, A. B. Electroactivity of Polyaniline Multilayer Films in Neutral Solution and Their Electrocatalyzed Oxidation of  $\gamma$ -Nicotinamide Adenine Dinucleotide. *Advanced Functional Materials* **2003**, 13 (6), 473-479.
259. Tian, S.; Liu, J.; Zhu, T.; Knoll, W. Polyaniline/Gold Nanoparticle Multilayer Films: Assembly, Properties, and Biological Applications. *Chem. Mater.* **2004**, 16 (21), 4103-4108.
260. Ge, C.; Armstrong, N. R.; Saavedra, S. S. pH-Sensing Properties of Poly(aniline) Ultrathin Films Self-Assembled on Indium-Tin Oxide. *Anal. Chem.* **2007**, 79 (4), 1401-1410.
261. Raposo, M.; Oliveira, O. N. Adsorption of Poly(*o*-methoxyaniline) in Layer-by-Layer Films. *Langmuir* **2002**, 18 (18), 6866-6874.
262. Krogman, K. C.; Zacharia, N. S.; Schroeder, S.; Hammond, P. T. Automated Process for Improved Uniformity and Versatility of Layer-by-Layer Deposition. *Langmuir* **2007**, 23 (6), 3137-3141.
263. Portnov, S.; Yashchenok, A.; Gubskii, A.; Gorin, D.; Neveshkin, A.; Klimov, B.; Nefedov, A.; Lomova, M. An automated setup for production of nanodimensional coatings by the polyelectrolyte self-assembly method. *Instruments and Experimental Techniques* **2006**, 49 (6), 849-854.
264. Cheung, J. H.; Stockton, W. B.; Rubner, M. F. Molecular-Level Processing of Conjugated Polymers. 3. Layer-by-Layer Manipulation of Polyaniline via Electrostatic Interactions. *Macromolecules* **1997**, 30 (9), 2712-2716.
265. Dong-Mei Zhou; Jing-Juan Xu; Hong-Yuan Chen; Hui-Qun Fang Ascorbate sensor based on 'self-doped' polyaniline. *Electroanalysis* **1997**, 9 (15), 1185-1188.
266. Granot, E.; Katz, E.; Basnar, B.; Willner, I. Enhanced Bioelectrocatalysis Using Au-Nanoparticle/Polyaniline Hybrid Systems in Thin Films and Microstructured Rods Assembled on Electrodes. *Chem. Mater.* **2005**, 17 (18), 4600-4609.
267. Bartlett, P. N.; Wallace, E. N. K. The oxidation of ascorbate at poly (aniline)-poly (vinylsulfonate) composite coated electrodes. *Physical Chemistry Chemical Physics* **2001**, 3 (8), 1491-1496.
-

## 8. CURRICULUM VITAE

### ***PERSONAL DATA***

---

Name : Fredy Kurniawan  
Date of birth : 28-04-1974  
Place of birth : Cepu, Indonesia  
Marital status : Married  
E-Mail : fredy@chem.its.ac.id

### ***EDUCATIONAL BACKGROUND***

---

1992-1997 Bachelor of Chemistry, Chemistry Department of Institute Technology of Sepuluh Nopember (ITS) Surabaya – Indonesia

2001 – 2004, Master of analytical chemistry, Chemistry Department –of Institute Technology Bandung (ITB), Bandung - Indonesia

2004 - present, PhD student of Institute of Analytical Chemistry, Chemo- and Biosensor, Regensburg University Germany.

### ***EMPLOYMENT***

---

1998 – present, Lecturer of chemistry department, Faculty of Mathematics and Natural Sciences, Institute Technology of Sepuluh Nopember (ITS) Surabaya - Indonesia

### ***PROFESSIONAL MEMBERSHIP***

---

Member of environmental society of ITS research center, Indonesia.

Member of basic science society of ITS research center, Indonesia.

## 9. LIST OF PUBLICATIONS AND PRESENTATIONS

### ***BACHELOR AND MASTER THESIS***

---

1. Graft copolymerization of potato starch by trimethyl ammonium chloride (TAC)
2. Preliminary study of construction of polypyrrole-humic acid electrode for stripping voltammetric analysis of Cd<sup>2+</sup> ion

### ***LIST OF PUBLICATIONS***

---

1. Fredy Kurniawan, Buchari, Indra Noviandri, "Application of polypyrrole-humic acid electrode in determination of Cd<sup>2+</sup> ion", MIPA, 2007
2. Fredy Kurniawan, Vessela Tzakova, Vladimir M. Mirsky, "Gold Nanoparticles in Nonenzymatic Electrochemical Detection of Sugar", Electroanalysis, Vol 18, Issue 19-20, October 2006.
3. Fredy Kurniawan, Vessela Tsakova, Vladimir M. Mirsky "Analytical applications of electrodes modified by gold nanoparticles: dopamine detection", Accepted in Journal Nanotechnology and Nanoscience, 2008

### ***LIST OF PRESENTATIONS***

---

1. Fredy Kurniawan, Vessela Tzakova, Vladimir M. Mirsky, "Detection of glucose by gold nanoparticles modified electrode", International Workshop Shedding Light in the Nanoworld : Ordered and Disordered Nanostructures, Sunny Beach, Bulgaria, 2006.
2. Feyzim Hodzhaoglu, Fredy Kurniawan, Vladimir M. Mirsky, and Christo Nanev, "Nucleation and growth of protein crystal in the presence of gold, nanoparticles", Pilot program for coupled multidisciplinary training and fundamental knowledge on nanoscale phenomena, Sofia, Bulgaria, 2007
3. Fredy Kurniawan, Vessela Tzakova, Vladimir M. Mirsky, "Application of gold nanoparticles for non-enzymatic electrochemical detection of sugars", 5. Deutsches BioSensor Symposium, 2007

### ***IN PROGRESS***

---

1. Feyzim Hodzhaoglu, Fredy Kurniawan, Vladimir M. Mirsky, and Christo Nanev Gold nanoparticles induce protein crystallization Protein, submitted to Jurnal of Crystal Research and Technology

## **10. ACKNOWLEDGEMENTS**

I would like to thank the following people who contributed to the success of my work:

Generally I wish to give my grateful acknowledgements to all members of our institute, who provide a pleasant atmosphere where I spent more than 3 years of happy time.

First of all, I appreciate my supervisor, *Prof. Dr. Vladimir M. Mirsky*. I would like to thank him for giving me the opportunity to study and work under his instruction, for his selfless supervision and assistance, for his intelligent guidance and discussion. I also would like to acknowledge *Prof. Dr. Otto. S. Wolfbeis*, our chief, for offer me a chance to study, his valuable discussion and his warm assistance;

*Mrs. Angela Haberkern, Mr. Thomas Hirsch and Joachim Rewitzer*, my lab colleagues giving me plenty of valuable advice, warm help and care, with whom I had a happy time during the past period;

*Mrs. A. Stoiber*, who often helped me to search for chemicals without hesitation;

*Miss Emmert Gisela* who patiently assisted me to solve computer problems;

*Mrs. Edeltraud Schmid and Mrs. M. Bauer*, our secretaries, whom I always caused trouble;

*Prof.D. Weiss and Dr. J. Stahl* who performed scanning electron microscopy of the gold nanoparticles modified electrode.

*Nataliya V. Roznyatovskaya, PhD* for the fruitful discussion

*Dr. Vessela Tsakova and Dr. S. Ivanov* in Bulgarian Academy Sciences for helping me to get the accommodation during my stay in Sofia, and also for the fruitful discussions.

*Prof. Dr. Christo Nanev and Feyzim Hodzhaoglu* in Bulgarian Academy Sciences for the cooperation in protein crystallization research.

*Dr. Tz. Tzacheva and Dr. I. Dimitrov* for the discussion in protein crystallization.

## ACKNOWLEDGEMENTS

---

My Indonesian friends, *the family Muhammad Dardi, Alfa ferri and Eko* in Regensburg, who gave me great support in life and spirit, offering me warm hospitality and care, which presented me a feeling of home;

Furthermore, **special appreciation** given to:

Indonesian government who provides me the fellowship through SPMU TPSDP Sepuluh Nopember Institute of Technology.

DAAD and Bulgarian Ministry of Education and Science who gave me the collaboration grant in 2005 and 2005.

*My dear wife and the whole family.....*